CHALMERS

Structural analysis of main deck of RoPax vessels

A finite element analysis approach combining hull girder loads and local loads for buckling assessment

Examensarbete inom högskoleingenjörsprogrammet maskinteknik

YUYANG WU

INSTITUTIONEN FÖR MEKANIK OCH MARITIMA VETENSKAPER

CHALMERS TEKNISKA HÖGSKOLA
Göteborg, Sverige 2025
www.chalmers.se

Examensarbete 2025

Structural analysis of main deck of RoPax vessels
A finite element analysis approach combining hull girder loads and local loads for buckling assessment

YUYANG WU

CHALMERS

Institutionen för Mekanik och maritima vetenskaper
CHALMERS TEKNISKA HÖGSKOLA
Göteborg, Sverige 2025

Structural analysis of main deck of RoPax vessels
A finite element analysis approach combining hull girder loads and local loads for buckling assessment

YUYANG WU

Supervisor/Examiner: Zhiyuan Li, Department of Mechanics and Maritime Sciences, Chalmers University of Technology

Examensarbete MMSX25
Institutionen för Mekanik och Maritima vetenskaper
Chalmers tekniska högskola 412 96
Göteborg Sverige
Telefon + 46 (0)31-772 1000

Omslagsbild: RoPax vessel Stena Edda (Nash, 2020)

Structural analysis of main deck of RoPax vessels
A finite element analysis approach combining hull girder loads and local loads for buckling assessment
YUYANG WU

Department of Mechanics and Maritime Sciences
Chalmers University of Technology

ABSTRACT

This thesis develops a finite element analysis-based methodology for assessing the buckling behavior of vehicle deck structures in RoPax vessels under combined global and local loading conditions. The proposed approach combines rule-based calculation of hull girder loads, midship section modeling, sub-modeling, and the application of local wheel loads.

The methodology is demonstrated on Deck 3 and Deck 5 of a reference RoPax vessel. The global hull girder loads are calculated according to DNV formulations and applied to a finite element model of the midship section. The resulting boundary response is then transferred to refined local deck models, where linear buckling analyses are performed under both pure hull-girder loading and combined hull-girder and wheel loading conditions.

The results show that both deck structures maintain sufficient margins against buckling under the investigated design load cases. For Deck 3, the influence of the hull girder load is limited due to its location close to the neutral axis. For Deck 5, the top plate panels are identified as the main buckling-sensitive regions. The local wheel load reduces the buckling load multiplier and shifts the critical deformation towards the loaded areas; however, the structures remain within a safe range.

This thesis is written in English.

Keywords: RoPax vessel, deck structure, finite element analysis, FEA, hull girder load, wheel load, sub-modeling, linear buckling analysis, DNV

Structural analysis of main deck of RoPax vessels

A finite element analysis approach combining hull girder loads and local loads for buckling assessment

YUYANG WU

Institutionen för Mekanik och maritima vetenskaper
Chalmers Tekniska Högskola

SAMMANFATTNING

Detta examensarbete utvecklar en finita-elementbaserad metod för att bedöma knäckningsbeteendet hos fordonsdäck i RoPax-fartyg under kombinerade globala och lokala lastförhållanden. Metoden kombinerar regelbaserad beräkning av skrovbalkslaster, modellering av midskeppssektionen, submodellering och applicering av lokala hjullaster.

Metoden demonstreras på däck 3 och däck 5 i ett referensfartyg av RoPax-typ. De globala skrovbalkslasterna beräknas enligt DNV:s formuleringar och appliceras på en global FE-modell. Den resulterande randresponsen överförs därefter till förfinade lokala däckmodeller, där linjära knäckningsanalyser utförs för både ren skrovbalkslast och kombinerad skrovbalks- och hjullast.

Resultaten visar att båda däckstrukturerna har tillräckliga marginaler mot knäckning under de undersökta dimensionerande lastfallen. För däck 3 är påverkan från skrovbalkslasten begränsad eftersom däcket ligger nära den neutrala axeln. För däck 5 identifieras topp-plåtens paneler som de mest knäckningskänsliga områdena. Den lokala hjullasten reducerar knäckningsmultiplikatorn och förskjuter den kritiska deformationen mot lastytorna, men strukturerna förblir inom ett säkert område.

Examensarbetet är skrivet på engelska.

Nyckelord: RoPax-fartyg, däckstruktur, finita element analys, FEA, skrovbalkslast, hjullast, sub-modellering, linjär knäcknings analys, DNV

Acknowledgements

This work corresponds to 15hp and has been written by YUYANG WU within the Mechanical Engineering (Maskinteknik) program at Chalmers University of Technology.

I want to express my sincere gratitude to my examiner and my supervisor, Zhiyuan Li. His guidance and support throughout this project have been highly educational and have opened the door for me into the field of marine and ship engineering.

I would also like to express my sincere gratitude to Jörgen Andersson from Stena. In particular, his help in evaluating the accuracy of the buckling results, together with his constructive suggestions and guidance, contributed significantly to the quality of this work.

Last but not least, I would also like to thank my family who have always been my support on my academic journey.

YUYANG WU, Göteborg, 2025

Contents

List of Nomenclature

Abbreviations	
BS	Beam sea
CG	Class guideline
CS	Classification society
DNV	Det Norske Veritas
DoF	Degree of freedom
FE	Finite element
FEA	Finite element analysis
FEM	Finite element method
FS	Follow sea
HBM	Horizontal bending moment
HS	Head sea
LCF	Load combination factors
MPC	Multi-Point Constraint
OS	Oblique sea
PULS	Panel ultimate limit state
RoPax	Roll on/Roll off passenger
RU	Rules for classification
TM	Torsional moment
ULS	Ultimate limit state
VBM	Vertical bending moment
VSF	Vertical shear force

Geometry and main vessel parameters		
g	gravitational acceleration	m/s^2
L	vessel length	m
B	vessel breadth (width)	m
D	vessel depth	m
T_{sc}	scantling draught	m
T_{LC}	midship draught in the considered loading condition	m

C_B	block coefficient	m
C_w	wave coefficient	$-$
x	longitudinal coordinate (positive forward)	m
y	transverse coordinate (positive transverse)	m
z	vertical coordinate (positive upwards)	m

Hull girder loads		
M_{bv-tot}	total vertical bending moment (still-water + wave)	kNm
M_{sw}	still-water vertical bending moment	kNm
M_{wv}	wave vertical bending moment	kNm
M_{bh-tot}	total horizontal bending moment	kNm
M_{wh}	wave horizontal bending moment	kNm
M_{t-tot}	total torsional moment	kNm
M_{wt}	wave torsional moment	kNm
Q_{tot}	total vertical shear force (still-water + wave)	kN
Q_{sw}	still-water vertical shear force	kN
Q_{wv}	wave vertical shear force	kN
M_{st}	still-water torsional moment	kNm

Load Combination Factors		
C_{WV}	load combination factor for vertical bending moment	$-$
C_{QW}	load combination factor for vertical shear force	$-$
C_{WH}	load combination factor for horizontal bending moment	$-$
C_{WT}	load combination factor for torsional moment	$-$

Other factors		
f_{lp}	factor depending on longitudinal position along the ship	$-$
f_T	draught ratio between loading condition and scantling draught	$-$
f_p	probability factor	$-$
f_{vib}	correction for the minimum contribution from hull girder vibration	$-$
f_R	factor related to operational profile	$-$

f_{beta}	wave heading correction factor	$-$
f_{nl-vh}	non-linear effect factor for vertical hogging bending	$-$
f_{nl-vs}	non-linear effect factor for vertical sagging bending	$-$
f_m	distribution factor for wave vertical bending moment along ship length	$-$
f_{sw}	distribution factor for still-water vertical bending moment along ship length	$-$
f_{q-pos}	distribution factor for positive wave vertical shear force along ship length	$-$
f_{q-neg}	distribution factor for negative wave vertical shear force along ship length	$-$
f_{qs}	distribution factor for still-water vertical shear force along ship length	$-$

Ship motions and accelerations		
a_{heave}	heave acceleration	m/s^2
a_{roll}	roll acceleration	m/s^2
a_{pitch}	pitch acceleration	m/s^2
T_θ	roll motion period	s
θ	roll angle	$°\ (degree)$
T_φ	pitch motion period	s
φ	pitch angle	$°(degree)$
$a_{pitch-z}$	vertical component of pitch acceleration at a given position	m/s^2
a_{roll-z}	vertical component of roll acceleration at a given position	m/s^2
a_z	vertical envelope acceleration	m/s^2

Local loads (Wheel loads)		
P_{wl}	wheel-load pressure acting on deck	kN/m^2
Q	axle load	ton
n_0	number of load areas (wheels) on one axle	$-$
a_1	effective length of tire–deck contact area	mm
b_1	effective width of tire–deck contact area	mm

List of Tables

List of Figures

1. Introduction

1.1. Background and motivation

As its name suggests, the RoPax (roll-on/roll-off passenger) vessel is a ship type designed to transport vehicles and passengers across short-sea routes. The emergence and proliferation of RoPax vessels are primarily driven by geographical features, particularly in Europe, where narrow waterways exist between land, such as the Baltic Sea and the North Sea.

Figure 1: RoPax Vessel "Stena Edda" (Nash, 2020)

In recent years, growing global concern over environmental sustainability has led to a requirement to reduce emissions in the shipping industry. As ecological impact becomes a core design concept for a ship, reducing fuel consumption is an intuitive and effective strategy for meeting emission-reduction goals. One promising approach to reducing fuel consumption is to optimize a vessel's structural weight. Reduced weight lowers propulsion power requirements, thereby reducing fuel consumption without affecting the vessel's performance. Against this background, increasing attention has been directed toward research on alternative materials. By replacing the current material with a higher-strength steel, the ship components can be redesigned to use less material while maintaining the same strength. However, the application of alternative materials also requires re-evaluating existing structures to capitalize on their performance while preventing over-design. To ensure safety and compliance, the structure must undergo reliability assessments, including buckling analysis.

1.2. Objectives

This study aims to establish a FEM (Finite Element Method) for the buckling assessment of ship deck structures. The proposed methodology shall account for the influence of hull girder loading and local loading to achieve more realistic ship loading conditions. Its application in FEA (Finite Element Analysis) software shall enable the identification of the critical buckling behavior and failure mechanisms. In addition, this method is intended to support the structural optimization process, improving performance while ensuring compliance with relevant CS (Classification Society) requirements.

1.3. Scope and limitations

This study focuses on the structural analysis of selected deck structures within a RoPax vessel. Particular attention is paid to the possible buckling behavior of the structure under design loads. The scope of work is limited to decks 3 and 5, the primary vehicle-carrying decks, rather than all decks. Due to the design characteristics of RoPax vessels, there is usually a lack of vertical support, such as bulkheads and pillars, between decks. Therefore, the performance of these deck structures under concentrated wheel loads is of particular interest.

Although the analysis centers on these decks, models of non-deck structures are also essential to account for the influence of hull girder loads. All structural components are modeled based on the midship section of a reference vessel and the relevant requirements in DNV (Det Norske Veritas) - CG (Class Guidelines).

As mentioned in Section 1.1, one of the underlying motivations for this work is the potential replacement of existing steel with other materials for the ship structures. However, the material substitution itself is not the primary focus of the present study. Instead, the methodology proposed in this thesis is intended to support such studies by enabling buckling analysis with different material properties assigned to the FE models. Therefore, to simplify the development and verification of the methodology, all FE models are built using material properties for AH36 shipbuilding steel, in accordance with the drawings of the reference vessel. The possible consequences of replacing AH36 with other materials will not be analyzed in the present study.

In addition, the investigation is further limited to linear buckling analysis, which is used to identify critical instability modes and locations. Initial imperfections, non-linear buckling behavior, and ULS (Ultimate Limit State) of the structure are beyond the scope of this study. All these neglected aspects are proposed as directions for future work.

In general, the main emphasis of this thesis is on developing and demonstrating an analysis framework that consistently combines global hull-girder loads and local wheel loads for the structural assessment of RoPax vehicle decks.

2. Literature review

In an earlier study done by Humia (2019), unstiffened plates and stiffened panels of large cruise vessels were investigated using PULS (Panel Ultimate Limit State) and non-linear FEA (Humia, 2019). At the same time, empirical loads were applied instead of CS rule-based load values. The study highlighted the influence of boundary conditions, welding-induced imperfections, and the effects of surrounding members on buckling behavior and strength. The importance of FEA was thereby emphasized for achieving an optimized, reliable ship structural design.

Beyond shipbuilding, methodological advances in offshore engineering provide valuable insights into the analysis of on-sea structures. Research by Yi and Park (2025) introduced an FEA strategy for floating offshore substations that integrate cargo-hold modeling with sub-model refinement (Yi & Park, 2025). The methodology achieved both computational efficiency and local accuracy. Although the study did not focus on ships, the concept of sub-modeling remains inspiring.

More recently, Jang and Kim (2025) discussed the challenges and constraints associated with rule-based hull girder load adjustment in ship structural FE analysis (Jang & Kim, 2025). Their study focused on applying rule-based procedures to a cargo hold model, in which local loads derived from classification rules were integrated and compared with target hull girder loads. Since the calculated hull girder loads may not directly satisfy the required design values, additional load adjustment procedures are required for components such as vertical shear force, vertical bending moment, horizontal bending moment, and torsional moment. As the adjustment procedure adopted in their study is derived from the DNV-CG-0127, the work provides a highly relevant reference for the present thesis, particularly regarding the definition of boundary conditions, load application, and hull girder load representation in FE-based ship structural assessment (DNV, 2021a).

In summary, the reviewed studies demonstrate that buckling is a critical failure mechanism in ship structures and that reliable structural assessment can be achieved through FE-based approaches. Previous research has also shown that boundary conditions, initial imperfections, surrounding structural members, and load application methods can significantly influence the predicted buckling response and ultimate strength. In addition, sub-modeling techniques provide an effective way to improve local stress resolution while maintaining computational efficiency in large-scale structural analysis.

Although these studies provide valuable insights into buckling assessment, FE modeling strategies, sub-modeling techniques, and hull girder load adjustment, specific investigations focusing on main deck structures remain relatively limited. In particular, an integrated methodology for analyzing deck structures under the combined effects of hull girder loads and local loads has not been sufficiently established. This research gap forms one of the main motivations of the present thesis, as introduced in Section 1.3.

3. Hull girder loads

Hull girder loads represent the load combinations acting on the vessel's entire hull structure. In the design process for a vessel, the ship's hull is often idealized as a hollow beam structure floating on the sea surface. This allows the estimation of moments and forces (induced by onboard cargo, structures, and seawater buoyancy) using beam theory. These hull-girder loading conditions serve as the basis for evaluating the vessel's overall structural response. This section provides principles and calculations for hull girder loads, with reference to the methodologies and formulas outlined in DNV-RU (Rules for classification)-SHIP pt.3 (DNV, 2022). Before proceeding with the calculation of hull girder loads, it is essential to clarify several key concepts related to vessel loading.

3.1. Static and dynamic loads

A hull girder load is a combination of two corresponding load types: static (S) and dynamic (D). Static loads refer to moments or forces acting on vessels under still-water conditions. These loads are always present and influence the ship regardless of external environmental factors. In contrast, dynamic loads arise from wave-induced effects and represent the additional forces/moments imposed by the ship's interaction with a varying sea state.

When estimating dynamic loads, the standard practice is to consider the extreme sea-state scenario, in which the vessel is assumed to experience the maximum possible wave-induced loads. It ensures that the structural analysis accounts for the most critical and demanding scenarios that the ship may face during its operational life.

In addition, this study will conduct the assessment in accordance with the conservative approach recommended in DNV-CG-0127, namely, the standard quasi-formulation (DNV, 2021b). This approach involves transforming dynamic loads into equivalent static loads, which are then applied to the model to evaluate its performance under the most critical potential conditions. In other words, the maximum possible dynamic load has been calculated and applied as a static load while conducting the static analysis.

3.2. Hull girder load overview

This section will present different types of hull girder loads, which are the combined forces and moments acting over the entire hull. These loads can be classified into four primary components that play critical roles in assessing the vessel's structural behavior, see Table 1.

Table 1: Load components

VBM	Vertical Bending Moment
HBM	Horizontal Bending Moment
VSF	Vertical Shear Force
TM	Torsional Moment

As mentioned in the previous section, each of these load components is derived as a combination of static and dynamic loads. Static load refers to loads that occur while the vessel is in still water, for example, in regions around a harbor. Dynamic loads are additional loads that arise when vessels travel on the sea surface. The combined loads lead to a more realistic simulation of the operational environment. The governing formulations for calculating hull girder loads are prescribed in DNV-RU-SHIP, thereby obviating the necessity for independent derivation within the scope of this work (DNV, 2022).

Finally, from a safety perspective, all load combinations should reflect extreme design scenarios. This means that the applied loads must represent credible maximum values based on environmental conditions and vessel usage profiles, see Table 2. For the RoPax vessel in this study, *normal operation at sea* shall apply as the design load scenario. Noticing that *special operations* refer to the loading condition of a semi-submersible heavy transport vessel (DNV, 2022).

Table 2: Hull girder load components for strength assessment (DNV, 2022)

		Design load scenario						
		1	*2*	*3*	*4*	*5*	*6*	*7*
		Normal operations at harbor and sheltered water	*Normal operation at sea*	*Flow through ballast water exchange*	*Overfilling of ballast tanks and tank testing*	*Flooding*	*Special operation still-water*	*Special operations at sea*
		Static (S)	*Static+ Dynamic (S + D)*	*Static+ Dynamic (S + D)*	*Accidental (A) and Testing (T)*	*Accidental (A)*	*Static (S)*	*Static+ Dynamic (S + D)*
Hull girder loads	VBM	M_{sw}	$M_{sw} + M_{wv-LC}$	$M_{sw} + M_{wv-LC}$	M_{sw}	M_{sw}	M_{sw_i}	$M_{sw\_i} + M_{wv-LC}$
	HBM	-	M_{wh-LC}	M_{wh-LC}	-	-	-	M_{wh-LC}
	VSF	Q_{sw}	$Q_{sw} + Q_{wv-LC}$	$Q_{sw} + Q_{wv-LC}$	-	-	Q_{sw_i}	$Q_{sw\_i} + Q_{wv-LC}$
	TM	M_{st}	$M_{st} + M_{st-LC}$	$M_{st} + M_{st-LC}$	M_{st}	M_{st}	M_{st_i}	$M_{st\_i} + M_{st-LC}$

☐ - Load cases directly relevant to the analysis of the deck structure

☐ - Load cases of secondary relevance

3.3. Wave headings

To calculate the dynamic loads, it is necessary to consider the various wave types that the ship may encounter during navigation. Unlike the constant static loads, dynamic loads are induced by the ship's interaction with the wave environment. The magnitude of hull girder loads can vary significantly depending on wave direction (DNV, 2022). The waves can be categorized into four principal types:

- **Head Sea (HS):**
  Refers to waves approaching from the forward longitudinal direction of the vessel. This kind of wave is considered the most structurally demanding wave in terms of vertical bending moment (VBM) and is therefore central to design load scenarios.
- **Following Sea (FS):**
  Refers to waves propagating from the backward longitudinal direction of the vessel. Compared with HS, FS will produce an opposing force of equal or lesser magnitude. In the design process, the effects of following seas may be neglected, unless the vessel's structural design makes them

significant.

- **Beam Sea (BS):**
  Refers to waves impacting the vessel from the transverse direction (port or starboard side). These waves primarily affect HBM, while their influence on VBM is typically negligible.
- **Oblique Sea (OS):**
  Refers to waves impacting the vessel from oblique directions. Its direction is usually idealized as the diagonal line between the vertical and horizontal axes. These waves are causing both smaller VBM and HBM but introducing TM.

It is essential to declare that one type of wave heading might not have contributed to each dynamic hull girder load. For instance, HS does not cause any HBM or TM. In contrast, BS will cause dynamic HBM, but not to the same extent as HS.

The influence of wave heading is not applied directly in the calculation of dynamic loads. Instead, the magnitude of dynamic load is adjusted by LCF (Load Combination Factors), which accounts for wave-heading effects. In addition to appropriately scaling the loads, these LCFs align the load directions with the vessel's global coordinate system. The global coordinate system is presented in Section 7.2, while the LCFs are listed in Section 3.4.

According to DNV-RU-SHIP pt.3, each type of wave heading corresponds to a specific load case (DNV, 2022). The HS, BS, and OS wave cases correspond to the HSM (Head Sea moment), BSR (Beam Sea roll), and OST (Oblique Sea torsion) load cases, respectively.

Table 3: Load cases

Load case	Implication
HSM	Load case where the dynamic **VBM** minimizes/maximizes
BSR	Load case where the **roll motion** of the vessel is minimized/maximized
OST	Load case where the **TM** of the vessel minimizes/maximizes

Furthermore, each load case is associated with a suffix indicating the magnitude of its load components. The same suffix conventions are used in subsequent references to load types to maintain consistency. A reference table summarizing the suffix system is provided for facilitating clarity and traceability.

Table 4: Suffix for LCFs

Suffix	Meaning
1	Minimize
2	Maximize
S	Starboard side
P	Port side

3.4. Load combination factors

This section presents the LCFs and their magnitude under different wave headings. Tables come from DNV-RU-SHIP pt.3, and the factors shown in the tables are described in Section 4.2 (DNV, 2022).

Table 5: LCF for HSM load case (DNV, 2022)

Load component		LCF	HSM-1	HSM-2
Hull girder loads	M_{WV}	C_{WV}	-1.0	1.0
	Q_{WV}	C_{QW}	$-1.0f_{\ell p}$	$1.0f_{\ell p}$
	M_{WH}	C_{WH}	0	0
	M_{WT}	C_{WT}	0	0

Table 6: LCF for BSR-load case (DNV, 2022)

Load component		LCF	BSR-1P	BSR-2P	BSR-1S	BSR-2S
Hull girder loads	M_{WV}	C_{WV}	$0.1-0.2f_T$	$0.2f_T-0.1$	$0.1-0.2f_T$	$0.2f_T-0.1$
	Q_{WV}	C_{QW}	$(0.1-0.2f_T)f_{\ell p}$	$(0.2f_T-0.1)f_{\ell p}$	$(0.1-0.2f_T)f_{\ell p}$	$(0.2f_T-0.1)f_{\ell p}$
	M_{WH}	C_{WH}	$1.2-1.1f_T$	$1.1f_T-1.2$	$1.1f_T-1.2$	$1.2-1.1f_T$
	M_{WT}	C_{WT}	0	0	0	0

Table 7: LCF for OST load case (DNV, 2022)

Load component		LCF	OST-1P	OST-2P	OST-1S	OST-2S
Hull girder loads	M_{WV}	C_{WV}	$-0.3-0.2f_T$	$0.3+0.2f_T$	$-0.3-0.2f_T$	$0.3+0.2f_T$
	Q_{WV}	C_{QW}	$(-0.35-0.2f_T)f_{\ell p}$	$(0.35+0.2f_T)f_{\ell p}$	$(-0.35-0.2f_T)f_{\ell p}$	$(0.35+0.2f_T)f_{\ell p}$
	M_{WH}	C_{WH}	-1.0	1.0	1.0	-1.0
	M_{WT}	C_{WT}	$-f_{\ell p-OST}$	$f_{\ell p-OST}$	$f_{\ell p-OST}$	$-f_{\ell p-OST}$
$f_{\ell p-OST}$ is a specified longitudinal distribution factor given in DNV-RU-SHIP Pt.3 Ch.4 Sec. 4 [3.4.1] (DNV, 2022)						

4. Calculation of hull girder loads

Having established the conceptual framework for hull girder loads in the structural response of a vessel, the next step is to determine these loads. The calculation procedures are governed by the rules and recommendations set forth by DNV-RU-SHIP pt-3, which provide standardized formulations for each load component under both static and dynamic conditions (DNV, 2022).

The parameters, factors, and coefficients required for the calculation of load components are listed in Section 4.1 and Section 4.2. Their numerical values are specified in Ch.4 of DNV-RU-SHIP pt.3, and therefore are not explicitly listed in this study (DNV, 2022). However, the magnitudes of the load components under different load cases are summarized in Section 4.7.

4.1. Vessel-related parameters

The following table lists the parameters that recur in the load calculation formula. Among these parameters, the gravitational acceleration and the wave coefficient are specified in DNV-RU-SHIP pt.3 (DNV, 2022). The other vessel-related parameters should be adjusted based on the data for the vessel under study. In the current case, these parameters are defined with respect to the reference vessel.

Table 8: Table of parameters

Symbol	Description	Unit
g	Gravitation acceleration	$\left[\frac{m}{s^2}\right]$
L	Vessel length	$[m]$
B	Vessel width	$[m]$
D	Vessel depth	$[m]$
T_{sc}	Scantling draught	$[m]$
T_{LC}	Midship draught at the considered loading condition	$[m]$
C_B	Block coefficient	-
C_w	Wave coefficient	-
x	Coordinate along the longitudinal direction of the vessel	-
y	Coordinate along the transversal direction of vessel	-
z	Coordinate along the vertical direction of vessel	-

4.2. Factors and coefficients

The magnitudes or calculations of the factors and coefficients are given by DNV-RU-SHIP pt.3 (DNV, 2022).

Table 9: Table of factors and coefficients

Symbol	Description
$f_{\ell p}$	Factor depending on longitudinal position along the ship
f_T	Ratio between draught at loading condition and scantling draught
f_p	Probability factor
f_{vib}	Correction for the minimum contribution from hull girder vibration
f_R	Factor related to the operational profile
f_β	Heading correction factor
f_{nl-vh}	Coefficient considering non-linear effects applied to hogging
f_{nl-vs}	Coefficient considering non-linear effects applied to sagging
f_m	Distribution factor for wave VBM along the ship's length
f_{sw}	Distribution factor for still-water VBM along the ship's length
f_{q-pos}	Distribution factor for positive wave VSF along the ship's length
f_{q-neg}	Distribution factor for negative wave VSF along the ship's length
f_{qs}	Distribution factor for still-water VSF along the ship's length

4.3. VBM (Vertical Bending Moment)

VBM represents the primary hull girder load effect acting on a vessel's hull girder. It arises from the combined action of still-water and wave loads in the vertical plane. Under still-water conditions, VBM is generated by the vessel's self-weight, cargo weight, and buoyancy forces distributed along the ship's length, resulting in vertical deformation of the hull girder. However, these parameters are usually not known in sufficient detail during the preliminary design stage. Therefore, the target vertical bending moment (VBM) is calculated using DNV's rule-based equations, in which the principal vessel parameters define the design hull girder load for structural assessment.

For RoPax vessels, VBM is critical due to their relatively large length-to-width and length-to-depth ratios, the limited number of transverse bulkheads, and extensive uninterrupted vehicle decks. These structural features increase demands on the deck structures. Based on the curvature of the hull girder deflection, the structural loading conditions are classified as sagging or hogging.

- Sagging – midship is depressed, top plate is in compression.
- Hogging - midship is elevated, top plate is in tension.

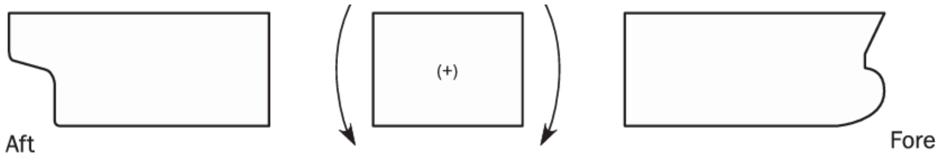

Figure 2: Vertical Bending Moment (DNV, 2022)

The total VBM is the sum of still-water VBM and wave VBM from dynamic load cases. During the calculation, the wave VBM must be computed first. Its value will subsequently be applied to the calculation of still-water VBM and wave VBM in different dynamic load cases.

$$M_{bv-tot} = M_{sw} + M_{wv-LC}\ [kNm] \tag{1}$$

Where:

M_{bv-tot} = The total vertical bending moment

M_{sw} = The still-water vertical bending moment

M_{wv-LC} = The wave vertical bending moment under a specific load case

M_{wv} - Wave vertical bending moment

$$M_{wv-s} = -0.19 \times \frac{f_R}{0.85}\ f_{nl-vs}\ f_m\ f_p\ C_w\ L^2\ B\ C_B\ [kNm] \tag{2}$$

$$M_{wv-h} = 0.19 \times \frac{f_R}{0.85}\ f_{nl-vh}\ f_m\ f_p\ C_w\ L^2\ B\ C_B\ [kNm] \tag{3}$$

Where:

f_R = Factor related to the operational profile

- $f_R = 0.76$

f_{nl-vs} = Coefficient considering non-linear effects applied to hogging

- $f_{nl-vs} = 0.5789\left(\frac{C_B+0.7}{C_B}\right)$

f_{nl-vh} = Coefficient considering non-linear effects applied to sagging

- $f_{nl-vh} = 1.0$

f_m = Distribution factor for wave VBM along the ship's length

- $f_m = \begin{cases} 0 & \text{for } x \leq 0 \\ 1.0 & \text{for } 0.4L \leq x \leq 0.65L \\ 0 & \text{for } x \geq L \end{cases}$

f_p = Probability factor

- $f_P = 1.0$

f_{vib} = Correction for the minimum contribution from hull girder vibration

- $f_{vib} = \begin{cases} 1.10 & \text{for } B \leq 28 \text{ m} \\ 1.20 & \text{for } B > 40 \text{ m} \end{cases}$

C_w = Wave coefficient

- $C_W = \begin{cases} 0.0856L & \text{for } L < 90 \text{ m} \\ 10.75 - \left(\frac{300-L}{100}\right)^{1.5} & \text{for } 90 \text{ m} \leq L \leq 300 \text{ m} \\ 10.75 & \text{for } 300 \text{ m} < L \leq 350 \text{ m} \\ 10.75 - \left(\frac{L-300}{100}\right)^{1.5} & \text{for } 350 \text{ m} < L \leq 500 \text{ m} \end{cases}$

C_B = Block coefficient

- $C_B = 0.75$

M_{sw} - Still-water vertical bending moment

$$M_{sw-h} = f_{sw}(171\, C_w\, L^2\, B\, (C_B + 0.7)\, 10^{-3} - M_{wv-h})\ [kNm] \tag{4}$$

$$M_{sw-s} = -0.85\, f_{sw}(171\, C_w\, L^2\, B\, (C_B + 0.7)\, 10^{-3} + M_{wv-s})\ [kNm] \tag{5}$$

Where:

f_{sw} = Distribution factor for still-water vertical bending moment along the ship's length

- $f_{sw} = \begin{cases} 0.0 & \text{for } x < 0 \text{ m} \\ 0.15 & \text{at } x = 0.1L \\ 1.0 & \text{for } 0.3L \leq x \leq 0.7L \\ 0.15 & \text{at } x = 0.9L \\ 0.0 & \text{for } x \geq L \end{cases}$

C_B = Block coefficient

C_w = Wave coefficient

M_{wv} = Wave vertical bending moment

M_{wv-LC} - Wave vertical bending moment under a specific load case

When $C_{WV} \geq 0$:

$$M_{wv-h-LC} = f_\beta\, C_{WV}\, M_{wv-h}\ [kNm] \tag{6}$$

When $C_{WV} < 0$:

$$M_{wv-s-LC} = f_\beta\, C_{WV}\, |M_{wv-s}|\ [kNm] \tag{7}$$

Where:

f_β = Heading correction factor

- $f_\beta = 1.0$

C_{WV} =Load combination factor for vertical bending moment

- See Table 5

M_{wv} = Wave vertical bending moment

4.4. VSF (Vertical Shear Force)

The VSF represents the internal force acting on the hull girder in the vertical direction. For the RoPax vessel, the importance of VSF magnitude is secondary to that of VBM among the hull girder load components. However, due to the reduced number of bulkheads and vertical supports in RoPax designs, certain deck edges and bulkhead adjacent regions may experience higher stress concentration caused by shear force. Therefore, structural details need to be carefully evaluated to ensure structural compliance with performance requirements.

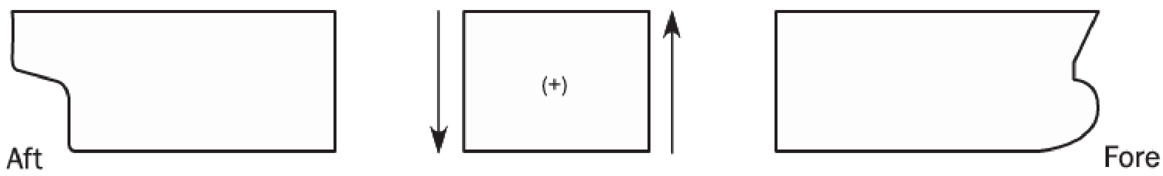

Figure 3: Vertical Shear Force (DNV, 2022)

The total VSF is a combination of still-water VSF and wave VSF in dynamic load cases. Noticing that shear force is a set of positive and negative forces. The application positions of positive force and opposing force are described in Ch.4 Sec.2 of DNV-RU-SHIP pt.3 (DNV, 2022).

$$Q_{tot} = Q_{sw} + Q_{wv-LC}[kN] \tag{8}$$

Where:

Q_{tot} = The total vertical shear force

Q_{sw} = The still-water vertical shear force

Q_{wv-LC} = The wave vertical shear force under a specific load case

Q_{sw} - Vertical still-water shear force

$$Q_{sw-pos} = \frac{5\, f_{qs}\, M_{sw}}{L}\ [kN] \tag{9}$$

$$Q_{sw-neg} = -\left(\frac{5\, f_{qs}\, M_{sw}}{L}\right)\ [kN] \tag{10}$$

Where:

f_{qs} = Distribution factor for still-water VSF along the ship's length

- $f_{qs} = \begin{cases} 0.0 & \text{for x} < 0 \text{ m} \\ 1.0 & \text{at } 0.15\text{L} \leq \text{x} \leq 0.3\text{L} \\ 0.8 & \text{for } 0.4\text{L} \leq \text{x} \leq 0.6\text{L} \\ 1.0 & \text{at } 0.7\text{L} \leq \text{x} \leq 0.85\text{L} \\ 0.0 & \text{for x} \geq \text{L} \end{cases}$

M_{sw} = Still-water vertical bending moment with $f_{sw} = 1$

Q_{wv} - Vertical wave shear force

$$Q_{wv-pos} = 0.52\, f_{q-pos}\, f_p\, C_w\, L\, B\, C_B\ [kN] \tag{11}$$

$$Q_{wv-neg} = -\left(0.52\, f_{q-neg}\, f_p\, C_w\, L\, B\, C_B\right)\ [kN] \tag{12}$$

Where:

f_{q-pos} = Distribution factor for positive wave vertical shear force along the ship's length

- $f_{q-pos} = \begin{cases} 0.0 & \text{for x} < 0 \text{ m} \\ 0.92\, f_{nl-vh} & \text{for } 0.2\text{L} \leq \text{x} \leq 0.3\text{L} \\ 0.7\, f_{nl-vs} & \text{for } 0.4\text{L} \leq \text{x} \leq 0.6\text{L} \\ 1.0\, f_{nl-vs} & \text{for } 0.7\text{L} \leq \text{x} \leq 0.85\text{L} \\ 0.0 & \text{for x} \geq \text{L} \end{cases}$

f_{q-neg} = Distribution factor for negative wave vertical shear force along the ship's length

- $f_{q-neg} = \begin{cases} 0.0 & \text{for x} < 0 \text{ m} \\ 0.92\, f_{nl-vs} & \text{for } 0.2\text{L} \leq \text{x} \leq 0.3\text{L} \\ 0.7\, f_{nl-vh} & \text{for } 0.4\text{L} \leq \text{x} \leq 0.6\text{L} \\ 1.0\, f_{nl-vh} & \text{for } 0.7\text{L} \leq \text{x} \leq 0.85\text{L} \\ 0.0 & \text{for x} \geq \text{L} \end{cases}$

f_p = Probability factor

- $f_p = 1.0$

C_w = Wave coefficient

C_B = Block coefficient

Q_{wv-LC} - Vertical wave shear force under a specific load case

When $C_{QW} \geq 0$:

$$Q_{wv-LC} = f_\beta\, C_{QW}\, Q_{wv-pos}\ [kN] \tag{13}$$

When $C_{QW} < 0$:

$$Q_{wv-LC} = f_\beta\, C_{QW}\, \left|Q_{wv-neg}\right|\ [kN] \tag{14}$$

Where:

f_β = Heading correction factor

C_{QW} =Load combination factor for vertical shear force

- See Table 6

Q_{wv} = Wave vertical shear force

4.5. HBM (Horizontal Bending Moment)

HBM describes the bending action of the hull girder within the horizontal plane. The deflections are induced by waves, since the still water generally does not cause any bending in the horizontal direction. Under sea-going conditions, HBM develops in response to BSR and OST load cases, resulting in lateral curvature of the vessel's longitudinal axis.

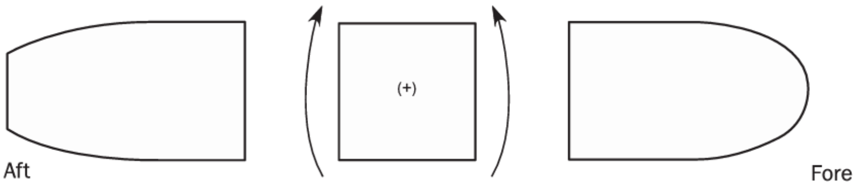

Figure 4: Horizontal Bending Moment (DNV, 2022)

The total HBM equals the HBM from dynamic load cases.

$$M_{bh-tot} = M_{wh-LC}\ [kNm] \tag{15}$$

Where:

M_{bh-tot} = The total horizontal bending moment

M_{wh-LC} = The wave horizontal bending moment under a specific load case

M_{wh} -Wave horizontal bending moment

$$M_{wh} = f_p \left(0.31 + \frac{L}{2800}\right) f_m\, C_w\, L^2\, T_{LC}\, C_B\ [kNm] \tag{16}$$

Where:

f_p = Probability factor

- $f_p = 1.0$

f_m = Distribution factor for wave vertical bending moment along the ship's length

C_w = Wave coefficient

C_B = Block coefficient

M_{wh}, Wave horizontal bending moment under a specific load case

$$M_{wh-LC} = f_\beta \, C_{WH} \, M_{wh} \; [kNm] \tag{17}$$

Where:

f_β = Heading correction factor

C_{WH} =Load combination factor for horizontal bending moment

- See Table 6

M_{wh} = Wave horizontal bending moment

4.6. TM (Torsion Moment)

The TM refers to the twisting action experienced by the hull girder about its longitudinal axis, primarily induced by asymmetric loading conditions or waves. According to DNV-RU-SHIP pt.3, only container ships need to consider the still-water torsion moments due to their open cross-section (DNV, 2022). In contrast, only the TM wave will be considered in the design process for the RoRax vessel. Among those wave headings, TM only generates under oblique or beam sea conditions, where wave crests and troughs create differential buoyancy on the port and starboard sides.

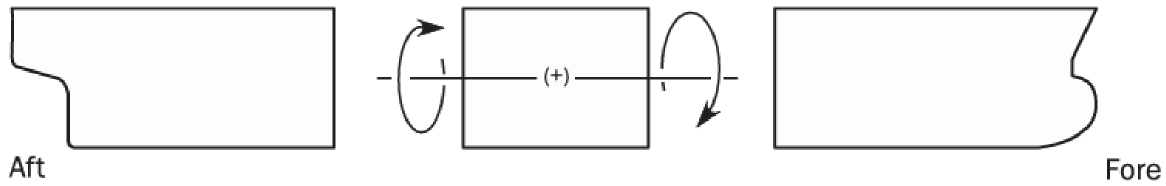

Figure 5: Torsional Moment (DNV, 2022)

Similar to HBM, the total TM consists of TM from dynamic load cases.

$$M_{t-tot} = M_{wt-LC} \; [kNm] \tag{18}$$

M_{wt} - Wave torsional moment

$$M_{wt} = f_p (M_{wt1} + M_{wt2}) \; [kNm] \tag{19}$$

Where:

$M_{wt1} = 0.4 \, f_{t1} \, C_w \sqrt{\frac{L}{T_{LC}}} \, B^2 \, D \, C_B$

$M_{wt2} = 0.22 \, f_{t2} \, C_w \, L \, B^2 \, C_B$

f_{t1} = Distribution factor = $\left|\sin\left(\frac{360x}{L}\right)\right|$

f_{t2} = Distribution factor = $\sin^2\left(\frac{180x}{L}\right)$

M_{wt-LC} - Wave torsional moment – dynamic load

$$M_{wt-LC} = f_{\beta}\, C_{WT}\, M_{wt}\ [kNm] \tag{20}$$

Where:

f_{β} = Heading correction factor

C_{WT} =Load combination factor for torsion moment

- See Table 7

M_{wt} = Wave torsion moment

4.7. Hull girder load result

In the structural analysis of the ship deck system, the VBM is recognized as the dominant load effect. Under loads from the vertical direction, the hull experiences large deflection at the midship regions, which in turn induces tensile and compressive stresses in longitudinal members. Therefore, the VBM plays a decisive role in determining the structural hull strength.

In contrast, the influence of the HBM is localized, and it is limited by the width of the ship. It results in comparatively lower stress on deck structures. For RoPax vessels, the torsional response is also moderate since the hull cross-section is closed. According to the classical thin-walled beam torsion theory, known as Saint-Venant torsion, a closed cross-section develops a continuous shear flow. It thus exhibits a much higher torsional stiffness than open-deck cross-sections. This conclusion is also supported by DNV's rule-based formulations. For container ships with large deck openings, the rules explicitly require the calculation and control of the still-water TM. In contrast, for most ship types with closed-deck structures, the still-water TM is typically not explicitly evaluated (DNV, 2022).

Consequently, VBM is regarded as the primary governing load effect, with HBM and TM treated as secondary load components. Their importance lies primarily in evaluating specific structural details, such as wide deck openings for vehicle entry rather than car-carrying decks.

Accordingly, the present study will focus on the HSM load case, which yields the largest VBM. In hull bending, sagging and hogging can lead to different critical failure modes. In a sagging condition, compressive stress primarily promotes buckling of the deck plates and stiffeners. This case is of critical interest because the midship region under sagging conditions deforms further under the self-weight of loaded vehicles.

In summary, the present study focuses on the target hull girder load associated with load case HSM-1. This load case is considered particularly relevant because it induces the maximum compressive stress in the deck structure, thereby increasing the likelihood of buckling. The detailed implementation of the corresponding loads in the FE model will be described in Section 7.6.1 and Section 7.6.2.

At the end of this section, the calculated magnitudes of moments and forces (calculated according to the formulas given in Section 4.3 to Section 4.7) will be presented in Table 10.

Table 10: Calculated loads for buckling assessment

	VBM [kNm]	**VSF** [kN]		**HBM** [kNm]	**TM** [kNm]
		Positive	Negative		
HSM-1	-2 794 912	40 860	-40 860	0	0
HSM-2	2 952 944	40 860	-40 860	0	0
BSR-1P	-1 047 465	25 412	-25 412	-65 034	0
BSR-2P	1 391 617	25 412	-25 412	65 034	0
BSR-1S	1 047 465	-25 412	25 412	65 034	0
BSR-2S	-1 391 617	-25 412	25 412	-65 034	0
OST-1P	-1 845 212	33 136	-33 136	-812 919	-172 687
OST-2P	2 104 397	33 136	-33 136	812 919	172 687
OST-1S	1 845 212	-33 136	33 136	812 919	172 687
OST-2S	-2 104 397	-33 136	33 136	-812 919	-172 687

5. Local loads

In the context of ship structural analysis, local loads generally refer to combinations of external, internal, distributed, heavy-unit, and wheel loads, see Table 11.

Table 11: Local load components for strength assessment (DNV, 2021b)

<table>
<tr><td colspan="3" rowspan="4"></td><td colspan="7">Design load scenario</td></tr>
<tr><td>1</td><td>2</td><td>3</td><td>4</td><td>5</td><td>6</td><td>7</td></tr>
<tr><td>Normal operations at harbor and sheltered water</td><td>Normal operation at sea</td><td>Flow through ballast water exchange</td><td>Overfilling of ballast tanks and tank testing</td><td>Flooding</td><td>Special operation still-water</td><td>Special operations at sea</td></tr>
<tr><td>Static (S)</td><td>Static+ Dynamic (S + D)</td><td>Static+ Dynamic (S + D)</td><td>Accidental (A) and Testing (T)</td><td>Accidental (A)</td><td>Static (S)</td><td>Static+ Dynamic (S + D)</td></tr>
<tr><td rowspan="9">Local loads</td><td rowspan="4">P_{ex}</td><td>Exposed decks</td><td>-</td><td>P_D</td><td>-</td><td>-</td><td>-</td><td>P_S</td><td>$P_S + P_W$</td></tr>
<tr><td>External shell</td><td>P_S</td><td>$P_S + P_W$</td><td>$P_S + P_W$</td><td>P_S</td><td>-</td><td>P_S</td><td>$P_S + P_W$</td></tr>
<tr><td>Superstructure sides</td><td>-</td><td>$\max(P_W; P_{SI})$</td><td>-</td><td>-</td><td>-</td><td>P_S</td><td>$P_S + P_W$</td></tr>
<tr><td>Superstructure end bulkheads and deckhouse walls</td><td>-</td><td>P_A</td><td>-</td><td>-</td><td>-</td><td>P_S</td><td>$P_S + P_W$</td></tr>
<tr><td rowspan="5">P_{in}</td><td>Boundaries of water ballast tanks</td><td rowspan="2">P_{ls-3}</td><td rowspan="2">$P_{ls-1} + P_{lD}$</td><td>$P_{ls-2} + P_{lD}$</td><td>$\max(P_{ls-4}, P_{ls-ST})$</td><td>-</td><td>$P_{ls-3}$</td><td>$P_{ls-1} + P_{lD}$</td></tr>
<tr><td>Boundaries of tanks other than water ballast tanks</td><td>-</td><td>P_{ls-ST}</td><td>-</td><td>P_{ls-3}</td><td>$P_{ls-1} + P_{lD}$</td></tr>
<tr><td>Watertight boundaries</td><td>-</td><td>-</td><td>-</td><td>-</td><td>P_{fs}</td><td>-</td><td>-</td></tr>
<tr><td>Boundaries of bulk cargo holds</td><td>P_{bs}</td><td>$P_{bs} + P_{bd}$</td><td>-</td><td>-</td><td>-</td><td>-</td><td>-</td></tr>
<tr><td>Internal structures in</td><td>P_{int}</td><td>-</td><td>-</td><td>-</td><td>-</td><td>-</td><td>-</td></tr>
</table>

		tanks								
	P_{dl}	Exposed decks and non-exposed decks and platforms	P_{dl-s}	$P_{dl-s} + P_{dl-d}$	-	-	-	P_{dl-s}	$P_{dl-s} + P_{dl-d}$
	F_U	Heavy units on internal and external decks	F_U	$F_{U-s} + F_{U-d}$	-	-	-	F_U	$F_{U-s} + F_{U-d}$
	P_{wl}	Decks and hatch covers/RoRo equipment	P_{wl-1}	P_{wl-2}	-	-	-	-	-

□-Load cases directly relevant to the analysis of the deck structure

□- Load cases of secondary relevance

However, not all these categories are directly relevant to the structural assessment of car-carrying decks.

- **External loads**

  It includes green sea pressures, hydrostatic and hydrodynamic pressure, acting on the shell plating, and load from the weight of superstructures on exposed decks. Since the present study will focus on the deck structures, namely Deck 3 & 5 (which are internal decks), external loads will not be involved.

- **Internal loads**

  It primarily refers to the pressures exerted by liquids carried in onboard tanks. While significant for tank top structures and certain lower decks, such loads are irrelevant to the inner vehicle decks under investigation in this work.

- **Distributed loads**

  It is an idealized representation of densely arranged point loads, often employed in the design of passenger decks or storage areas.

- **Heavy unit loads**

  In contrast to distributed loads, it intends to model the impact of a large, concentrated cargo item. For example, containers that are carried on a container ship.

- **Wheel loads**

  It is a specific category of concentrated load representing the contract forces between the vehicle wheel and the top plate of the decks. For RoPax vessels, where vehicle transport is a primary operational function, wheel loads are particularly relevant.

In summary, for deck analysis of RoPax vessels, only distributed loads and wheel loads are of practical significance. According to recommendations from engineering experts at Stena, refined FE models of vehicle decks should explicitly represent vehicles using wheel loads to capture the highly concentrated stresses and deflections in the deck panels.

In this case, the wheel load is combined with the hull girder loads to obtain the overall stress level in the decks. Referring to the conclusions in Section 4.7, compressive stress due to hull girder loads may trigger buckling. The additional compressive stress induced by wheel load further increases the likelihood of buckling.

For the buckling assessment in this study, the deck response under combined hull girder loads and wheel loads is compared with the response under pure hull girder loading (without wheel loads) in order to demonstrate the influence of the local wheel loads (Section 9).

6. Calculation of local loads

When evaluating local loads on the car-carrying decks of RoPax vessels, the formulation should focus on two interrelated components: the vertical envelope acceleration under sea-going conditions and the wheel loads induced by vehicles. Since the magnitude of wheel loads is directly affected by the vertical acceleration acting on the vessel, the derivation of vertical envelope acceleration will be presented first. According to the governing formulations, the vertical acceleration varies with location on the ship. For simplicity, the vertical envelope acceleration is taken to be the maximum possible value. It should be noted that this simplification should be regarded as a conservative assumption and may lead to some overestimation of the wheel loads. But the calculated wheel loads, taking into account vertical envelope acceleration, shall provide a more realistic representation of operational loading scenarios.

6.1. Vertical envelope acceleration

The evaluation of vertical envelope acceleration is carried out through several steps.

1. Identify related ship motions that are related to vertical acceleration.
2. Use formulas to calculate the magnitude of acceleration associated with each type of motion.
3. An appropriate directional coefficient shall be applied to acceleration components to extract their magnitude in the vertical direction.
4. Calculate the total vertical envelope acceleration as the combined acceleration of them.

The formulas for estimating ship motion and calculating accelerations are also covered in DNV-RU-SHIP pt.3 (DNV, 2022).

6.1.1. Ship motion

The visualized figure of ship motions and direction is shown in Figure 6. Motions related to vertical acceleration are heave, pitch, and roll.

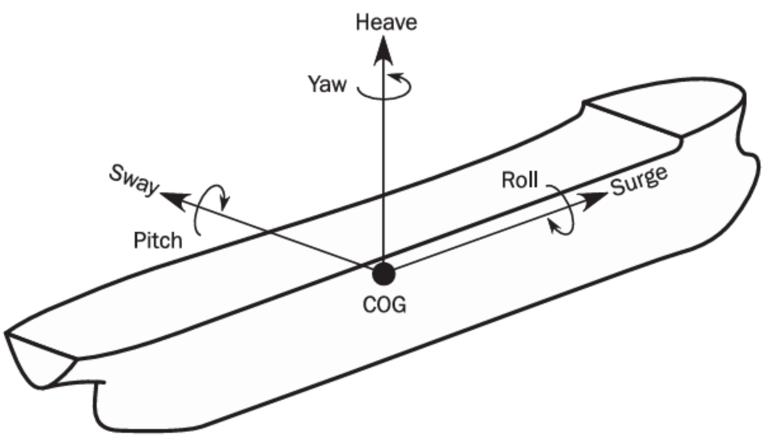

Figure 6: Visualized ship motion (DNV, 2022)

Heave acceleration can be obtained directly with a formula, shown in Section 6.1.2, thereby eliminating the necessity to determine the heave motion.

T_θ - Roll period

$$T_\theta = \frac{2.3\pi k_r}{\sqrt{g\ GM}}\ [seconds] \tag{21}$$

Where:

k_r = Radius of gyration = $0.39B$

GM = Metacentric height = $0.07B$

θ - Roll angle, in degrees (angle unit)

$$\theta = \frac{9000(1.4 - 0.035T_\theta)f_p f_{BK}}{(1.15\ B + 55)\pi}\ [°(degree)] \tag{22}$$

Where:

f_p = Probability factor

$$f_{BK} = \text{Bilge keel factor} = \begin{cases} 1.0 & \text{for ship with bilge keel} \\ 1.2 & \text{for ship without bilge keel} \end{cases}$$

T_φ – Pitch period

$$T_\varphi = \sqrt{\frac{2\pi\lambda_\varphi}{g}}\ [seconds] \tag{23}$$

Where:

$\lambda_\varphi = 0.6(1 + f_T)L$

φ – Pitch angle

$$\varphi = 920\ f_p\ L^{-0.84}\left\{1.0 + \left(\frac{2.57}{\sqrt{gL}}\right)^{1.2}\right\}\ [°(degree)] \tag{24}$$

Where:

f_p = Probability factor

6.1.2. Motion accelerations

It should be noted that these formulas are strictly valid only for vessels with a length equal to or longer than 150 m, which corresponds to the typical dimensional range of modern RoPax vessels. For ships of shorter length, the calculation of heave acceleration shall follow the other formulations prescribed in DNV-RU-SHIP pt.3 (DNV, 2022).

a_{heave} – heave acceleration

$$a_{heave} = \left(1.15 - \frac{6.5}{\sqrt{gL}}\right) f_p a_0 g \left[\frac{m}{s^2}\right] \tag{25}$$

Where:

f_p = Probability factor

a_0 = Acceleration parameter = $(1.58 - 0.47C_B)\left(\frac{2.4}{\sqrt{L}} + \frac{34}{L} - \frac{600}{L^2}\right)$

a_{roll} – roll acceleration

$$a_{roll} = f_p \theta \frac{\pi}{180}\left(\frac{2\pi}{T_\theta}\right)^2 \left[\frac{m}{s^2}\right] \tag{26}$$

Where:

f_p = Probability factor

θ = Roll angle

T_θ = Roll period

a_{pitch} – pitch acceleration

$$a_{pitch} = f_p \left(1.75 - \frac{22}{\sqrt{gL}}\right) \varphi \frac{\pi}{180}\left(\frac{2\pi}{T_\varphi}\right)^2 \left[\frac{m}{s^2}\right] \tag{27}$$

Where:

f_p = Probability factor

φ = Pitch angle

T_φ = Pitch period

6.1.3. Vertical envelope accelerations

Since heave motion acts in the vertical direction, its contribution to the vertical envelope acceleration can be taken directly without further transformation. In contrast, the vertical components of pitch and roll motions depend on the position along the vessel's length. (x) and breadth (y). These coordinates vary along the ship's geometry. Accordingly, the vertical acceleration components due to pitch and roll are calculated as follows:

$$a_{pitch-z} = a_{pitch}(1.08x - 0.45L)\left[\frac{m}{s^2}\right] \tag{28}$$

$$a_{roll-z} = a_{roll}\, y \left[\frac{m}{s^2}\right] \tag{29}$$

Thereby, the vertical envelope acceleration, a_z, can be calculated.

$$a_z = \sqrt{a_{heave}^2 + \left[\left(0.95 + e^{-\frac{L}{15}}\right)a_{pitch-z}\right]^2 + (1.2a_{roll-z})^2}\left[\frac{m}{s^2}\right] \tag{30}$$

Where:

a_{heave} = Heave acceleration

$a_{pitch-z}$ = Vertical component of pitch acceleration at a given position

a_{roll-z} = Vertical component of roll acceleration at a given position

6.1.4. Vertical envelope accelerations result

Accelerations	Magnitude	Unit
a_{heave}	3.08	$[m/s^2]$
$a_{pitch-z}$	0.78	$[m/s^2]$
a_{roll-z}	1.08	$[m/s^2]$
a_z	4.03	$[m/s^2]$

6.2. Wheel loads

The wheel load acting on the deck structure is calculated according to the formula below:

$$P_{wl} = \frac{Q}{n_0 a_1 b_1}(g + a_z)10^6 \left[\frac{kN}{m^2}\right] \tag{31}$$

Where:

Q = Axle load $[ton]$

n_0 = Number of load areas on the axle

a_1 and b_1 = Length and width of the tire-deck contact patch

a_z = Vertical envelope acceleration $\left[\frac{m}{s^2}\right]$, calculated according to the procedure described in Section 6.1.3

Parameters a_1 and b_1 define the effective footprint of the tire on the deck surface. For RoPax vessels, cargo typically consists of double-wheel trailers or smaller passenger vehicles. In the context of structural analysis, the wheel load induced by double-wheel trailers is taken as the reference and the upper limit of the design load. It ensures a conservative representation of service conditions. The schematic of a double wheel trailer's footprint is provided in Figure 7.

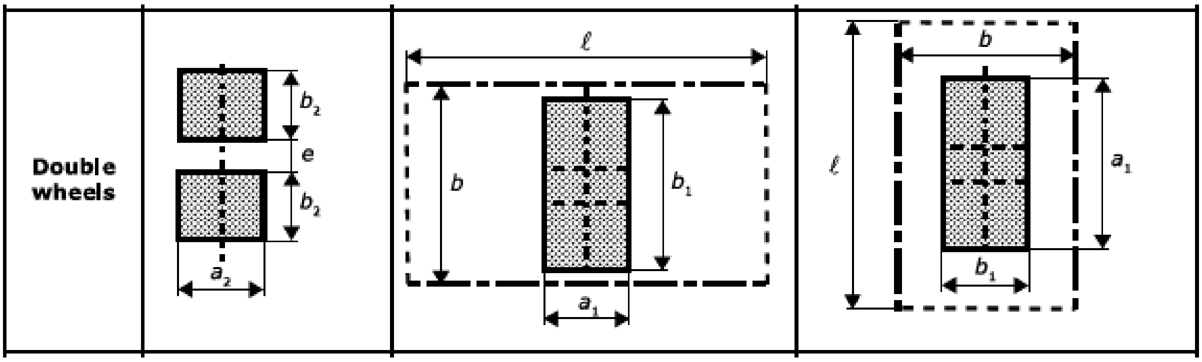

Figure 7: Visualization of vehicle footprint (DNV, 2022)

DNV-RU-SHIP pt.3 provides no references to tire footprints or spacing (DNV, 2022). Therefore, practical data from shipyards or vessel operators should be employed. In the present study, reference values were obtained in accordance with the Stena expert's recommendation (Stena, personal communication, August 2025). Specifically, the MAFI 40'/60 t trailer is recommended as the reference wheel load for Deck 3, while the MAFI 40'/40 t trailer is applied for Deck 5.

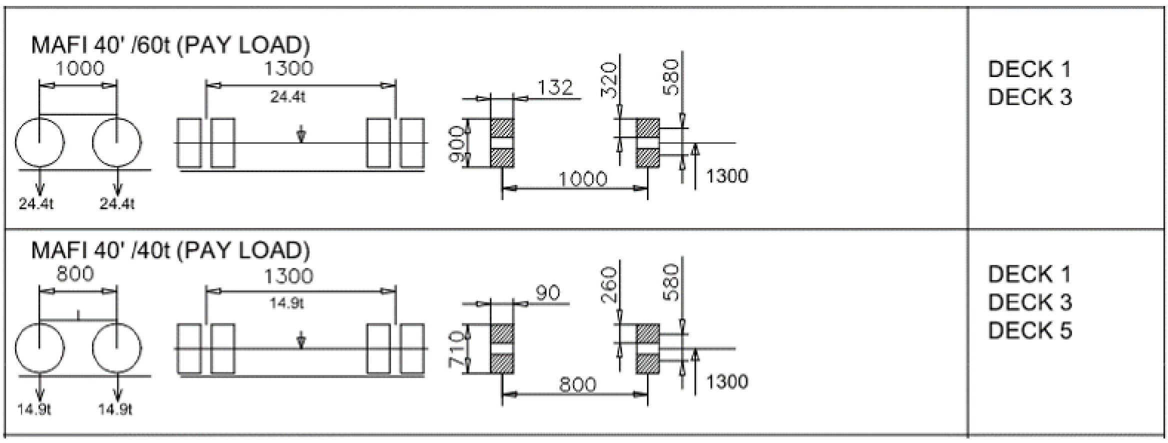

Figure 8: Recommended footprint data

6.3. Data justification

The wheel-load data used in this thesis is based on operational data provided by Stena for typical MAFI trailers on Decks 3 and 5. To evaluate the reliability of these values, the given payloads and wheel configurations have been compared with publicly available data of similar trailers. Manufacturer data for 40 ft MAFI-type trailers indicate payload capacities up to 70 tonnes, carried on multi-axle bogies with twin wheels, resulting in wheel loads of a similar order of magnitude to those adopted in this study (MAFI Transport-Systeme GmbH, n.d.).

Furthermore, the tire arrangement provided by Stena's engineering experts has been checked against the typical tire footprint given in DNV's vehicle-deck design rules. The patterns are consistent with the arrangement of the contact patch between the wheel and the top deck in Ch.10 of DNV-RU-SHIP pt.3 (as shown in Figure 7 and Figure 8), confirming that the expert's data closely aligns with DNV regulations (DNV, 2022).

From a structural point of view, the assumed vehicle distributions on Deck 3 and Deck 5 are also considered reasonable. Deck 3 is located closer to the bottom of the hull and is directly supported by more continuous longitudinal and transverse structural members, including bulkheads and girders. It is therefore structurally more efficient to allocate heavier vehicles with higher axle loads to Deck 3. In contrast, Deck 5 is mainly supported by pillars and has fewer continuous supporting members beneath it, making it better suited to carrying lighter vehicle types with lower axle loads.

Consequently, these data are considered reasonable for calculating wheel load. The calculated wheel load is given in Section 6.4.

6.4. Local load result

According to the methodology described in Section 6.2, the wheel load magnitudes for Decks 3 and 5 have been calculated and summarized in Table 12.

Table 12: Wheel load – deck 3

MAFI 40'/60t		Wheel load deck 3		
Parameters	**Value**	**Symbol**	**Value**	**Unit**
Q	24.4	P_{wl}	1421.326	$\left[\frac{kN}{m^2}\right]$
n_0	2			
a_1	132			
b_1	900			

Table 13: Wheel load – deck 5

MAFI 40'/40t		Wheel load deck 5		
Parameters	**Value**	**Symbol**	**Value**	**Unit**
Q	14.9	P_{wl}	1613.637	$\left[\frac{kN}{m^2}\right]$
n_0	2			
a_1	90			
b_1	710			

7. Global model

To conduct reliable structural and mechanical analysis, it is essential to establish a numerical representation of the deck structure in a computational environment. In the present study, the FE software ANSYS was employed, with the modeling approach and evaluation procedures developed in accordance with the design principles specified by DNV-RU-SHIP pt.3 (DNV, 2022). In addition to the Rules for classification, DNV-CG-0127 (DNV, 2021a) and DNV-CG-0128 (DNV, 2021b)were incorporated to account for the unique structural characteristics of RoPax vessels.

To ensure computational efficiency without compromising compliance with DNV requirements, the FE model was limited to the vessel's central part, a methodology commonly referred to as midship cargo hold analysis (DNV, 2021a) . In this approach, only the midship section (approximately 0.3L to 0.7L of the vessel's overall length) will be modeled.

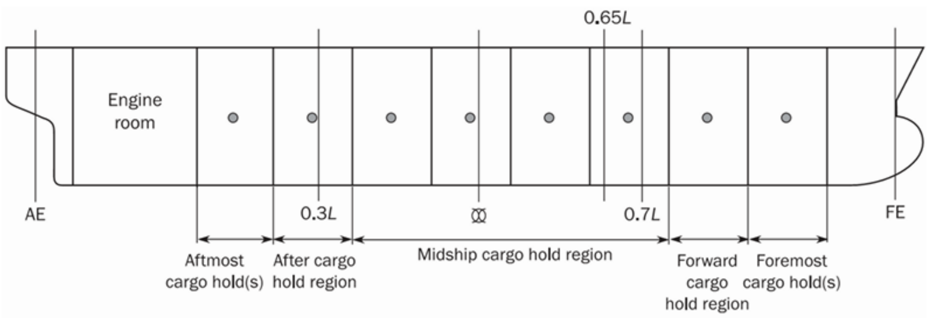

Figure 9: Cargo hold regions (DNV, 2021a)

This modeling scope is justified since the hull girder loads and structural responses in the midship region are usually representative of the vessel's most critical longitudinal bending and shear conditions. Another practical reason is the lack of a complete structural drawing for the vessel. Therefore, the mid-section model of the ship in this study will be based on the typical cross-section of the reference ship.

7.1. Reference ship dimensions

Table 14: Main dimensions of the reference ship model

Symbol	Value	Description
L	$212[m]$	Vessel length
B	$26.7[m]$	Vessel width
D	$21.5[m]$	Vessel depth

T_{sc}	$6.3[m]$	Scantling draught

In addition to the main dimensions, the detailed local structural dimensions are based on the drawing of the reference vessel. These drawings provide the geometric references needed to build FE models. Structural details, such as plate thickness, stiffener spacing, stiffener scantling, et.c., are given in the drawing.

7.2. Reference global coordinate system

To ensure consistent interpretation of loading directions and displacement results during simulation, the model adopts the vessel's global coordinate system as defined by (DNV, 2022). This standardization is essential for aligning the calculated hull girder loads with the FE model boundary conditions and for ensuring compatibility with classification society assessment procedures. The vessel's global coordinate follows DNV's instructions.

In addition, the reference global coordinate system is of great importance for implementing sub-modeling in ANSYS. In this approach, nodal displacements from the main model are transferred to the cut boundaries of the sub-model and used as boundary conditions. A consistent coordinate definition is consequently required to ensure that the transferred displacements are applied with the correct magnitude and direction. A more detailed description of this procedure is provided in Section 8.1.

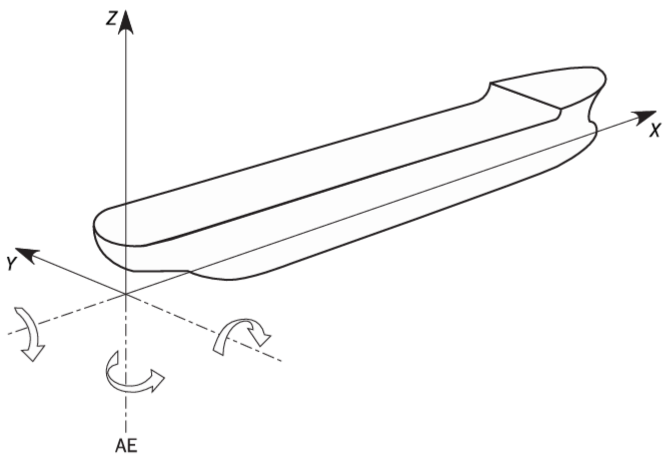

Figure 10: Reference coordinate system (DNV, 2022)

7.3. Modeling of global model

In the present study, the global model refers to midship cargo hold regions as described at the beginning of Section 7. The midship cargo hold model of the RoPax vessel was developed in ANSYS SpaceClaim. The model geometry includes all primary structural members, such as decks, longitudinal/transversal/vertical girders, bulkheads, and longitudinal stiffeners. Photographic and rendering views of the current model are presented in this section for visual reference.

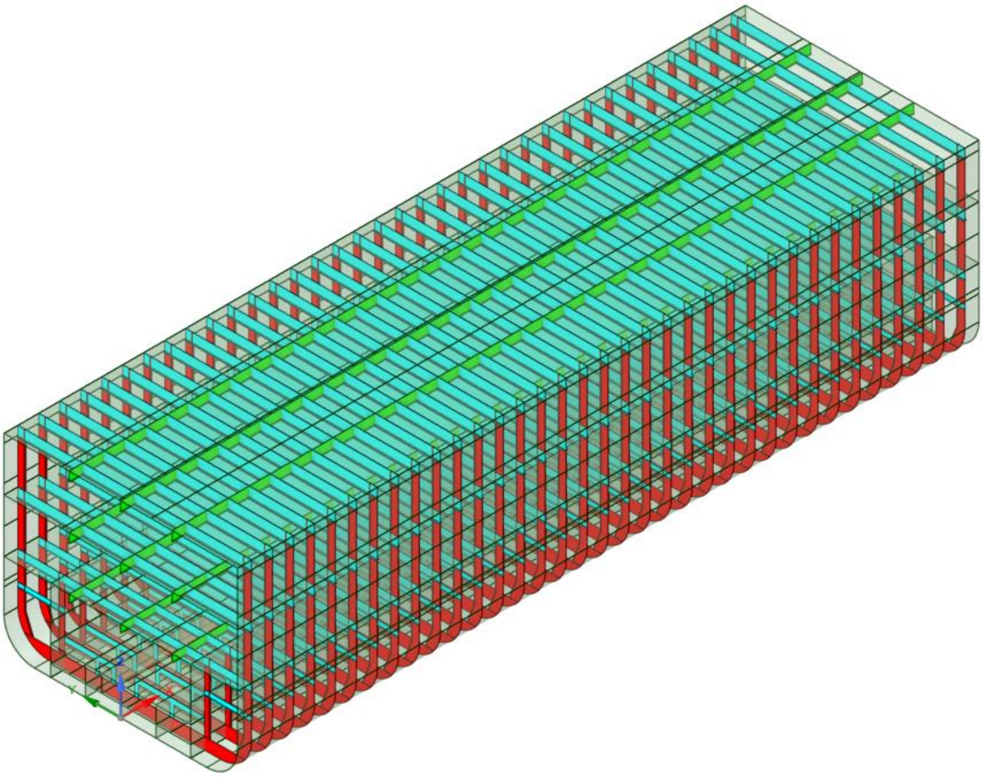

Figure 11: Midship cargo hold model with hidden stiffeners

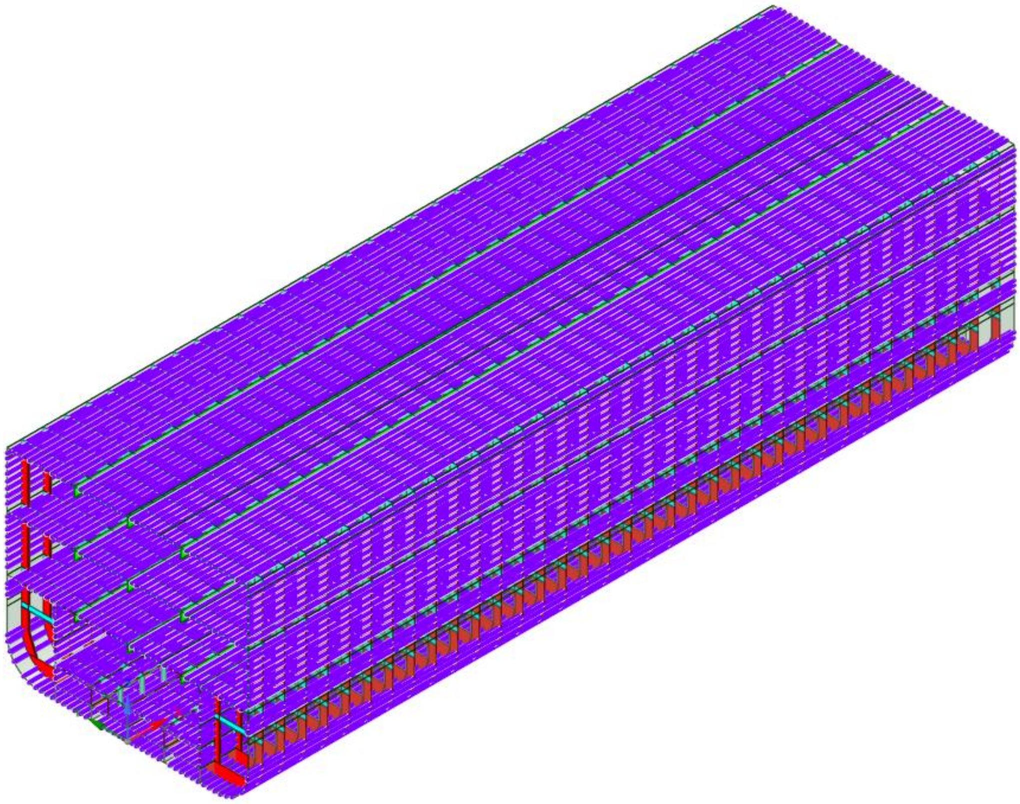

Figure 12: Midship cargo hold model with visible stiffeners

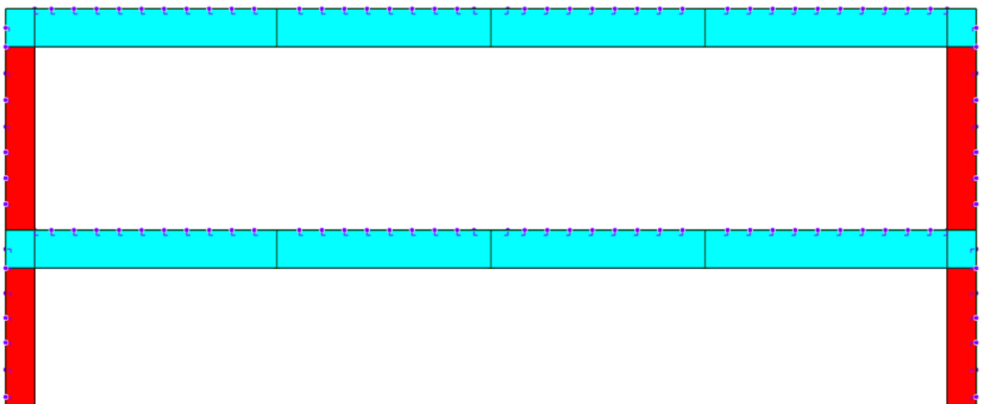

Figure 13: Midship cargo hold model - front view

To optimize computational efficiency, the smaller longitudinal stiffeners are represented using beam elements rather than shell elements (DNV, 2021a). The use of the shell–beam mixed model is a common modeling approach in FEA, since these stiffeners have relatively small cross-sectional areas compared with other structural elements.

7.4. Mesh size of global model

In accordance with DNV's recommendations (DNV, 2021a), the mesh size of the midship cargo hold FE model shall be defined by the spacing of longitudinal stiffeners, where the spacing is represented by the variable $'s'$. A $s \times s$ element size is therefore applied to balance computational efficiency with the need for structural detail accuracy. This approach ensures that the mesh can correctly capture stress distributions in plating and primary members.

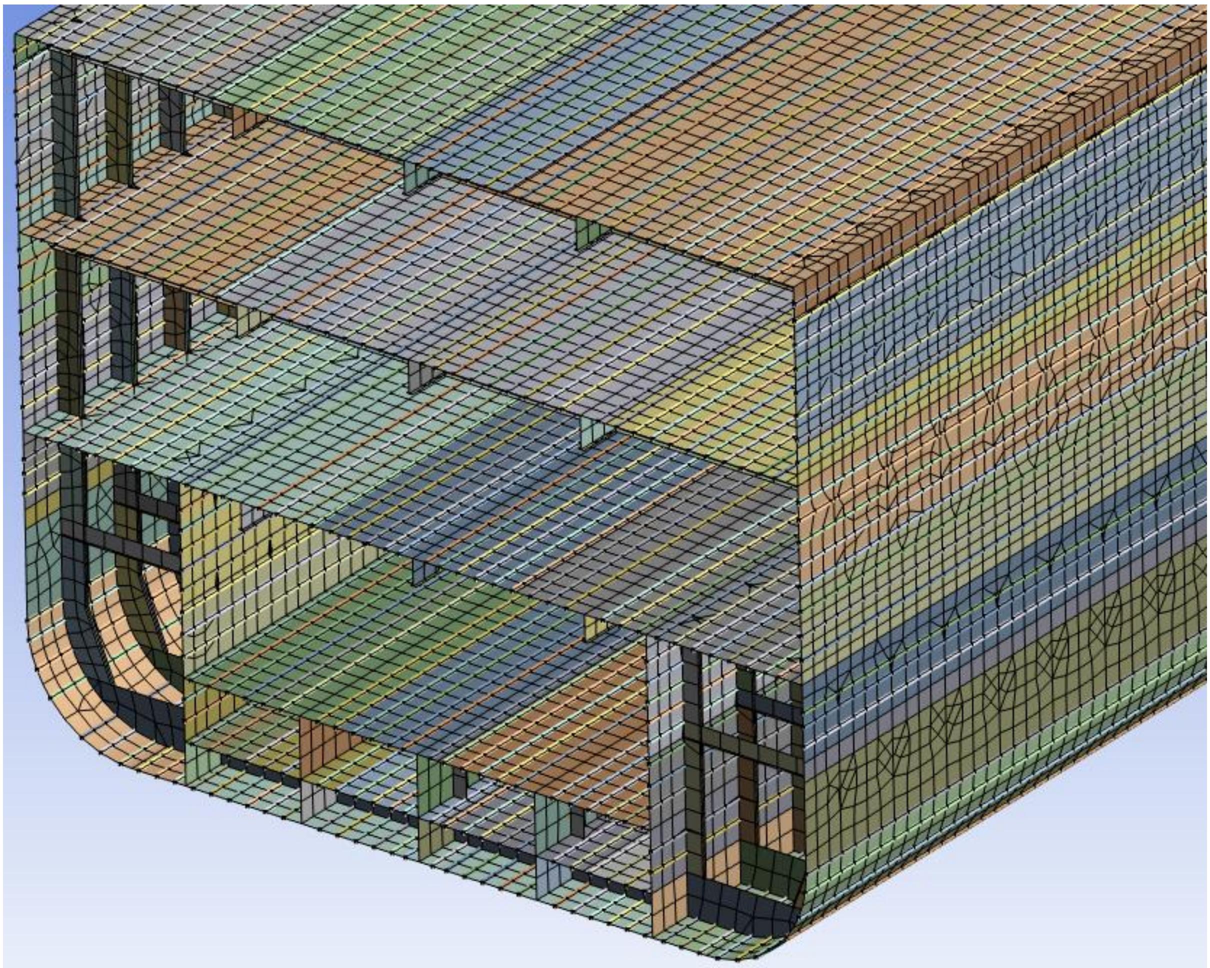

Figure 14: Mesh of cargo hold model (620mm)

7.5. Boundary conditions of the cargo hold model

The midship cargo hold model shall be supported at the ends to provide constraint of the model and support of the unbalanced force (DNV, 2022). The applicable boundary condition is specified in DNV-CG-0127, see Table 15 (DNV, 2021a). In cases where TM is present, it shall be applied to an independent point located at the fore end of the vessel model. Conversely, if TM does not exist, the rotation DoF (degree of freedom) around the x-axis shall be constrained as *Free*.

Table 15: Boundary condition for midship cargo hold model (DNV, 2022)

		Displacement			Rotation		
		δ_x	δ_y	δ_z	θ_x	θ_y	θ_z
Fore end	Independent Point	-	fix	fix	TM adjustment/Free	-	-
	Cross section	-	Rigid	Rigid	Rigid	-	-
Aft end	Independent Point	-	fix	fix	fix	-	-
	Cross section	-	Rigid	Rigid	Rigid	-	-
	Centerline inner bottom Point	fix	-	-	-	-	-
Reversed boundary conditions at the fore and aft ends are permitted							

7.5.1. Independent point

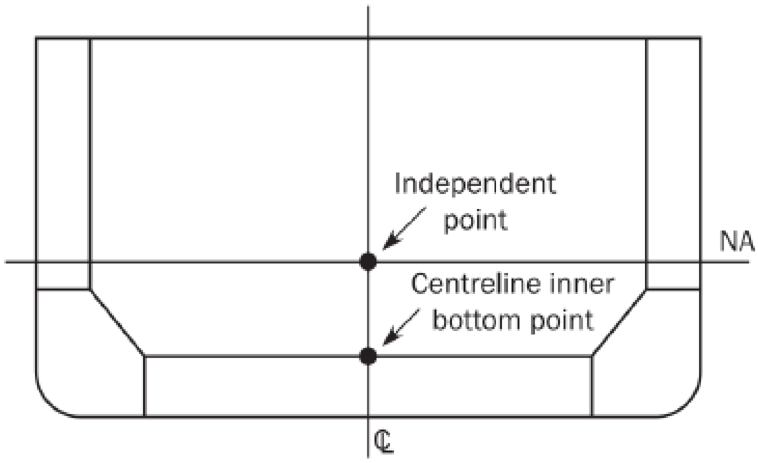

Figure 15: Independent point and centerline inner bottom point (DNV, 2021a)

According to requirements outlined in DNV-CG-0127 (DNV, 2021a), the independent point is expected to be positioned at the neutral axis of the ship section. Within ANSYS Mechanical, this point is implemented as a remote point using the MPC (Multi-Point Constraint) formulation. The location of the MPC point is therefore defined according to the position of the neutral axis of the corresponding boundary section.

However, it is essential to note the limitations of ship models using shell elements, in which the cross-section is represented only by edges. In such a case, the software does not take plate thickness into account when evaluating the neutral axis. To overcome this limitation, the section must be processed and converted into a geometry that includes the surfaces as a boundary section, with defined areas and thicknesses. In the present study, the boundary cross-sections used for analysis were therefore prepared with thickness-inclusive geometry. After this preparation, the coordinates of the MPC point can be determined from the calculated NA position, as shown in Figure 16.

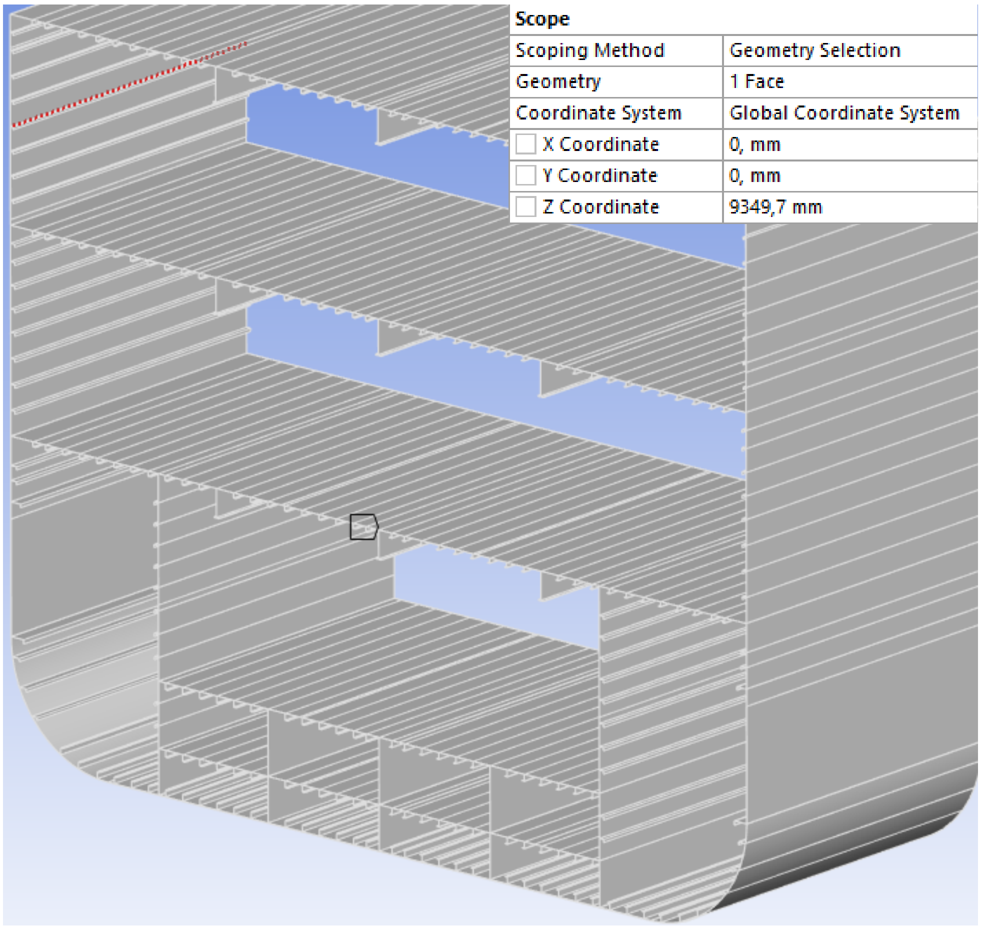

Figure 16: Boundary section modeled as a solid element & coordinate of the neutral axis

Subsequently, in the Geometry setting, the corresponding boundary section can be selected so it can be controlled by the remote point. The selection will establish the constraint relationship between the remote point and the selected section. According to Table 15, the remote point should be coupled to the boundary edges, and the connection behavior should be set to be rigid. This coupling ensures that any displacement or rotation at the remote point will be transferred to the selected cross-section, thereby providing the kinematic response. This implementation is used in the present study for both end sections of the midship cargo hold model.

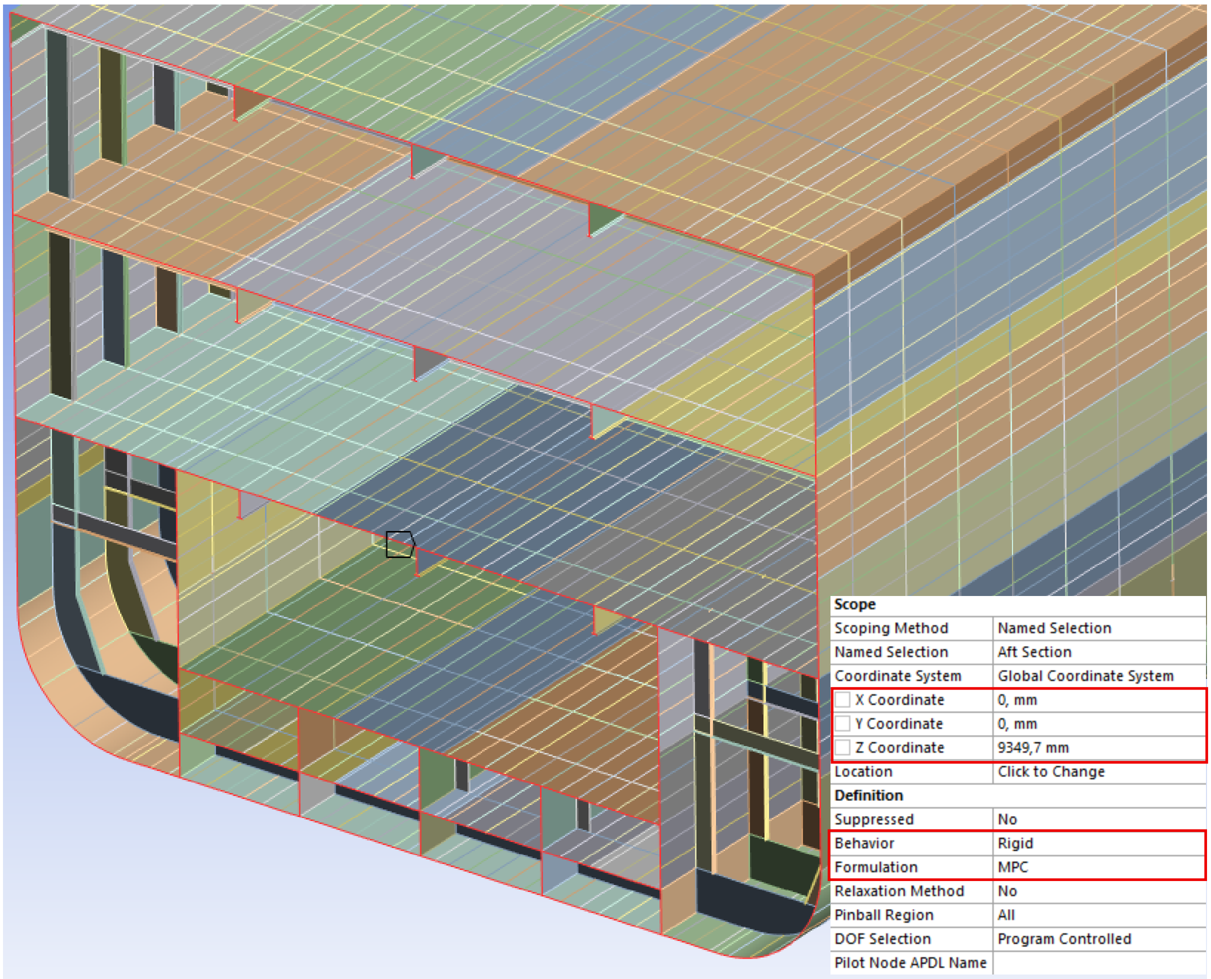

Figure 17: Edges connected to the remote point and connection behavior

What should also be mentioned is how the positions of the remote points are defined. Within the context of midship cargo hold analysis, one point is located at the aft boundary section, and the other one is located at the fore boundary section. Hence, the remote point at the aft has its x-coordinate equal to zero, which corresponds to the aft section located at $0.3L$ of the vessel. For the other one, its x-coordinate corresponds to $0.7L$, so its x-coordinate shall be adjusted to $(0.7 - 0.3)L = 0.4L$.

7.5.2. Centerline inner bottom point

The centerline inner bottom point refers to the intersection between the vessel's vertical centerline and the tank top (see Figure 18). It constrains the section of the aft end's movement along the x-axis. Consequently, the boundary condition creates a situation that is similar to a simply supported beam, which is a reasonable setup for analyzing the ship's structural behavior since it is treated as a hollow beam.

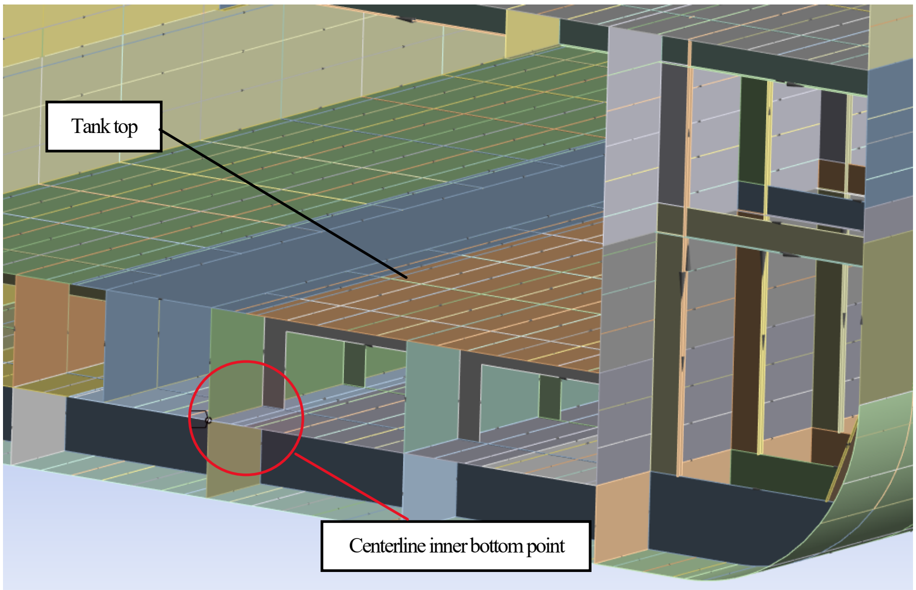

Figure 18: Centerline inner bottom point

7.6. Hull girder load application

In a strict rule-based FE analysis procedure, the hull girder load shall not be applied directly as an isolated load (DNV, 2021a). Instead, a complete loading condition should first be established by applying the relevant local loads, including structural weight, cargo or ballast loads, hydrostatic pressure, wave pressure, and other rule-defined pressure components as mentioned in report by Jang and Kim (2025) (Jang & Kim, 2025) with respect to DNV-CG-0127 (DNV, 2021a). The resultant hull girder loads from these local loads are then compared with the target hull girder loads calculated in Section 4, and additional load adjustments are made until the required target values are met. This procedure ensures consistency between the local load distribution and the global hull girder response.

However, the present study lacks access to sufficiently detailed loading information, such as the complete cargo, ballast, lightweight, and pressure distributions required to construct a fully rule-compliant load case. Therefore, instead of reproducing the full DNV load-generation and load-adjustment process, the target hull girder loads calculated in Section 4 are applied directly to the FE model. Although this approach does not strictly follow the complete DNV rule-based loading procedure, it remains mechanically meaningful for the purpose of this study. The main objective is to investigate the buckling behavior of the deck structure under a representative global hull girder loading condition, rather than to perform a full classification-rule approval analysis. By directly applying the target VBM and VSF, the FE model can still reproduce the critical global compressive stress state in the deck region, which is the primary loading condition governing the buckling response considered in this thesis.

Based on this simplification and the focused load case HSM-1 in this study, the loading scenario shall produce the most critical compressive stress in the deck structure and is therefore suitable for observing deck buckling behavior. The vertical bending moment (VBM) was applied using beam theory, with prescribed bending moments at the aft and fore remote points. Meanwhile, the vertical shear force (VSF) was represented by introducing additional bending moments about the global Y-axis at the same boundary locations, following the load transformation concept described in DNV-CG-0127 (DNV, 2021a). The detailed implementation of the VSF and VBM in the FE model is presented in Section 7.6.1 and Section 7.6.2, respectively.

7.6.1. Vertical Shear Force applications

Due to the boundary condition, the VSF cannot be applied as concentrated forces at the aft and fore remote points. If concentrated vertical forces were directly applied at the remote points, the load would be balanced by the boundary constraints, and the intended internal shear force distribution would not be properly generated. Therefore, the VSF needs to be introduced as a distributed load along the model length. The same principle was adopted in this study, with further simplification based on the actual extent and loading conditions of the RoPax midship FE model.

Based on the above considerations, the VSF in the present study was applied using an equivalent shear force adjustment method. In DNV-CG-0127, two methods are presented for adjusting vertical shear forces (DNV, 2021a). Method 1 is used when the VSF needs to be adjusted to the target value at only one boundary section of the cargo hold model under consideration. However, in the present study, the target VSF needs to be satisfied at both the aft and fore sections of the midship model. Therefore, Method 2, namely the vertical shear force adjustment method at both bulkheads, was applied as the main reference.

In the original Method 2 procedure, the adjustment is divided into two steps. First, a pair of additional vertical bending moments in the same direction is applied at both ends of the model. Second, additional vertical forces are distributed among the model's stations to correct the shear force level.

For the first step, the vertical bending moments applied at the aft and fore ends are expressed as:

$$M_{Y\_fwd} = \frac{x_{fwd} - x_{aft}}{2} \cdot \frac{(Q_{targ-fwd} - Q_{fwd}) + (Q_{targ-aft} - Q_{aft})}{2} \qquad (32)$$

$$M_{Y\_aft} = M_{Y\_fore}$$

Where:

M_{Y_aft}
M_{Y_fwd} = VBM (in same direction) applied at the aft and fore ends

x_{aft}
x_{fwd} = the longitudinal coordinates of the aft- and fore section.

Q_{aft}
Q_{fwd} = the local load induced VSF

$Q_{targ-aft}$
$Q_{targ-fwd}$ = the target VSF as calculated in Section 4.4

However, the corresponding local load condition was not available in this study. Therefore, the initial VSF generated by local loads on the model is taken as zero, i.e.

$$Q_{aft} = Q_{fore} = 0$$

In addition, the target vertical shear forces at the two ends have the same magnitude but opposite signs. Substituting these values into Eq. 32 gives a zero result, since the shear forces cancel each other out. This implies that the VBM pair included in the first step of Method 2 is not required for the present loading case in this study. As a result, the target VSF condition is introduced only through the distributed vertical forces applied along the selected transverse stations of the model.

For the second step, the required shear force corrections at the fore and aft bulkheads are calculated as:

$$\Delta Q_{fwd} = \frac{\left(Q_{targ-fwd} - Q_{fwd}\right) - \left(Q_{targ-aft} - Q_{aft}\right)}{2} \qquad (33)$$
$$\Delta Q_{aft} = -\Delta Q_{fwd}$$

Where:

ΔQ_{aft}
ΔQ_{fwd} = the required vertical shear force adjustments at the aft and fore sections

Based on the same reason, since no local load induced VSF was present in the model, the required VSF adjustments are equal in magnitude to the target VSF values calculated in Section 4.4. In other words, the adjustment does not need to compensate for an existing shear force field, but directly represents the full target shear force to be introduced into the FE model. Therefore, the required shear force corrections can be expressed as:

$$\Delta Q_{aft} = Q_{targ-aft}$$
$$\Delta Q_{fore} = Q_{targ-fore}$$

In the DNV-based method, the cargo-hold model is divided into three regions: the aft hold, the midship hold and the fore hold. The corresponding lengths are denoted as $l_1, l_2, l_3, \Delta l_{fore}$ and Δl_{aft} respectively. Hence, the total cargo-hold model length is defined as:

$$l = l_1 + l_2 + l_3 + \Delta l_{aft} + \Delta l_{fore}$$

As a reference, DNV-CG-0127 provides an illustration of applied distributed vertical force on the model, see Figure 19. Jang and Kim (2025) gives a schematic illustration of VSF adjustment based on DNV-CG-0127, while the vertical force distribution and VSF distribution under HSM-1 are shown, see Figure 20.

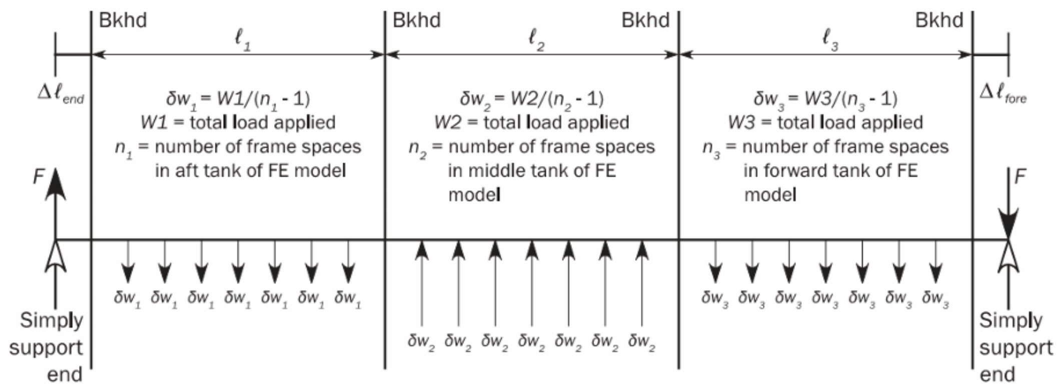

Figure 19: Original DNV scheme for VSF adjustment at stations (DNV, 2021a)

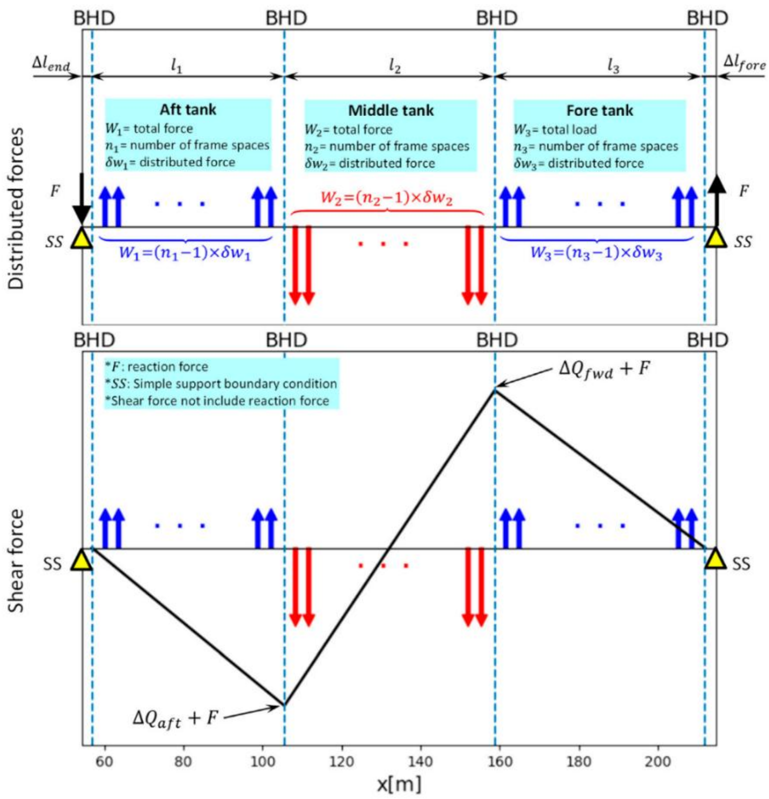

Figure 20: Schematic illustration of VSF adjustment by distributed vertical forces and the resulting shear force distribution, produced by Jang and Kim (2025), based on DNV-CG-0127

But it should be noted that the original DNV formulation is defined for a three-cargo-hold FE model, where l_1, l_2, and l_3 represent the aft, middle, and fore cargo holds, as shown in Figure 19 and Figure 20. In contrast, the present FE model does not include the adjacent aft and fore cargo holds. It represents only a RoPax midship segment within the midship cargo-hold region. Therefore, the complete three-region force distribution was not directly adopted. Instead, the model was treated as the middle evaluation segment, and the VSF was applied as an equivalent downward vertical load distributed along the length of the analyzed model.

For this reason, l_1 and l_3 does not have a direct physical meaning in the present model, while the analyzed model length corresponds to the middle region only. The following simplification is therefore adopted:

$$\delta w_1 = 0$$
$$\delta w_2 = \frac{\left(\Delta Q_{aft} - \Delta Q_{fore}\right)}{n_2 - 1} \tag{34}$$
$$\delta w_3 = 0$$

Where:

δ_{w2} = distributed load, in kN

n_2 = number of frame spaces in the FE model

For the current loading condition HSM-1, the resulting vertical shear force is:

$$\delta w_{2,HSM-1} = \frac{\left(40\,860 - (-40\,860)\right)}{36 - 1} \approx 2334.857\ [kN]$$

The total applied vertical force over the model length is $F_{total} = 81\,720$ kN. For verification, the reaction forces at the supported boundaries should be checked to ensure force equilibrium:

$$\sum F_z + R_{z-aft} + R_{z-fwd} = 0 \tag{35}$$

Where

$\sum F_z$ = the total applied vertical load

R_{z-aft}
R_{z-fwd} = the vertical reaction forces at the aft and fore boundaries

For the present RoPax model, the load was applied to the web plates of the transverse and vertical girders. These members were selected because they provide the primary vertical load-transfer path in the simplified midship structure. The flanges are not used as the primary load application region. However, they remain connected to the web structure and therefore participate in the load transfer through the FE connectivity. In ANSYS Mechanical, the load was applied to the edges of the girder web regions rather than to the shell/face element. The force was defined by components in the global coordinate system, with only the F_Z component activated, see Figure 21.

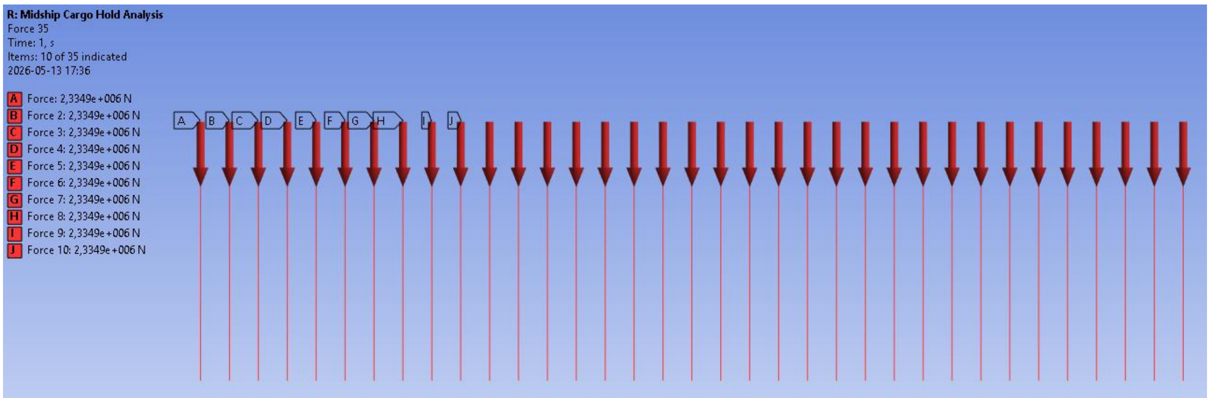

Figure 21: Loaded web plates of vertical and transversal girders

In addition, the reconstructed shear force distribution should be checked to confirm that the VSF reaches the target values at both boundaries. Therefore, the following conditions should be met.

$$R_{z-aft} = |Q_{targ-aft}|$$
$$R_{z-fwd} = |Q_{targ-fwd}|$$

For current loading conditions, the reaction forces $R_{z-aft} = R_{z-fore} = 40860\ [kN]$.

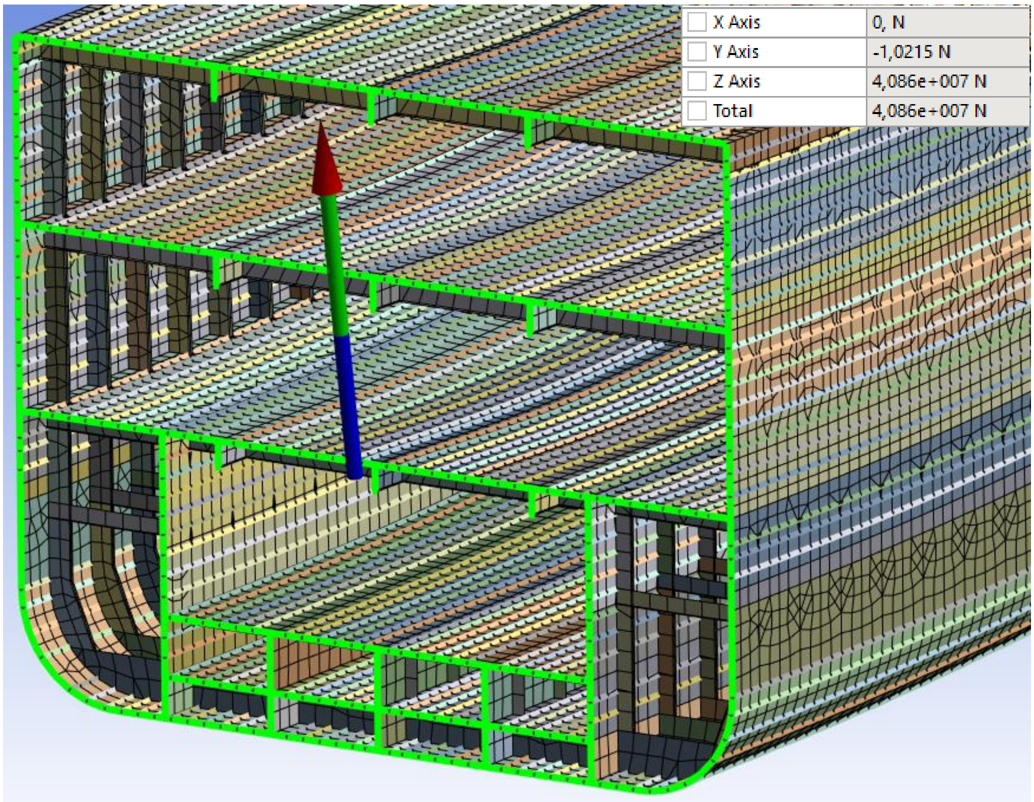

Figure 22: Reaction force at one of the boundary sections

7.6.2. Vertical Bending Moment applications

After the VSF application is submitted, the VBM shall also be applied in accordance with the instructions given by DNV-CG-0127 _(DNV, 2021a). According to the VBM adjustment procedure, the applied VBM should be determined from the difference between the target VBM and the peak VBM generated by the previously applied loads. This peak value includes the bending moment from local loads, the line loads used for VSF adjustment, and, if applicable, the end moment applied during the VSF adjustment step.

The additional VBM to be applied at the model ends is calculated as:

$$M_{v-end} = M_{v-targ} - M_{v-peak} \tag{36}$$

Where:

M_{v-end} =the additional vertical bending moment

M_{v-targ} = the target vertical bending moment

M_{v-peak} = the maximum/minimum vertical bending moment obtained from the applied loads

Following the DNV formulation, the peak bending moment is calculated as:

$$M_{v-peak} = \left[M_{v-FEM}(x) + M_{lineload}(x) + M_{Y-aft}\left(2\frac{x - x_{aft}}{x_{fore} - x_{aft}} - 1\right)\right] \qquad (37)$$

Where:

$M_{v-FEM}(x)$ = the bending moment caused by local loads

$M_{lineload}(x)$ = the bending moment caused by the vertical line loads used for VSF adjustment

M_{Y-aft} = the end bending moment introduced by the VSF adjustment step 1

The bending moment caused by the VSF line loads is calculated as:

$$M_{lineload}(x) = (x - x_{aft})F - \sum_{x_i<x}(x - x_i)\ \delta w_i \qquad (38)$$

Where:

F = the reaction force at model ends due to application of vertical loads to frames

x_i = the longitudinal position of the i-th loaded frame

δw_i = the vertical line load applied at that frame

In the present study, the local load induced bending moment does not exist. Therefore,

$$M_{v-FEM}(x) = 0$$

Meanwhile, as discussed in Section 7.6.1,

$$M_{Y-aft} = 0$$

Thus, the peak VBM depends only on the bending moment induced by the vertical line loads used for VSF adjustment.

$$M_{v-peak} = M_{lineload}(x)$$

As calculated in Section 7.6.1, the distributed vertical load:

$$\delta w_2 = 2\,476.36\ [kN]$$

And the boundary reaction force as shown in Figure 22:

$$F = 40\,860\ [kN]$$

Insertion of data into the DNV lineload bending moment expression Eq.38 gives the maximal bending moment at the middle of the ship.

$$M_{lineload-mid} = -875\,105\ [kNm]$$

Hence,

$$M_{v-peak} = -875\,105\ [kNm]$$

where the negative sign denotes sagging in the sign convention used in this study.

The target VBM for HSM-1 is:

$$M_{v-targ} = -2\,794\,912 \text{ kNm}$$

Therefore, the additional VBM required at the model ends would be:

$$M_{v-end} = -2\,794\,912 - (-875\,105\,) = -1\,919\,807\ [kNm]$$

This additional VBM shall be applied as an opposite moment pair at the aft and fore remote points. In accordance with DNV-CG-0127 _(DNV, 2021a), M_{v-end} is the end moment magnitude required to complete the VBM adjustment. Therefore, the applied moment pair is:

$$M_{Y-aft} = +1\,919\,807\text{kNm}$$

$$M_{Y-fore} = -1\,919\,807\text{kNm}$$

Where the signs are selected to produce the sagging deformation mode and the corresponding compressive longitudinal stress in the deck region, as shown in Figure 23.

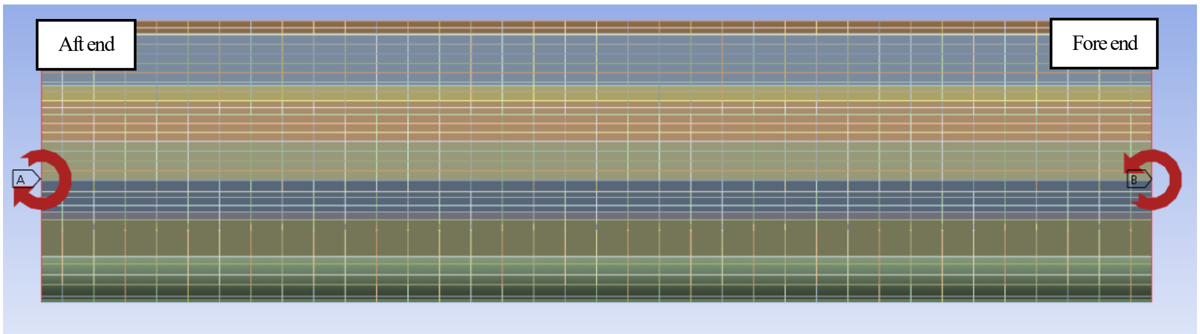

Figure 23: Applied VBM at boundaries in case of sagging

7.7. Global model results

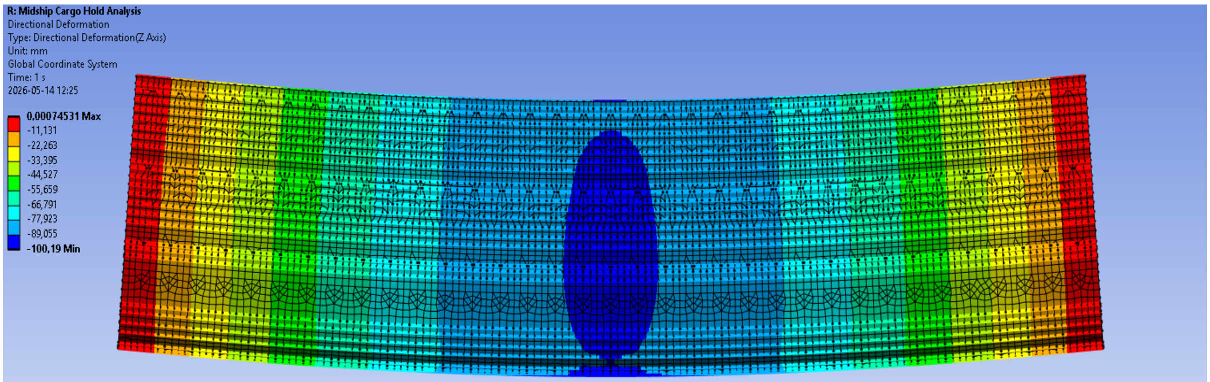

Figure 24: Directional deformation of the model in z-axis

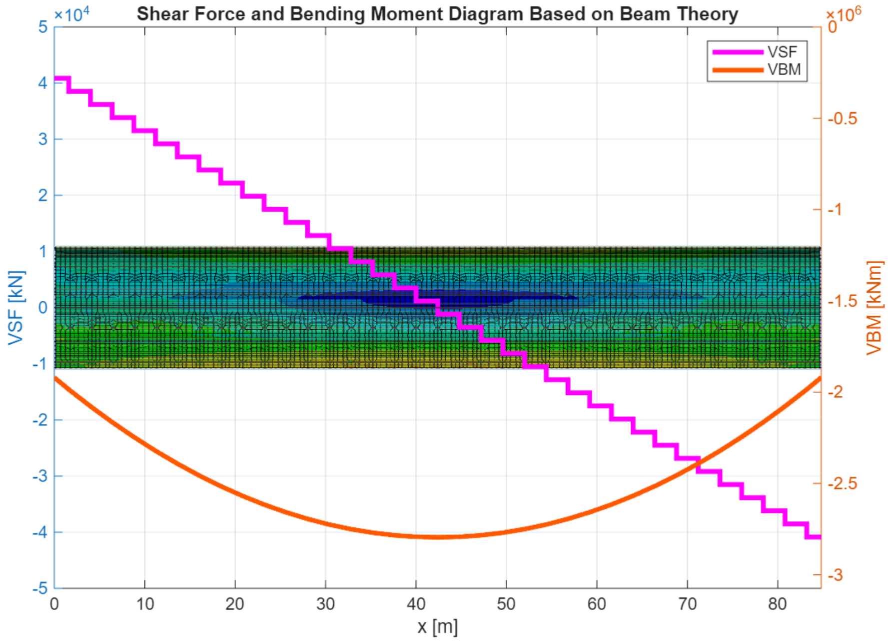

Figure 25: Shear Force and Bending Moment Diagram Based on Beam Theory

8. Local deck model

Since this study mainly focuses on the analysis of deck structures, local models in this context refer to the localized models of decks 3 and 5.

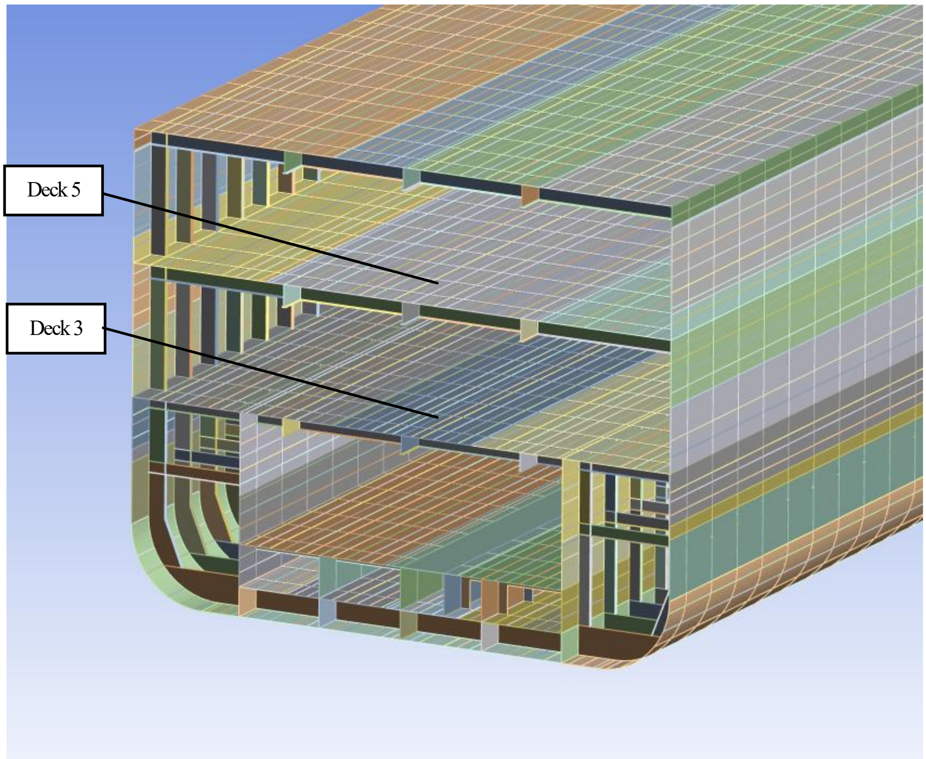

Figure 26: Deck 3 and deck 5 on midship cargo hold model

8.1. Modeling of local deck model

The dimensions of the local deck structure are presented in this section. It should be noted that the dimensions reported in this section refer specifically to the local deck model used in the subsequent sub-modeling and buckling assessment, rather than a full-breadth and full-length deck model in accordance with the midship cargo hold model. Therefore, these dimensions describe the extracted and modified deck region that is later analyzed as the local sub-model. The main dimensions of the modified local deck models are summarized in Tables 16 and Table 17. The spacing between the stiffeners is 620 mm.

Table 16: Dimension of top plate

	Top Plate		
	Length (x-axis) [mm]	Width (y-axis) [mm]	Thickness of top plate [mm]
Deck 5	21600	22320	10.5 & 12
Deck 3	21600	22320	11 & 12

Table 17: Dimension of supporting members

	Longitudinal Girder		Transverse Girder		Longitudinal Stiffeners
	Web [mm]	Flange [mm]	Web [mm]	Flange [mm]	L-beam [mm]
Deck 5	1050 x 10	200 x 30	1050 x 12	350 x 30	150 x 90 x 12
Deck 3	850 x 10	200 x 20	850 x 10	200 x 20	150 x 90 x 12

Since the local deck model is derived from the cargo hold model, it retains several characteristics of the global model. For example, the longitudinal stiffeners are represented by beam elements rather than being modeled explicitly as shell elements. For the purposes of the present strength and buckling assessment, this idealization is considered acceptable, as the beam representation captures the stiffeners' overall stiffness contribution while maintaining reasonable modeling efficiency. The local deck models of Deck 3 and Deck 5 are shown in Figure 27 and Figure 28 respectively.

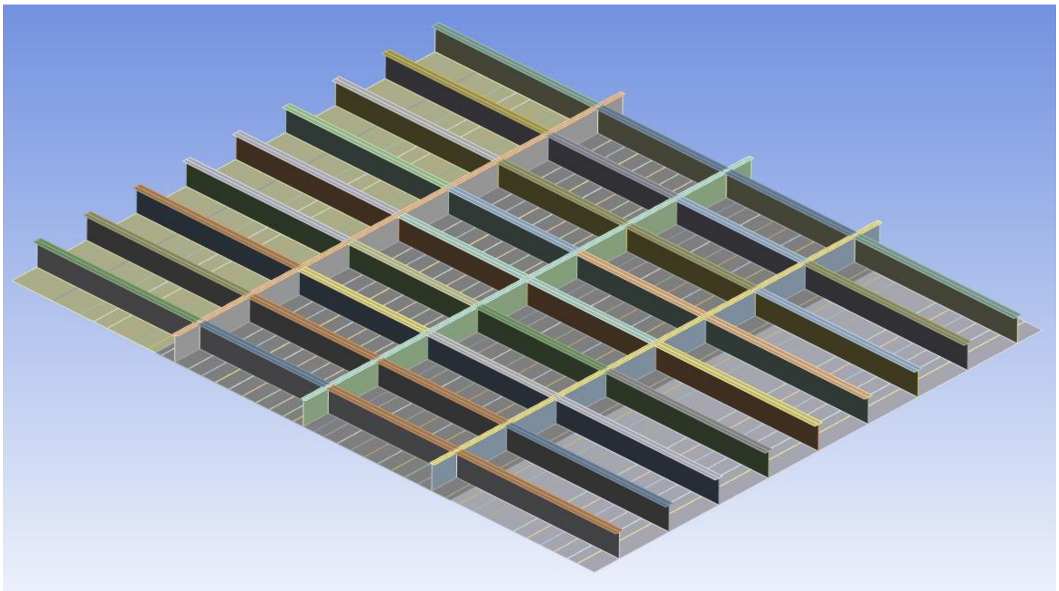

Figure 27: Local deck model of deck 5

8.2. Local mesh size

DNV's class guideline does not specify the mesh size for strength assessment. Therefore, mesh convergence will be performed to determine an appropriate mesh size. In this study, mesh convergence for strength assessment is evaluated by examining the deviation in load multipliers from the buckling analysis of the local model of deck 5. The mesh study of deck 3 has been considered unnecessary due to the structural similarity between decks.

Convergence analysis was achieved by progressively refining the model's mesh size and comparing the results with previous ones. The convergence deviation is expected to be as small as possible. Although a larger tolerance for deviation is typically allowed in practical engineering, deviations below 1% are considered reliable from a research perspective. Calculation of deviation according to the formula:

$$Deviation = \frac{\lambda_{i-1} - \lambda_i}{\lambda_{i-1}} * 100\% \tag{39}$$

Where:

$\lambda =$ Load multipliers

Table 18: Convergence study result

Mesh size	$200mm$	$150mm$	$100mm$	$75mm$	$50mm$
i	1	2	3	4	5
Mesh elements	26 167	43 744	93 226	161 841	358 601
Load multipliers	3.4934	3.2853	2.9796	2.8808	2.8533
Deviation	$-$	5.95%	9.31%	3.31%	0.95%

Since the deviation of the load multiplier from 75 mm to 50 mm is less than 1%, a mesh size of 75 mm is sufficient for the buckling analysis. Meanwhile, the first buckling mode did not change with the mesh size during the convergence analysis. So, the results of the convergence analysis are considered reliable.

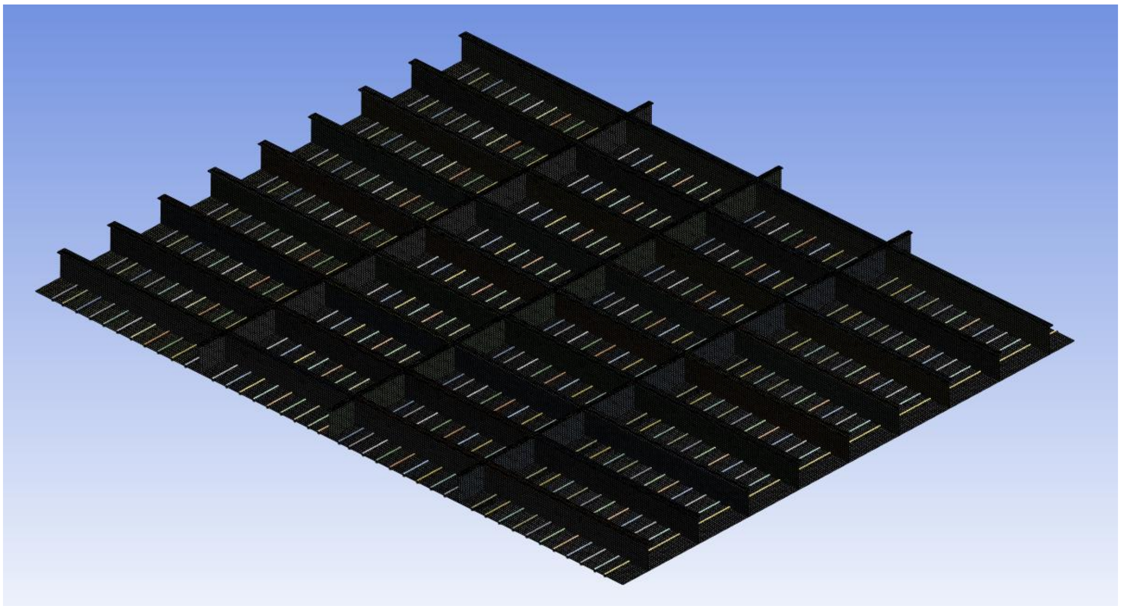

Figure 28: Mesh of local deck model - strength assessment (Mesh = 75mm)

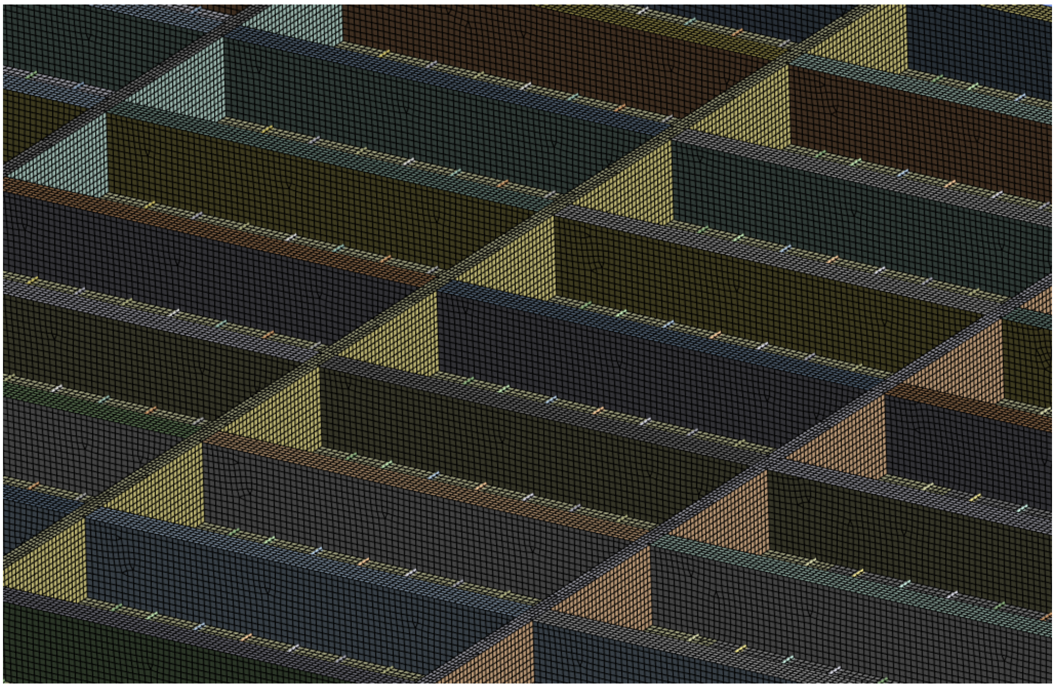

Figure 29: Partial enlargement of Figure 28 (Mesh = 75mm)

8.3. Sub-modeling

In the present study, the sub-modeling approach is employed to transfer the effects of the hull girder load to a localized structural model. The combined influence of loading conditions can be simulated by applying local loads to the sub-model. This interaction between hull girder and wheel loading effects constitutes one of the primaries focuses of this research.

Sub-modeling is a methodology commonly employed in FEA to improve the accuracy of stress and deformation within regions of local interest, without the need to refine the entire cargo hold model. The methodology was also applied to the structural analysis of a floating offshore substation to capture stress concentrations (Yi & Park, 2025).

This methodology is implemented by extracting the corresponding nodal displacements and rotations from the main model and applying them as cut-boundary constraints along the sub-model's cut boundaries. In ANSYS, the correspondence between the two models should already be ensured during the modeling stage by using the same reference coordinate system. As long as the sub-model's relative position with respect to the global coordinate system is correctly defined, the nodal displacements and rotations can be extracted from the main model and transferred to the sub-model. If the procedure is performed correctly, the displacement field obtained in the sub-model should be consistent with the displacement state at the corresponding location in the global model. This correspondence can also be used to demonstrate the validity of the sub-modeling procedure.

In addition, according to the official ANSYS guideline, the cut-boundary constraint primarily transfers nodal displacements and rotational degrees of freedom at the cut boundary (ANSYS Inc., n.d.). Therefore, if the same deformation state is to be fully reproduced in the sub-model, the corresponding loads acting on the sub-modeled region in the global model should also be applied to the sub-model, see Section 8.3.1. For academic completeness, the accuracy of the transferred nodal displacements and nodal rotations also needs to be verified, see Section 8.3.2.

8.3.1. Boundary conditions of sub-model

In the sub-modeling approach, the nodal displacement and nodal rotation results obtained from the cargo hold model are transferred to the sub-model as prescribed boundary conditions. It should be noted that ANSYS requires the global model and the sub-model to be defined consistently within the same coordinate system, as this ensures that nodal results are extracted from the correct locations and accurately transferred to the sub-model.

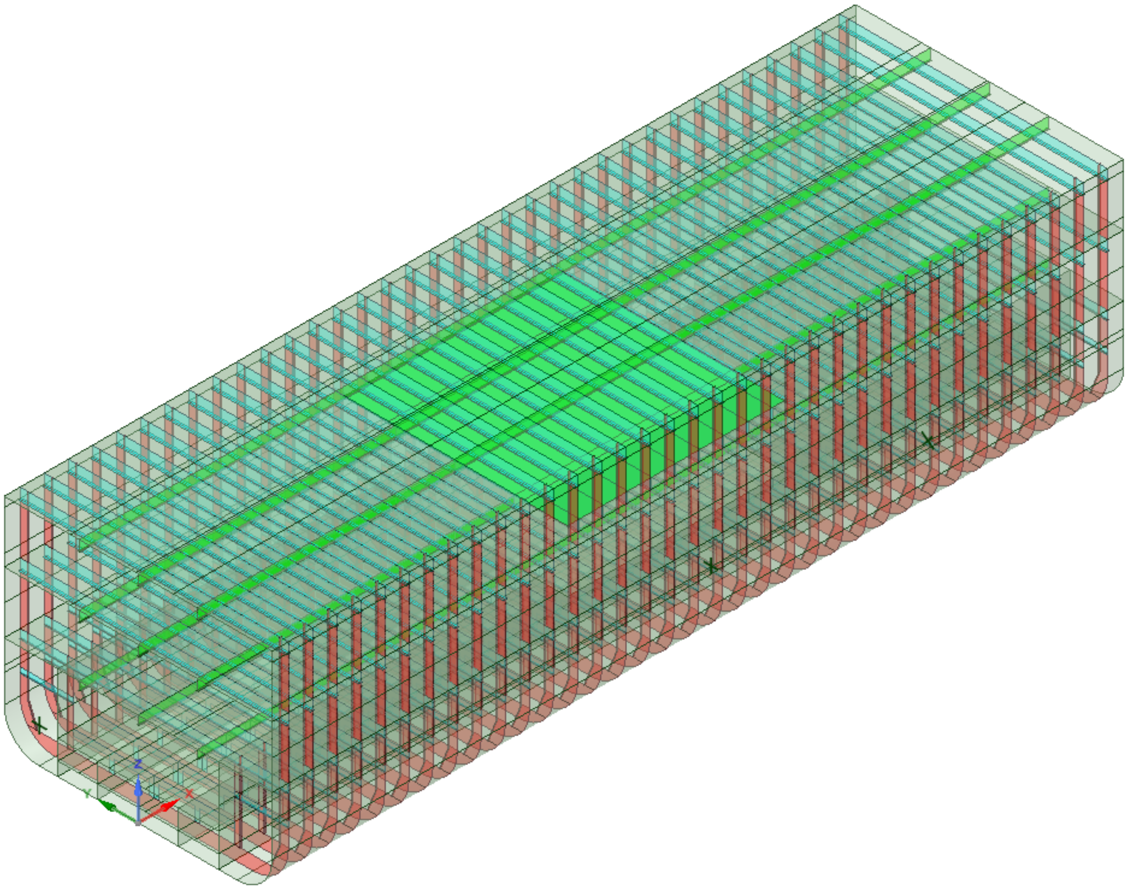

Figure 30: Global model and Sub-model in Space Claim

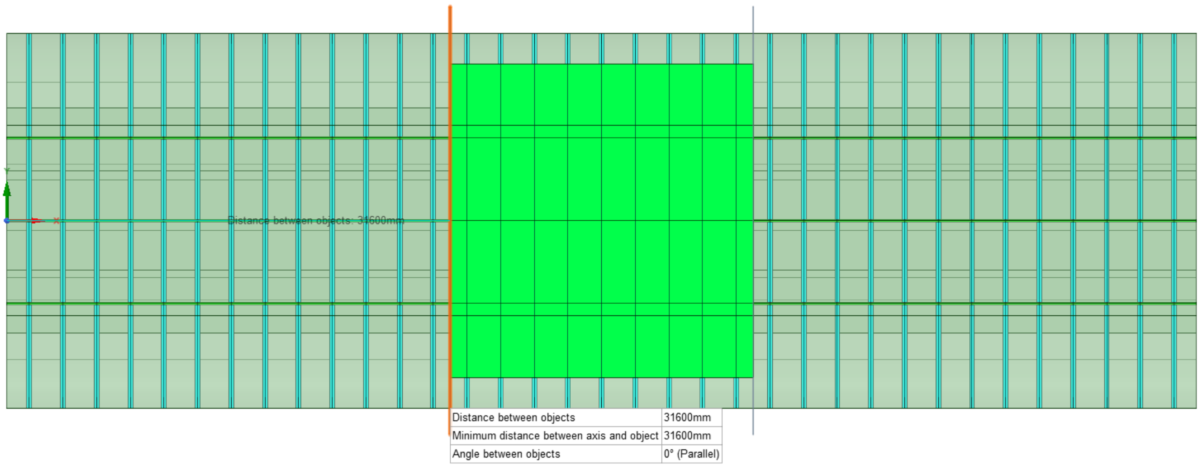

Figure 31: Global model and Sub-model in Space Claim – Top view

In ANSYS, these prescribed sub-model boundary conditions are named as cut-boundary constraints. It specifies the displacement and rotation of the nodes. In such a way, the boundary of the sub-model follows the deformation state extracted from the corresponding location in the cargo hold model. Once these cut-boundary constraints are applied, the displacement and rotation of the constrained boundary nodes are fixed according to the imported results. Therefore, any additional loads subsequently applied to the sub-model will not alter the prescribed boundary motion but will instead affect its internal stress and deformation response.

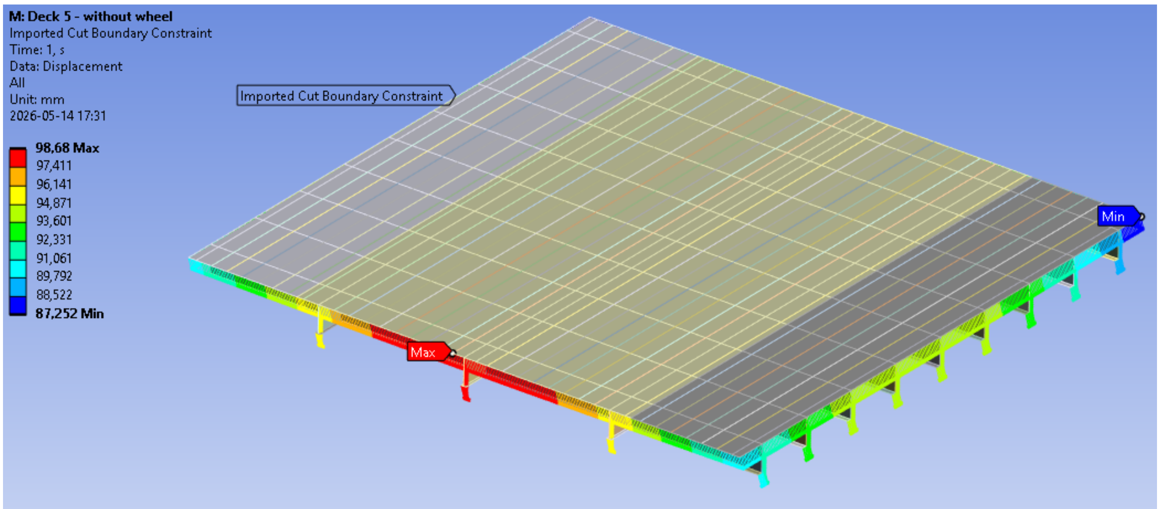

Figure 32: Visualized nodal displacement at cut boundaries of Deck 5

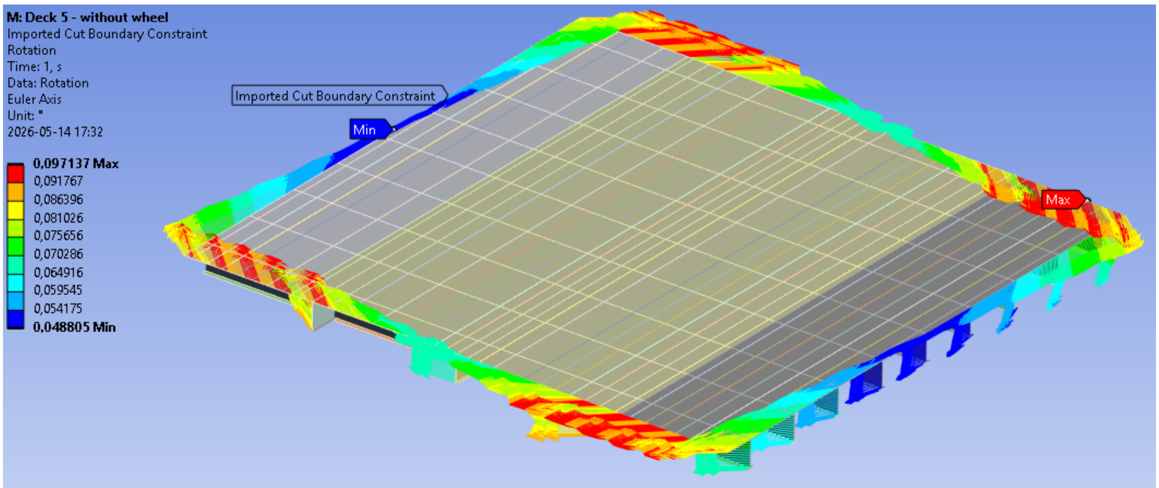

Figure 33: Visualized nodal rotation at cut boundaries of Deck 5

However, as pointed out in ANSYS guide, one limitation of the ANSYS sub-modeling procedure is that the cut-boundary constraints cannot fully reproduce the complete deformation field inside the extracted component (ANSYS Inc., n.d.). They impose the deformation state only along the cut boundaries, while the internal deformation of the sub-model still depends on the loads and structural conditions applied within the local model. For this reason, the relevant local loads acting on the component in the global model should also be reproduced in the sub-model, see Section 8.3.2.

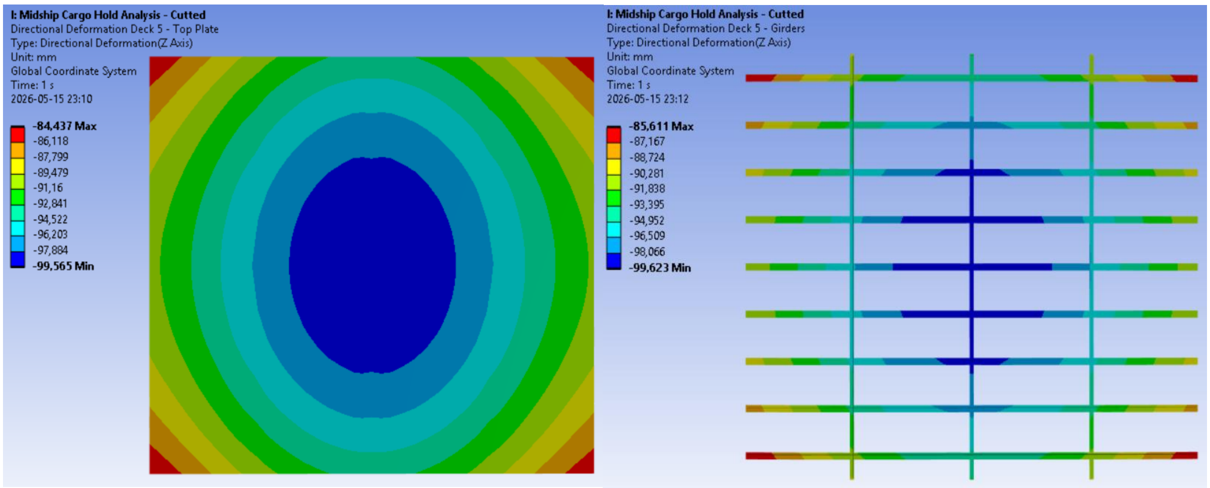

Figure 34: Global model results - vertical displacement of Top Plate (left) and girders (right)

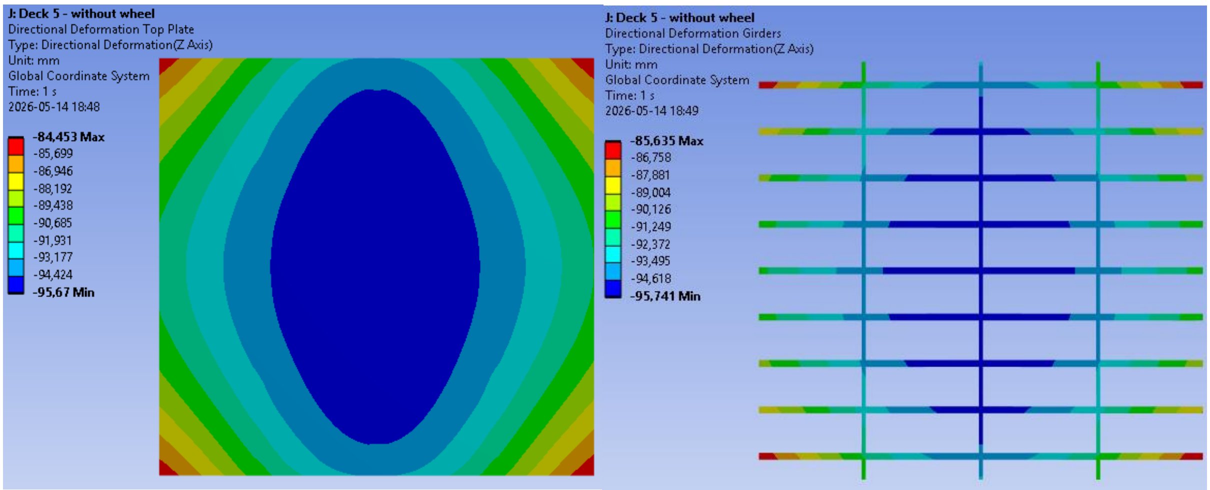

Figure 35: Sub-model results - vertical displacement of Top Plate (left) and girders (right)

8.3.2. Structural displacement reproduction

As described in Section 7.6.1, vertical downward forces were applied to all transverse web frames in the cargo hold model. Therefore, to reproduce the corresponding deformation behavior in the sub-model, the relevant vertical load needs to be reapplied. However, since the sub-model includes only partial transversal web plates connected to the corresponding deck structure, the magnitude of the applied vertical force will not be identical to that applied in the global model. After calculation and testing, a vertical force of $260\ [kN]$ should be applied to each transversal web plate of Deck 5. Under this loading condition, the difference between the displacement patterns obtained from the global and sub-models is negligible.

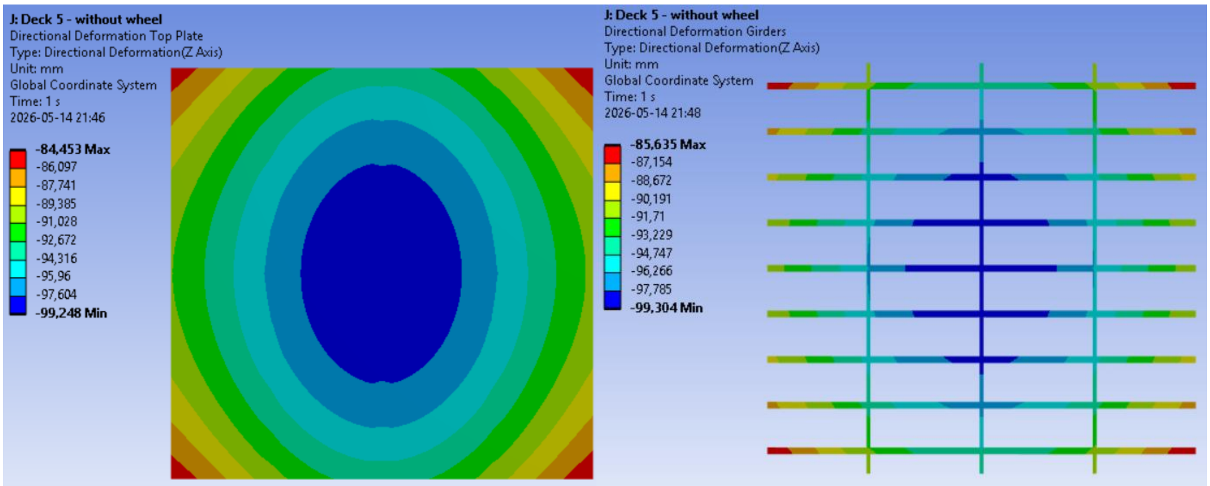

Figure 36: Corrected Deck 5 sub-model results - vertical displacement of Top Plate (left) and girders (right)

The same procedure had been repeated on the sub-model of Deck 3, while the required vertical forces for each transversal web plate had been calculated to $130\ [kN]$

8.3.3. Export of nodal results

To verify that the cut boundary constraints correctly import nodal results into the sub-model, nodal displacement and rotation results were extracted and compared with the corresponding results from the global model. Since the global model and the sub-model were meshed independently, their node numbering systems are different. Therefore, a direct comparison based on node numbers would not be possible. Instead, the comparison should be made based on the nodal locations relative to the global coordinate system (shared by the global model and the sub-model). In this way, nodes at the same position can be matched and compared. By default, ANSYS does not export the nodal position with result files. The function can be enabled through the following path in ANSYS Workbench:

$$File \longrightarrow Opotions \longrightarrow Mechanical \longrightarrow Export \longrightarrow Include\ Node\ Location \longrightarrow Yes$$

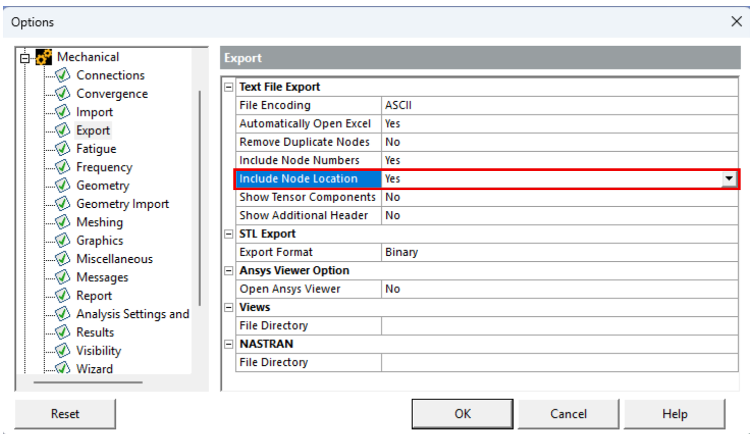

Figure 37: Enabling node location export in ANSYS Workbench Mechanical

The next step is to solve the model and obtain directional displacement results and nodal rotational results at the cut boundaries. In ANSYS Workbench, the directional displacement is a predefined result output, which can be created through the following steps:

$$Solution \longrightarrow Insert \longrightarrow Deformation \longrightarrow Directional\ deformation$$

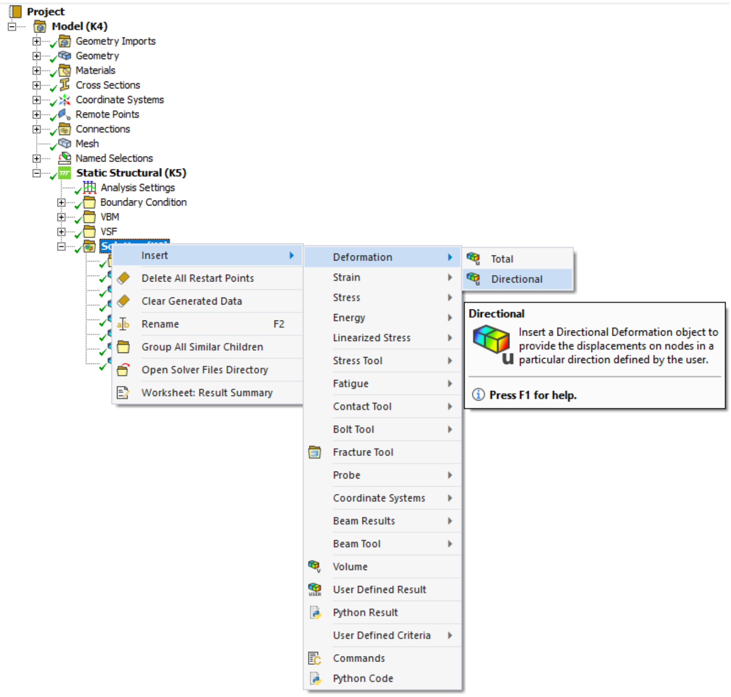

Figure 38: Creation of directional deformation

It can be used to extract the displacement component in any required direction, namely x-, y- or z-direction. The expected direction can be selected by changing the $Orientation$ option to the corresponding axis. The unit of the exported displacement result is determined by the current unit system used in the ANSYS model. As an example, the setups of extracting nodal displacement of aft cut-boundary in x-axis is shown in Figure 39.

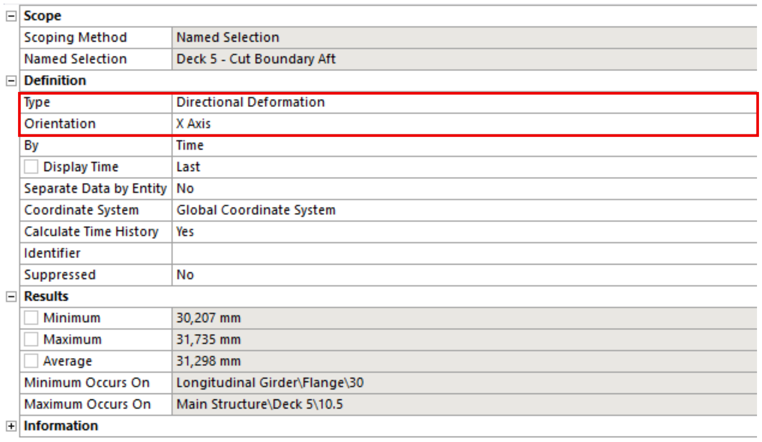

Scope	
Scoping Method	Named Selection
Named Selection	Deck 5 - Cut Boundary Aft
Definition	
Type	Directional Deformation
Orientation	X Axis
By	Time
Display Time	Last
Separate Data by Entity	No
Coordinate System	Global Coordinate System
Calculate Time History	Yes
Identifier	
Suppressed	No
Results	
Minimum	30,207 mm
Maximum	31,735 mm
Average	31,298 mm
Minimum Occurs On	Longitudinal Girder\Flange\30
Maximum Occurs On	Main Structure\Deck 5\10.5
Information	

Figure 39: Setups of directional deformation

In contrast, nodal rotation is not provided directly as an output result in the software. Therefore, it needs to be reported by defining a $\mathit{User\ Defined\ Result}$, which can be created through the following steps:

$$\mathit{Solution} \longrightarrow \mathit{Insert} \longrightarrow \mathit{User\ Defined\ Result}$$

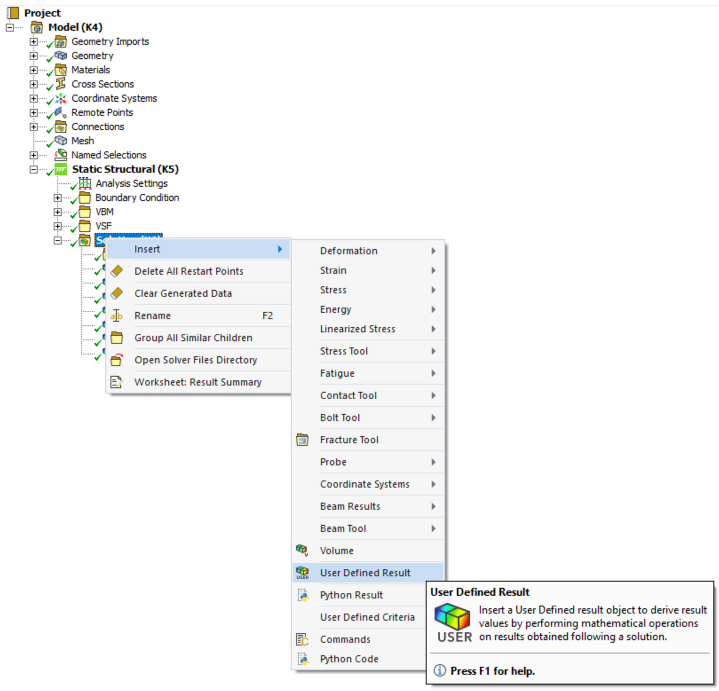

Figure 40: Creation of User Defined Result

To obtain the nodal rotation components, the expression of the $\mathit{User\ Defined\ Result}$ should be set as RX, RY or RZ, corresponding to the rotation about the global x-, y-, or z-axis. The $\mathit{Output\ Unit}$ should then be set to Angle. With this setting, the exported result represents the rotational degree of freedom of each node. The unit system in this project uses degrees $(°)$, but radius is also available in the software. As an example, the setups of extracting nodal rotation of aft cut-boundary around x-axis is shown in Figure

41.

Scope	
Scoping Method	Named Selection
Named Selection	Deck 5 - Cut Boundary Aft
Definition	
Source	Expression
Expression	= RX
Input Unit System	Metric (mm, kg, N, s, mV, mA)
Output Unit	Angle
By	Time
Display Time	Last
Separate Data by Entity	No
Calculate Time History	Yes
Identifier	
Suppressed	No
Results	
Minimum	-6,8468e-002 °
Maximum	6,7236e-002 °
Average	-6,0763e-004 °
Minimum Occurs On	Main Structure\Deck 5\10.5
Maximum Occurs On	Main Structure\Deck 5\10.5
Information	

Figure 41: Setups of User Defined Result

If other result components are required, or if a different expression needs to be used for creating a $User\ Defined\ Result$, the available predefined expressions can be checked in ANSYS Workbench through the following path:

$$Solution \longrightarrow Worksheet: Result\ Summary \longrightarrow Available\ Solution\ Quantities$$

Available Solution Quantities

Material and Element Type Information

Solver Component Names

Result Summary

Type	Data Type	Data Style	Component	Expression
R	Nodal	Scalar	X	RX
R	Nodal	Scalar	Y	RY
R	Nodal	Scalar	Z	RZ
REULER	Nodal	Euler Angles	VECTORS	REULERVECT
U	Nodal	Scalar	X	UX
U	Nodal	Scalar	Y	UY
U	Nodal	Scalar	Z	UZ
U	Nodal	Scalar	SUM	USUM
U	Nodal	Vector	VECTORS	UVECTORS
S	Element Nodal	Scalar	X	SX
S	Element Nodal	Scalar	Y	SY
S	Element Nodal	Scalar	Z	SZ
S	Element Nodal	Scalar	XY	SXY
S	Element Nodal	Scalar	YZ	SYZ
S	Element Nodal	Scalar	XZ	SXZ
S	Element Nodal	Scalar	1	S1
S	Element Nodal	Scalar	2	S2
S	Element Nodal	Scalar	3	S3
S	Element Nodal	Scalar	INT	SINT
S	Element Nodal	Scalar	EQV	SEQV
S	Element Nodal	Tensor	VECTORS	SVECTORS
S	Element Nodal	Scalar	MAXSHEAR	SMAXSHEAR

Figure 42: Several available solution quantities and expressions predefined in ANSYS

This list contains expressions that can be recognized by ANSYS for result extraction. It should be noted that the entered expression must be written exactly as it appears in this list. Otherwise, ANSYS would not be able to identify the expression, and the solution process would be aborted.

As a result, a list of solutions will be created in ANSYS Workbench as shown in Figure 43.

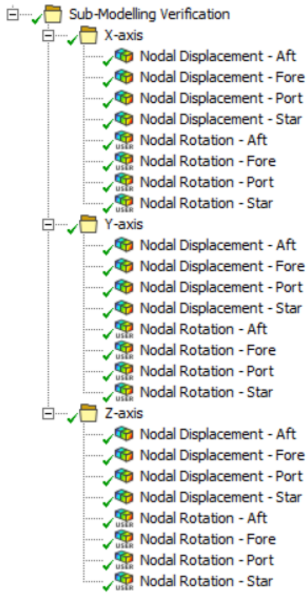

Figure 43: Created solutions for extracting nodal result components at each cut boundaries

While the export of a nodal result shall be done through following path:

$$Result \longrightarrow Export \longrightarrow Export\ Text\ File$$

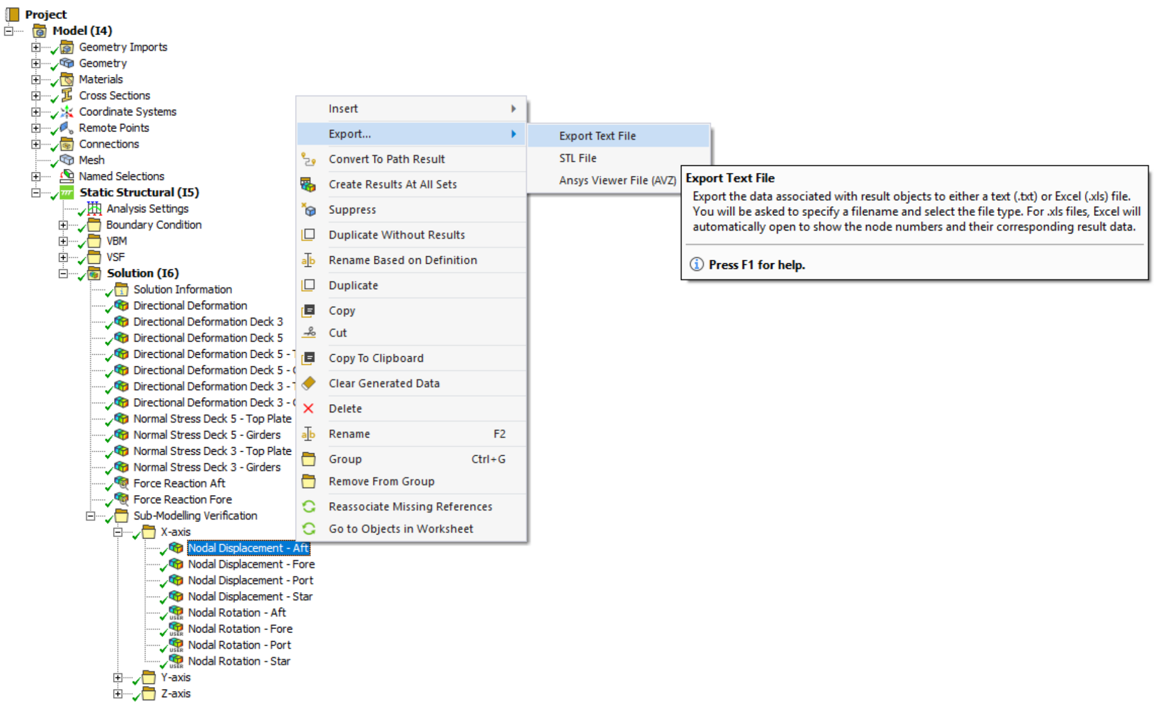

Figure 44: Export of nodal result

Following the above-mentioned process, the exported nodal result is stored as a .txt file, while its layout in Excel shall be formed as shown in Figure 45.

	A	B	C	D	E
1	Node Number	X Location (mm)	Y Location (mm)	Z Location (mm)	Directional Deformation (mm)
2	7279	31600	-5890	15400	31,457
3	7280	31600	-5890	14350	30,209
4	39965	31600	-5890	14875	30,828
5	8552	31600	5890	15400	31,637
6	8553	31600	5890	14350	30,385
7	43324	31600	5890	14875	31,006
8	8095	31600	0	15400	31,552
9	8096	31600	0	14350	30,286
10	42167	31600	0	14875	30,914
11	18323	31600	-100	14350	30,284
12	18325	31600	100	14350	30,287
13	18345	31600	5990	14350	30,385
14	18347	31600	5790	14350	30,385
15	18335	31600	-5790	14350	30,212
16	18337	31600	-5990	14350	30,207
17	7187	31600	-11160	15400	31,385
18	7189	31600	-10850	15400	31,384
19	7253	31600	-10230	15400	31,383
20	7272	31600	-9610	15400	31,386
21	7273	31600	-8990	15400	31,389
22	7274	31600	-8370	15400	31,395
23	7275	31600	-7750	15400	31,404
24	7276	31600	-7130	15400	31,418
25	7277	31600	-6760	15400	31,433
26	8544	31600	10850	15400	31,724
27	8545	31600	11160	15400	31,735
28	8587	31600	10230	15400	31,703
29	9033	31600	6760	15400	31,64
30	9034	31600	7130	15400	31,637

Figure 45: Example of exported nodal result in Excel

8.3.4. Verification of imported cut boundary constraints

To verify the accuracy of cut boundary constraints in the sub-model methodology, the nodal displacements and rotations at the four cut boundaries in the sub-model will be extracted and analyzed. For each cut boundary, the displacement components and the rotational components will be compared with the corresponding results from the cargo hold model.

After exporting the nodal results, the data are summarized in excel files for sub-modeling boundary transfer verification. Noticing that the mesh size of the global model and sub-model are different. Therefore, the verification of sub-modeling is done by comparing three datasets:

- Dataset 1

  The first dataset was obtained from a modified global model, in which the region corresponding to the sub-model was explicitly cut out, and the nodal results along the cut boundaries were exported. This dataset was used as a reference, and the result represents the deck deformation in the global model.

- Dataset 2

  The second dataset was obtained from the sub-model based on the modified global model, where the corresponding cut boundaries existed in the global mesh.

- Dataset 3

The third dataset was obtained from the sub-model based on the original global model, where the corresponding cut boundaries do not exist in the global model.

The comparison between Dataset 2 and Dataset 3 is of particular interest. Since the FE solution is evaluated at mesh nodes, different mesh sizes will lead to different numbers of nodes and nodal positions. In the modified global model, the sub-model cut boundaries are explicitly created in the global model. Therefore, mesh nodes must exist along the cut boundary lines. In contrast, mesh nodes may not exist in an unmodified global model due to the difference between the mesh size. The described situation is shown in Figure 46, where the black squares represent the global mesh element while the red square represents the cut boundary of the sub-model.

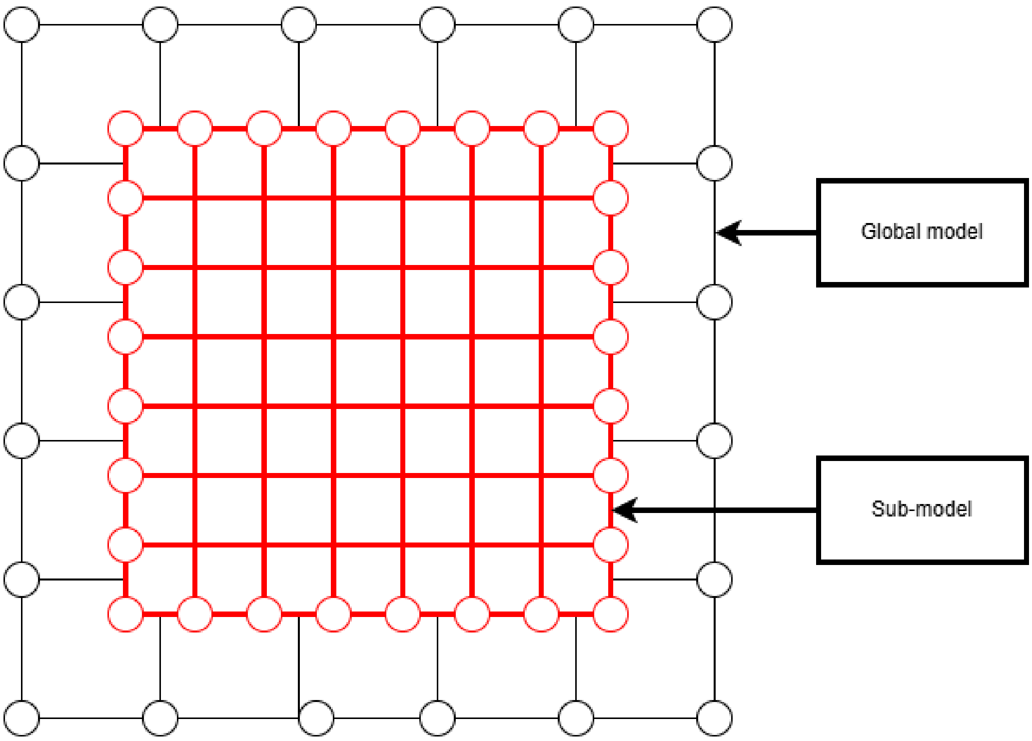

Figure 46: Illustration of possible miss match of nodes due to mesh size differences

According to the ANSYS guide, the non-existing nodes in global model are derived using linear interpolation with respect to closest existing nodes (ANSYS Inc., n.d.). However, a detailed interpolation formula used in ANSYS was not provided. Therefore, the verification of Dataset 3 focuses on the nodal results obtained from the sub-model boundary after the cut-boundary constraints have been applied. The exported nodal results from Dataset 3 are expected to be similar as those in Datasets 1 and 2.

The comparison of data sets is done based on following procedures.

1. The datasets are summarized in one excel file
2. All nodes are matched and re-ordered based on the node location
3. Comparing dataset 1 and dataset 2
4. Comparing dataset 2 and dataset 3

As an example, the comparison of nodal displacement on one edge can be done using Table 19.

Table 19: Comparison of nodal displacement

			Dataset 1				Dataset 2				Dataset 3			
Node Location			Node Number	Magnitude			Node Number	Magnitude			Node Number	Magnitude		
X	Y	Z		X	Y	Z		X	Y	Z		X	Y	Z
31600	-5890	15400	7279	31,457	-1,268	-90,016	575	31,457	-1,268	-90,016	575	31,399	-1,261	-90,240
31600	-5890	14350	7280	30,208	-2,192	-90,170	576	30,208	-2,192	-90,170	576	30,183	-2,203	-90,383
...			...				...				...			
31600	-11005	15400	-	31,384	-1,731	-84,607	25781	31,384	-1,731	-84,607	25781	31,414	-1,729	-84,766
31600	-11083	15400	-	31,384	-1,741	-84,530	25782	31,384	-1,741	-84,530	25782	31,415	-1,739	-84,695
-Non-existing node in global model. Magnitudes were manual calculated using linear interpolation														

The comparison of nodal results is done by calculating the average nodal result, the average error, and the relative error (%).

$$\bar{x} = \frac{1}{n}\sum_{i=1}^{n} x_{i,ref} \tag{40}$$

$$\bar{e} = \frac{1}{n}\sum_{i=1}^{n} x_{i,ref} - x_{i,comp} \tag{41}$$

$$\bar{e}\ (\%) = \frac{\bar{e}}{\bar{x}} * 100\% \tag{42}$$

Where:

$x_{i,\mathrm{ref}}$ = the nodal result of the reference dataset at the corresponding node i

$x_{i,\mathrm{comp}}$ = the nodal result of the compared dataset at the corresponding node i

n = the total number of compared nodes

$\bar{e}$ = averaged error

$\bar{x}$ = averaged nodal result

$\bar{e}(\%)$ = relative deviation in percentage

Results of the comparisons are summarized in tables below. Table 20 shows comparison results from Dataset 1 v.s. Dataset 2, which aims to verify the accuracy of nodal result transfer in sub-model methodology.

Table 20: Result comparison - Dataset 1 vs. Dataset 2

RESULT TYPE	BOUNDARY	COMPONENT	AVERAGED NODAL RESULT	AVERAGED ERROR	RELATIVE ERROR (%)
NODAL DISPLACEMENT	Aft	U_X	31,421	4,70E-06	0,000015%
		U_Y	-1,015	-2,04E-06	0,000201%
		U_Z	-90,088	-4,35E-05	0,000048%
	Fore	U_X	21,000	-1,63E-05	-0,000078%
		U_Y	-1,016	-4,03E-06	0,000397%
		U_Z	-90,087	-3,20E-05	0,000036%
	Port	U_X	26,211	-1,07E-05	-0,000041%
		U_Y	-0,109	2,07E-07	-0,000189%
		U_Z	-88,859	1,56E-05	-0,000018%
	Star	U_X	26,209	4,70E-05	0,000179%
		U_Y	-1,999	5,36E-06	-0,000268%
		U_Z	-88,597	2,16E-05	-0,000024%
NODAL ROTATION	Aft	R_X	-6,01E-04	8,42E-09	-0,001401%
		R_Y	6,94E-02	-1,16E-08	-0,000017%
		R_Z	-8,76E-04	2,30E-09	-0,000262%
	Fore	R_X	-7,56E-04	2,49E-09	-0,000329%
		R_Y	-6,94E-02	-1,62E-08	0,000023%
		R_Z	7,71E-04	2,12E-09	0,000275%
	Port	R_X	6,02E-02	-3,22E-08	-0,000053%
		R_Y	7,23E-06	4,68E-08	0,006477%
		R_Z	2,87E-06	1,46E-09	0,050899%
	Star	R_X	-6,22E-02	3,31E-08	-0,000053%
		R_Y	2,69E-06	-5,12E-08	-0,019014%
		R_Z	1,70E-06	-1,10E-09	-0,000648%

The results show very close agreement between Dataset 1 and Dataset 2 for both nodal displacement and nodal rotation at the cut boundaries. Relative errors remain extremely small, which indicates that the cut-boundary constraints applied in the sub-model can accurately reproduce the nodal response of the global model when the cut boundaries exist in both models.

Table 21 shows comparison results from Dataset 2 v.s. Dataset 3, which aims to verify the accuracy of nodal result transfer when corresponding nodes do not exist in the global model.

Table 21: Result comparison - Dataset 2 vs. Dataset 3

RESULT TYPE	BOUNDARY	COMPONENT	AVERAGED NODAL RESULT	AVERAGED ERROR	RELATIVE ERROR (%)
NODAL DISPLACEMENT	Aft	U_X	31,421	4,76E-02	0,15%
		U_Y	-1,015	1,40E-03	-0,14%
		U_Z	-90,088	2,24E-01	-0,25%
	Fore	U_X	21,000	-1,30E-01	-0,62%
		U_Y	-1,016	-8,91E-05	0,01%
		U_Z	-90,086	2,81E-01	-0,31%
	Port	U_X	26,211	-3,76E-02	-0,14%
		U_Y	-0,109	3,66E-04	-0,33%
		U_Z	-88,859	2,03E-01	-0,23%
	Star	U_X	26,209	-4,08E-02	-0,16%
		U_Y	-1,999	-1,81E-03	0,09%
		U_Z	-88,597	1,55E-01	-0,18%
NODAL ROTATION	Aft	R_X	-6,01E-04	-3,34E-07	0,06%
		R_Y	6,94E-02	2,97E-04	0,43%
		R_Z	-8,76E-04	-2,58E-06	0,29%
	Fore	R_X	-7,56E-04	-5,06E-07	0,07%
		R_Y	-6,94E-02	-3,96E-04	0,57%
		R_Z	7,71E-04	-4,23E-06	-0,55%
	Port	R_X	6,02E-02	1,12E-04	0,19%
		R_Y	6,76E-07	-9,35E-10	-0,14%
		R_Z	2,87E-06	-2,92E-09	-0,10%
	Star	R_X	-6,22E-02	-1,03E-04	0,17%
		R_Y	2,69E-04	-1,02E-06	-0,38%
		R_Z	1,70E-04	2,11E-07	0,12%

In Table 21, the cut-boundary nodes of the sub-model are not directly matched by corresponding nodes in the global model. As a result, the relative errors are noticeably larger than those reported in Table 20. However, the comparison results show that the relative errors of both displacement and rotation components remain within ±1%. So, the imported cut boundary constraint can still be regarded as reliable for the sub-modeling procedure. It demonstrates that the sub-modeling methodology can be used even when the cut-boundary nodes do not directly exist in the global model.

8.4. Local wheel load application

Within the context of deck structure analysis, local load refers to wheel loads. In the present study, the local load is represented by an axle load rather than by modeling an entire vehicle. In the FE model, the contact area of each wheel is idealized as a rectangular loading patch, with the calculated wheel load applied as a uniformly distributed vertical pressure over the patch area. Accordingly, one set of axle loads is represented by four wheel-loading patches on the deck surface.

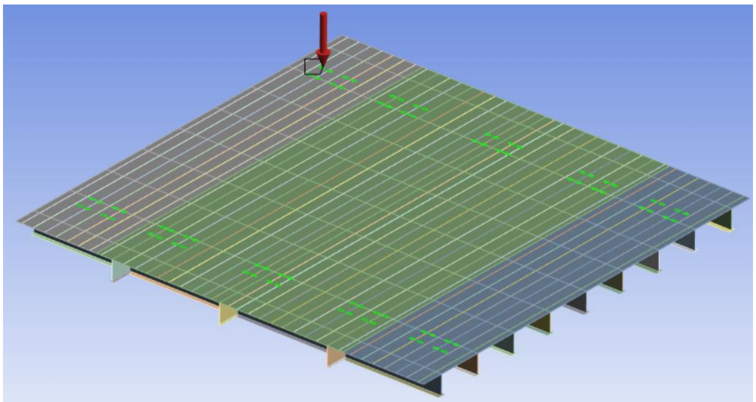

Figure 47: Applied wheel loads on loading patches in vertical direction

The local load is applied by assuming the parking positions of trailers on the deck. For the investigated deck width of 22.32 m, five trailers are assumed to be arranged in the transverse direction. This arrangement is adopted as a simplified representation of the vehicle-loading condition while still providing a reasonable and conservative local loading pattern for the deck structure. The corresponding loading arrangements for Deck 3 and Deck 5 are shown in Figure 48.

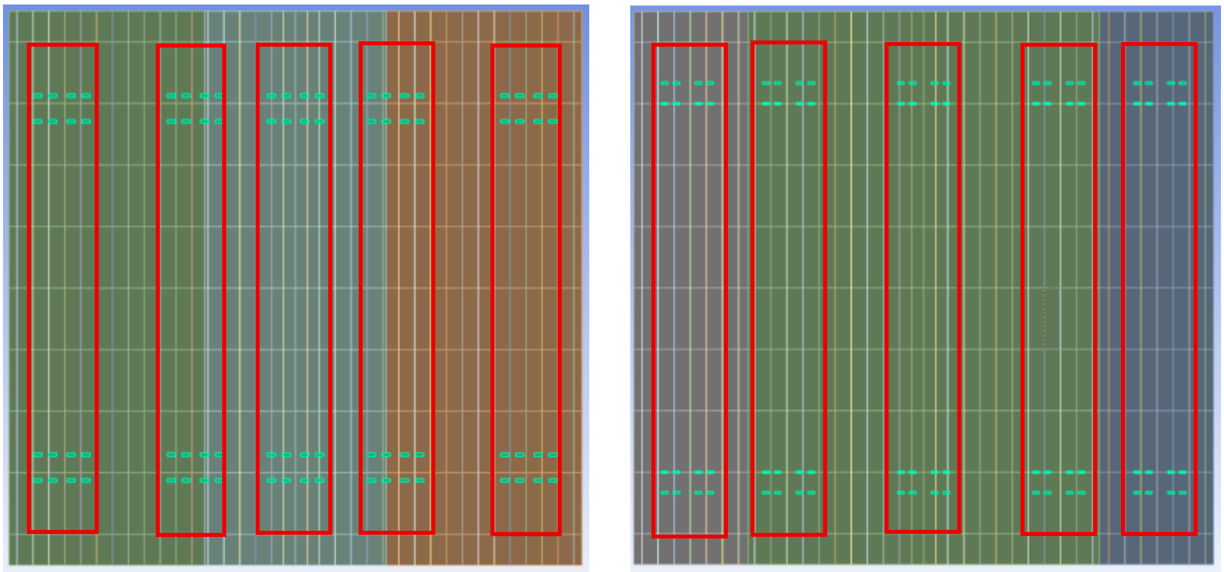

Figure 48: Wheel loading patches on Deck 3 (left) and Deck 5 (right)

9. Linear buckling analysis

Linear buckling analysis is used in this study as an efficient preliminary method to evaluate the stability behavior of the deck structures under the applied design load conditions. The analysis predicts the critical load multiplier and identifies the buckling-sensitive components or regions that may require further investigation. It should be emphasized that the obtained buckling mode shapes represent the relative instability pattern of the structure, rather than the actual magnitude of physical deformation after buckling. Therefore, the linear buckling results are primarily used to identify potential weak regions in the deck system and to guide a more comprehensive future nonlinear buckling analysis, in which the effects of initial imperfections, material nonlinearity, and large deformation can be considered.

According to beam bending theory, the VBM introduces maximal normal stress (longitudinal direction) in the hull girder, which can be expressed as:

$$\sigma_x = \frac{M_y z}{I_y} \tag{43}$$

Where:

M_y = the Vertical Bending Moment

z = the vertical distance from the neutral axis

I_y = the second moment of inertia of the hull cross-section

Since compressive stress is the primary driving factor for plate and stiffener buckling, the loading condition that maximizes VBM is of interest in buckling analysis. Among the hull girder loading conditions, the HSM-1 load case is selected because it represents sagging and produces the maximum compressive stress in the deck structure. Through the sub-modeling approach, the effect of the global hull girder loading has been transferred to the local deck model, and the resulting stress state is used as the pre-stress condition in the linear buckling analysis. To evaluate the influence of local wheel loads on the stability response, the buckling results will be divided into two parts: one load case that considers only the hull girder loading (implemented from the global model), and the other that considers the combined effect of hull girder and wheel loads.

9.1. General workflow

To clarify how the different load components are combined in the FE models, Figure 49 summarizes the overall workflow of buckling analysis adopted in this thesis. First, the hull girder loads are calculated using the formulas presented in Section 4. After that, the hull girder loads are applied to the midship cargo hold model described in Section 7. The resulting displacements of Deck 3 and Deck 5 are then exported and imposed as cut-boundary constraints on the corresponding local deck sub-models (Section 8), thereby reproducing the structural state due to hull-girder response. Subsequently, the local wheel loads defined in Section 6 are applied as pressure patches on the deck plating of the sub-models. For the linear buckling assessment, the hull girder loads for the critical sagging load case HSM-1 (Table 10) are combined with the wheel loads to form the design loading condition. In this way, the sub-modeling framework provides a consistent basis for evaluating buckling behavior under realistic combinations of hull girder loads and local loads.

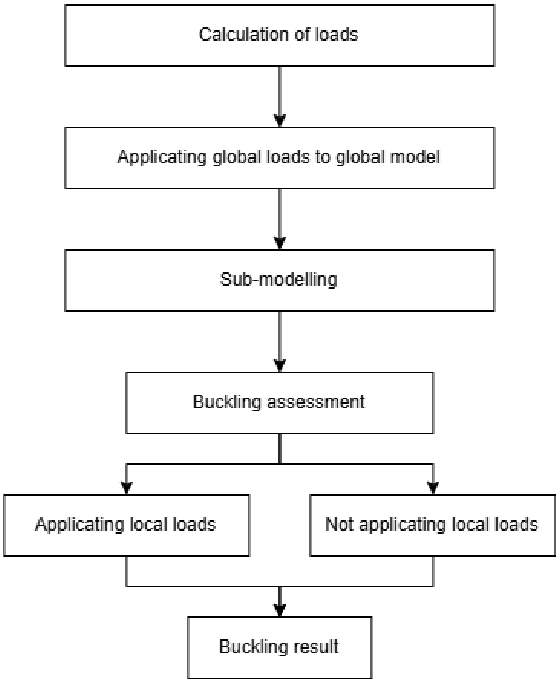

Figure 49: General workflow

9.2. Buckling result – Deck 3

Table 22: Linear buckling result - hull girder load

	Hull girder load	
	Hull girder load	Combined load
Mesh size $[mm]$	75	75
Number of elements	148 091	148 971
Load multiplier	12.74	7.7114

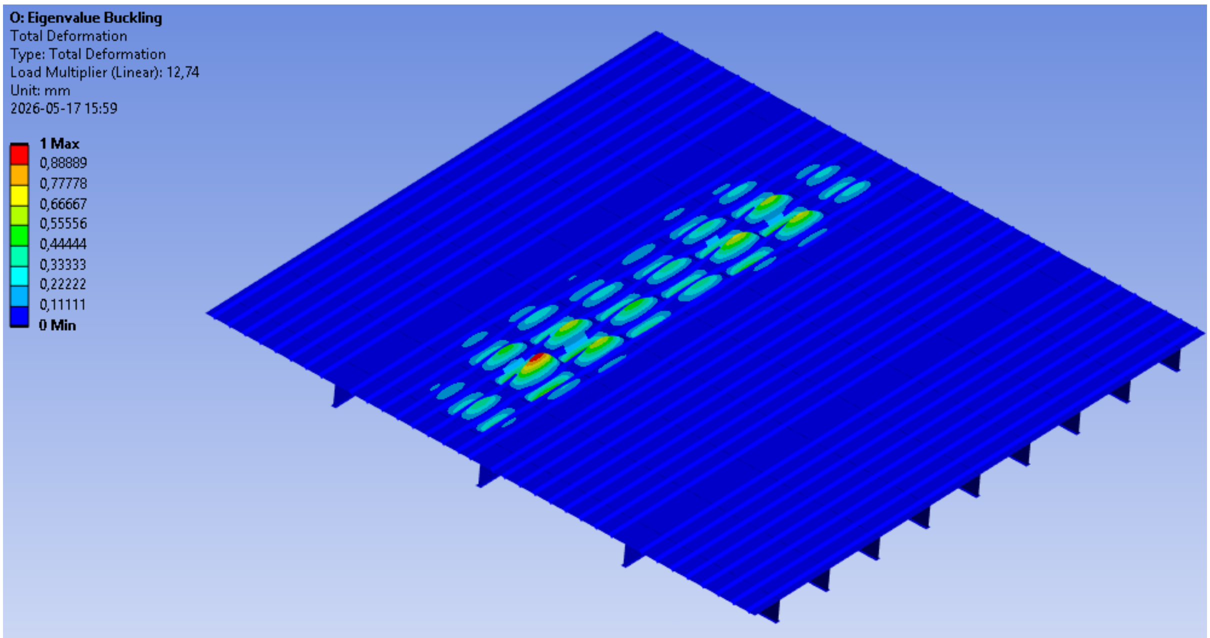

Figure 50: Buckling result – deck 3 without wheel load

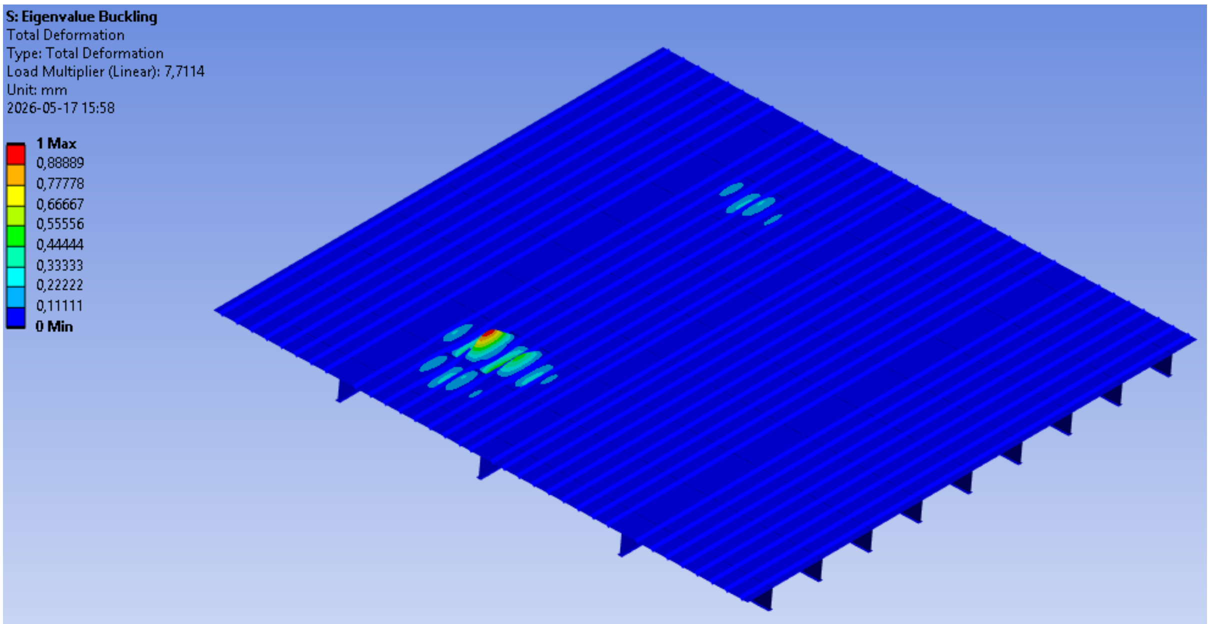

Figure 51: Buckling result – deck 3 with wheel load

For Deck 3, the first buckling load multiplier under pure hull girder loading is relatively high, reaching 12.74. This is mainly because Deck 3 is located close to the neutral axis of the hull girder section, see Figure 17. Therefore, the normal stress induced by hull girder load is relatively small, and the buckling load multiplier is high. Under pure hull girder load, the buckling pattern is relatively uniform and appears within the plate panels divided by the transverse and longitudinal stiffeners, indicating that the deck plating is the buckling-sensitive region under this loading condition. When the local wheel load is included in the combined load analysis, the buckling load multiplier decreases to 7.7114, and the buckling region shifts to the wheel-loaded position. It indicates that the buckling response is mainly governed by the local wheel load. However, the multiplier is still larger, which means that Deck 3 retains a sufficient safety margin against buckling and the structure can be considered safe under the applied design load condition.

9.3. Buckling result – Deck 5

Table 23: Linear buckling result - hull girder load & local load

	Hull girder load	
	Hull girder load	Combined load
Mesh size $[mm]$	75	75
Number of elements	161 841	163 452
Load multiplier	2.8808	2.6948

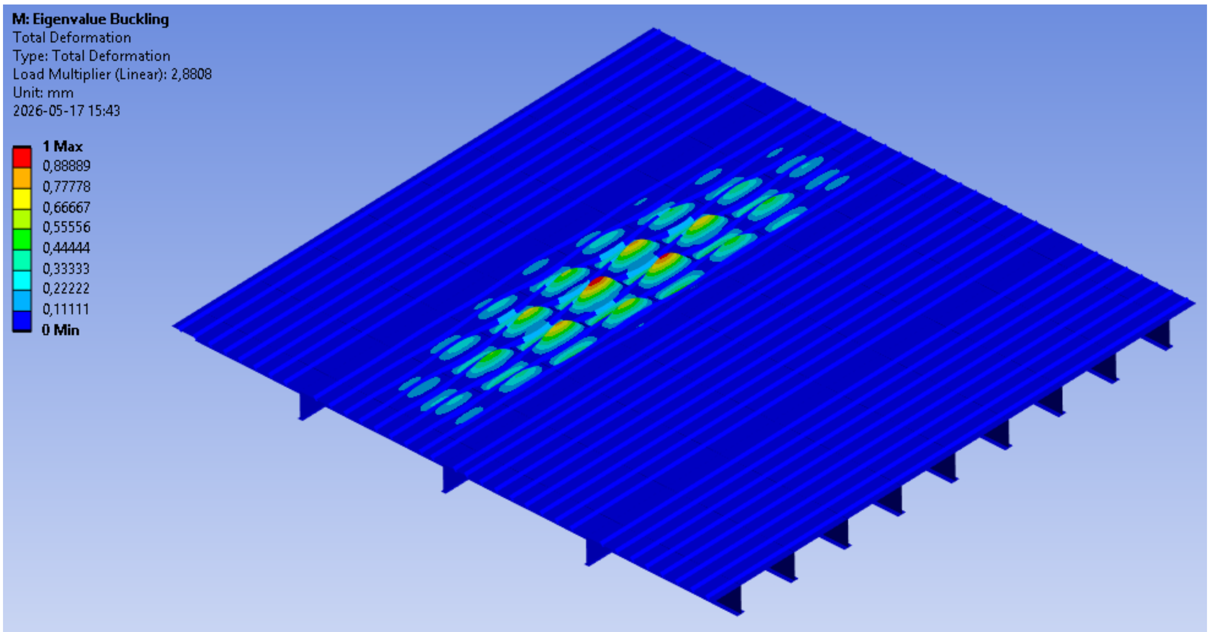

Figure 52: Buckling result – deck 5 without wheel load

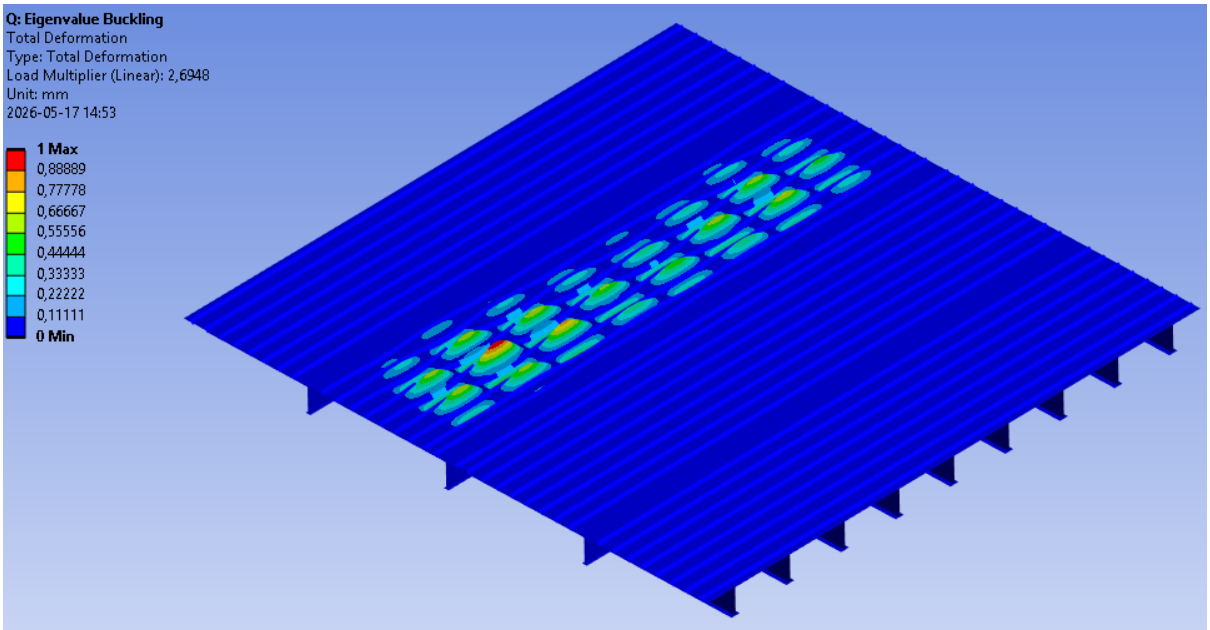

Figure 53: Buckling result – deck 5 with wheel load

Under pure hull girder loading, the linear buckling result of Deck 5 shows that the initial buckling deformation occurs mainly in the top plate. The buckling pattern is also relatively uniform and appears within the plate panels divided by the transverse and longitudinal stiffeners. When the local wheel load is included, the buckling load multiplier is slightly reduced. It is also worth noting that the location of the maximum buckling deformation shifts toward the deck loading patches, showing that the local wheel load affects the distribution of the buckling response. Nevertheless, Deck 5 still retains a reasonable safety margin against buckling, and the top plate is not close to its critical buckling state under the considered loading conditions.

9.4. Linear buckling result discussion

The linear buckling results indicate that the deck structures are not near their critical buckling state under the design load conditions investigated. This indicates that the applied design loads remain below the predicted elastic buckling loads for the deck structures.

The comparison between pure hull girder loading and combined loading also shows the influence of local wheel loads on the buckling response. Under pure hull girder loading, the stress state in the deck is mainly governed by the global bending behavior of the hull girder. When local wheel loads are applied, additional local bending and stress concentrations occur around the loading patches. These local effects disrupt the relatively uniform stress distribution imposed by the hull girder load, thereby making the buckling response more localized. Therefore, even if the global hull girder load remains unchanged, the presence of wheel loads can reduce the buckling load multiplier and shift the critical buckling deformation towards the loaded regions.

It should also be emphasized that the instability modes obtained in this study are mainly local buckling modes. The deformation is confined to limited plate regions, such as plate panels between stiffeners or near the wheel-loading patches. Therefore, the appearance of a local buckling mode in a linear buckling analysis should not be interpreted directly as global structural collapse. In practice, local buckling does not necessarily mean immediate structural failure, since the surrounding structural members may still redistribute loads and provide post-buckling resistance.

However, linear buckling analysis is based on idealized assumptions. It assumes linearly elastic material behavior and does not consider initial geometric imperfections, material plasticity, welding-induced residual stress, or large-deformation effects. Therefore, the calculated buckling load multiplier should not be treated as a direct safety factor for ultimate strength. Instead, it should be interpreted as an indicator of buckling sensitivity and as a useful tool for identifying potential weak regions in the structure.

Within the scope of this thesis, the linear buckling analysis is therefore used as a preliminary stability assessment. It helps to identify the structural regions that are more sensitive to instability and to compare the influence of different load combinations. The results indicate that the addition of local wheel loads reduces the buckling margin and alters the local buckling behavior, but the investigated deck structures still retain sufficient stability under the considered loading conditions.

For future work, a nonlinear buckling analysis is recommended to obtain a more realistic assessment of the ultimate buckling capacity. The first buckling mode obtained from the present linear analysis may be used as the basis for introducing initial geometric imperfections in a nonlinear model. Such an analysis would allow consideration of the effects of material nonlinearity, residual stress, geometric imperfections, and large deformation.

10. Conclusions

This study addresses the challenge of developing an analytical method to evaluate the structural behavior of deck structures with a focus on buckling performance. The aim is to develop a reliable, generalizable analysis framework that enables the assessment of deck structures under realistic loading conditions for a RoPax vessel. Unlike the conventional approach, which applies empirical or simplified loading conditions directly to an isolated deck model, this method seeks to incorporate the influence of hull girder loads into a localized analysis. This integrated setup shall allow the FE tools to capture the complex interplay between global and local structural responses, thereby improving the accuracy of reliability predictions under real loading conditions.

This methodology investigates the structural performance of the main deck of a RoPax vessel by combining hull girder loads and local loads using FEA. The methodology is based on the requirements of DNV-RU and DNV-CG and applies sub-modeling techniques to balance calculation efficiency and cost. This analysis covered linear buckling performance, providing insights into the structural reliability assessment of vehicle-carrying decks.

The linear buckling analysis indicates that the investigated deck structures are sufficiently stable under the design load cases considered. Under pure hull girder loading, the buckling load multipliers are well above unity, indicating that the decks are not close to their critical buckling state. After local wheel loads are introduced, the buckling load multipliers decrease, and the critical deformation region shifts towards the loading patches. However, the structures still retain adequate buckling margins under combined loading. Therefore, the observed local buckling modes should be regarded as indicators of potentially sensitive regions rather than signs of immediate structural failure.

Overall, the study confirms that integrating hull girder and local loads into FEA provides a more realistic and reliable representation of deck performance than traditional analyses based on empirical loads. The combined approach identifies critical components and clarifies potential buckling risks with higher accuracy. The methodology developed in this study can serve as a framework for future optimization of RoPax deck structures. It may also be adapted for analysis of other ship types after appropriate modifications.

11. Future work and improvement

Based on the findings and limitations of this study, several directions are suggested for future research:

1. More realistic load condition

One important improvement is to establish a more detailed and realistic loading condition for the global ship model. In a full CS-based procedure, the hull girder loads should not be applied only by directly adjusting the model to the target VBM and VSF values. Instead, the loading condition should first be generated from the actual load components acting on the vessel, including structural weight, cargo or vehicle loads, ballast loads, hydrostatic pressure, wave pressure, and other relevant local loads. The resulting hull girder loads should then be checked and adjusted to satisfy the target values required by the CS rules.

2. Non-linear buckling and ULS analysis

The present study is limited to linear buckling analysis, which is mainly used to identify buckling-sensitive regions and estimate the elastic critical load of the structure. However, linear buckling analysis does not consider important practical factors such as initial geometric imperfections, residual stresses from welding, material plasticity, and large-deformation effects. Therefore, future work should include non-linear buckling analysis and ultimate limit state (ULS) assessment. Such an extension would provide a more realistic evaluation of the post-buckling behavior and ultimate load-carrying capacity of the deck structures. It would also better align the assessment procedure with classification society requirements.

3. Material choice

A possible continuation of this work is to investigate the performance of the materials used in practical applications, such as EHSS. The potential weight-saving benefits of EHSS are significant in ship design, but its use raises questions about fatigue life and increased buckling sensitivity due to reduced plate thickness. Studies comparing conventional steels and EHSS supported by FEA shall provide valuable guidance for material selection in future ship design.

4. Structural fatigue analysis

Fatigue analysis was not included in the present study, but it remains an important direction for future work. RoPax vehicle decks are subjected to repeated wheel loads and wave-induced hull girder stress variations during operation, which may lead to fatigue damage over long-term service. Therefore, future research should evaluate fatigue-sensitive details such as welded connections, stiffener intersections, openings, plate edges, and regions near wheel-loading patches. A more complete fatigue assessment could include realistic operational load spectra, hot-spot stress evaluation, and fatigue-life estimation using appropriate S–N curves. This would complement the buckling-focused assessment carried out in the present study.

5. Optimization of structures

Given alternative material selection is possible, further structural optimization would be required. A lighter hull structure is desirable, but the reduction in structural weight must not compromise strength, buckling resistance, fatigue life, or compliance with classification society requirements. Potential optimization measures include modifying stiffener arrangements, adjusting plate thickness and scantlings, improving the geometry of openings, and refining intersections between structural members. These improvements could contribute to the development of more efficient RoPax deck structures while maintaining sufficient structural performance and safety.

12. References

ANSYS Inc. (n.d.). *Advanced Analysis Guide*. Retrieved May 1, 2026, from ANSYS Inc.: https://ansyshelp.ansys.com/public/account/secured?returnurl=//////Views/Secured/corp/v242/en/ans_adv/Hlp_G_AdvTOC.html

DNV. (2021a). *DNV-CG-0127: Finite Element Analysis.* Oslo: DNV AS.

DNV. (2021b). *DNV-CG-0128: Buckling.* Oslo: DNV AS.

DNV. (2022). *DNV-RU-SHIP Pt.3.* Oslo: DNV AS.

Humia, A. G. (2019). *Analytical and Numerical Buckling analysis for Cruise Vessel specific Structures.* University of Rostock, Chair of Ship Structures. Rostock: University of Rostock.

Jang, C. H., & Kim, D. K. (2025). Challenges and Constraints in the Application of Rule-Based Hull Girder Load Adjustments: Insights with Future Directions. *Applied Sciences, 15*(3), 1480. doi:10.3390/app15031480

MAFI Transport-Systeme GmbH. (n.d.). *Container Chassis*. Retrieved Dec. 28, 2025, from MAFI: https://mafi.de/en/product/container-chassis/

Nash, P. (2020). *Stena Edda at Birkenhead, 202003*. Retrieved Apr. 4, 2026, from Wikimedia Commons: https://commons.wikimedia.org/wiki/File%3AStena_Edda_at_Birkenhead%2C_202003.jpg

Yi, M. S., & Park, J. S. (2025). *Structural Integrity and Slamming Pressure Mitigation in Floating Offshore Substations: A Multi-Tiered Finite Element Analysis.* Article proof.

13. Appendix

APPENDIX A –Deformation and normal stress of midship cargo-hold model (Global-model)

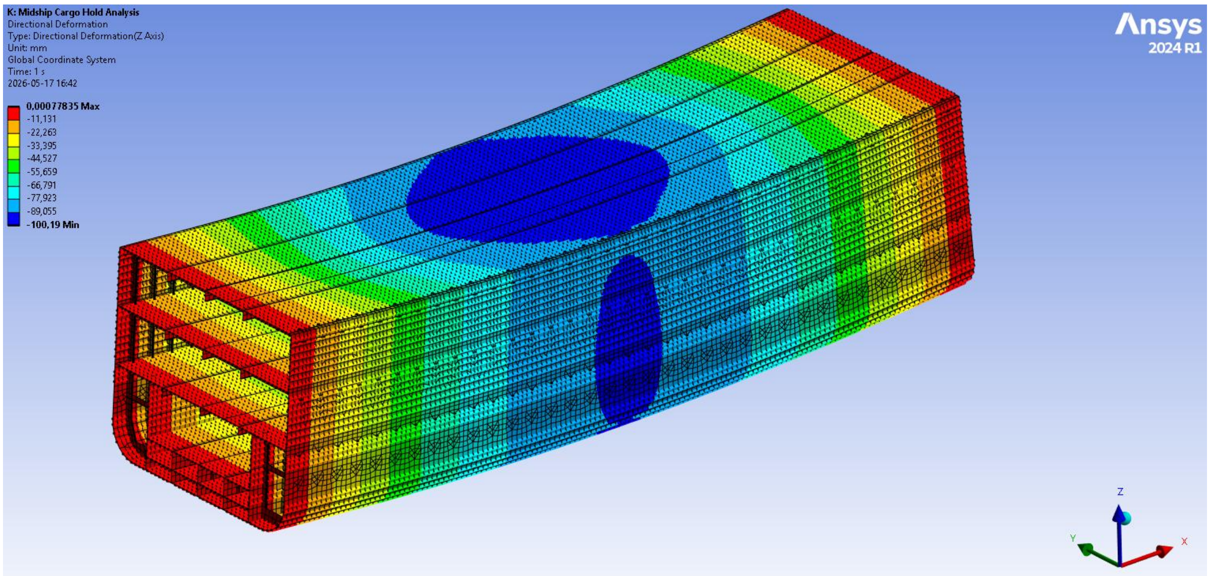

Figure A1: Directional deformation (z-axis) – Global model

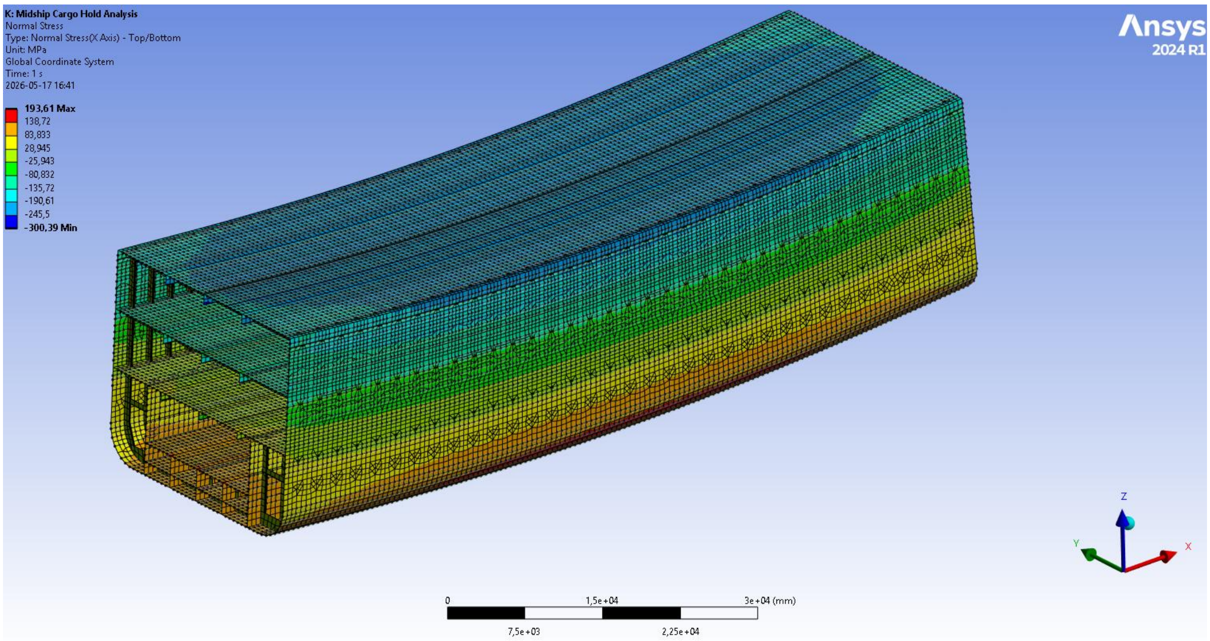

Figure A2: Normal stress (x-axis) – Global model

APPENDIX B – Directional deformation of Deck 3 (Sub-model)

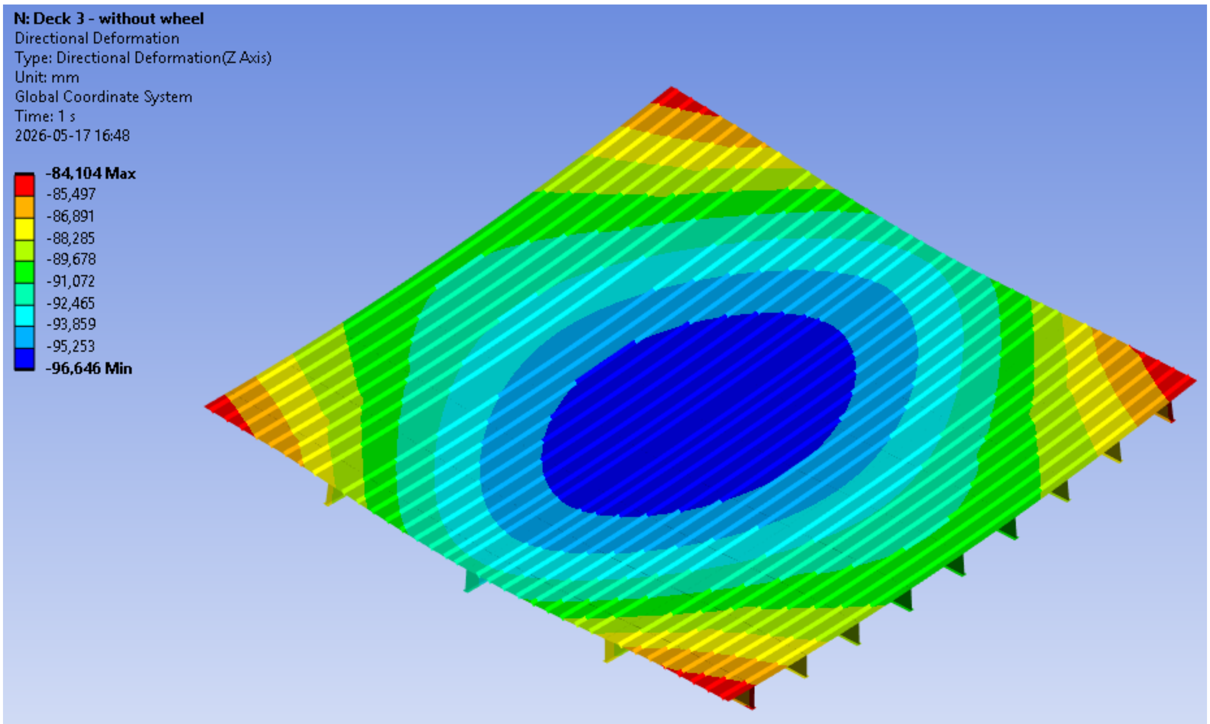

Figure B1: Directional deformation (z-axis) – Deck 3 without wheel load

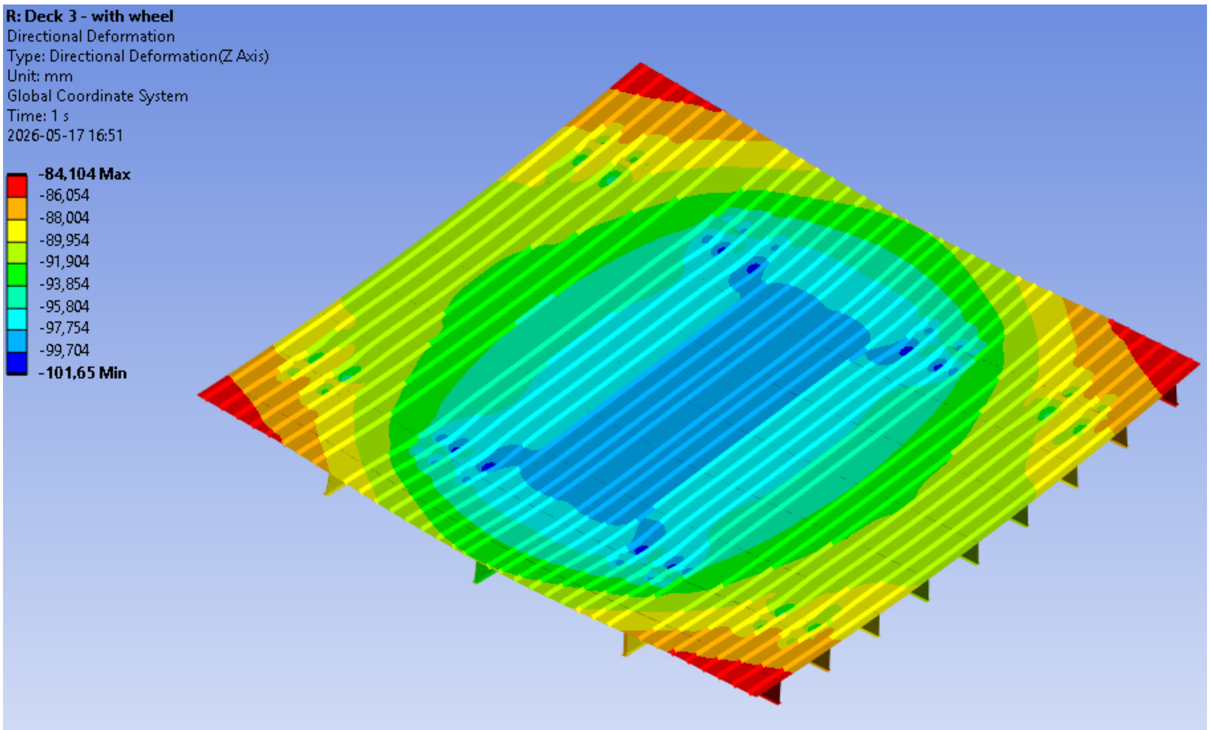

Figure B2: Directional deformation (z-axis) – Deck 3 with wheel load

APPENDIX C – Directional deformation Deck 5 (Sub-model)

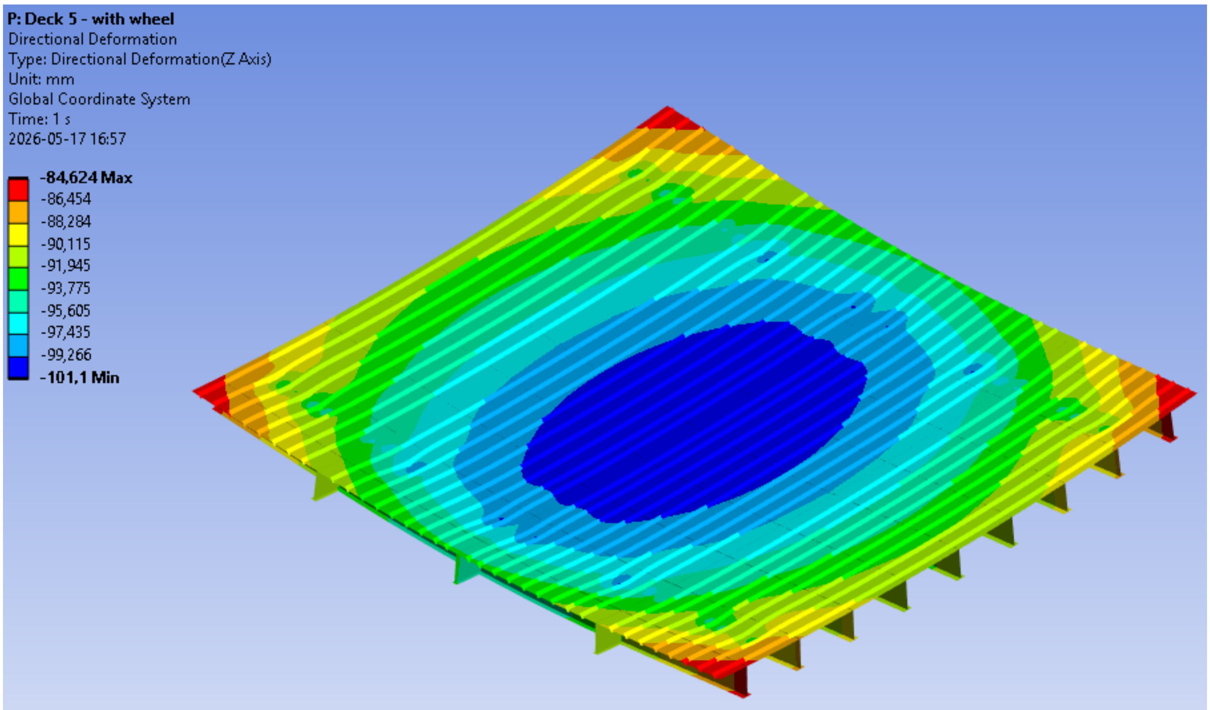

Figure C1: Directional deformation (z-axis) – Deck 5 without wheel load

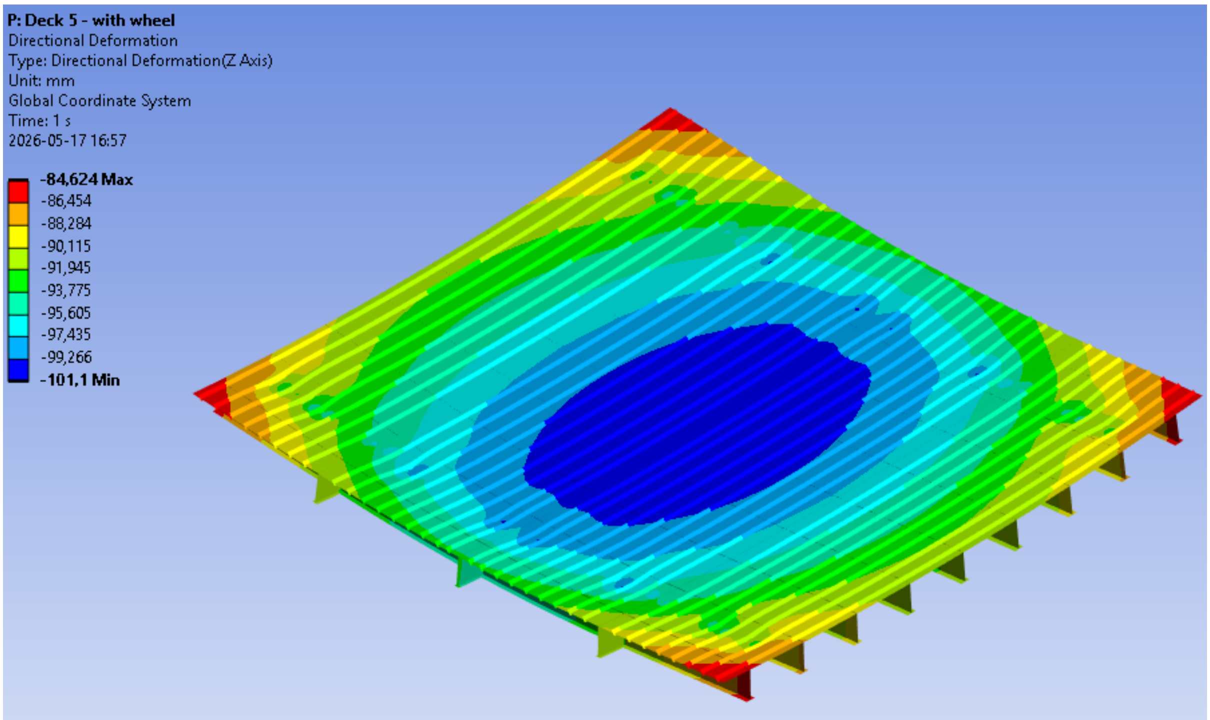

Figure C2: Directional deformation (z-axis) – Deck 5 with wheel load

APPENDIX D – MATLAB code for shear- bending diagram

```
%clear; clc; close all;

%% Basic data
L = 84.8;                          % Model length [m]
n_frame = 35;                      % Number of web frames
x_1 = 1.6;                         % First web frame position [m]
x_35  = L - 1.6;                   % Last web frame position [m]

R_aft = 40860;                     % Aft support reaction [kN]
R_fore = 40860;                    % Fore support reaction [kN]

delta_w = (R_fore+R_aft)/35;       % Vertical line load at each web frame [kN]

M_target = -2794912;               % Target VBM for HSM-1 [kNm], sagging negative


%% Web frame positions
x_frame = linspace(x_1, x_35, n_frame);

%% VSF diagram
x_vsf = [0, x_frame, L];
V_vsf = [R_aft - delta_w*(0:n_frame), R_aft - delta_w*n_frame];

%% VSF introduced VBM
x_VBM = linspace(0, L, 2000)';
M_VSF = -R_aft*x_VBM + delta_w*sum(max(x_VBM - x_frame, 0), 2);

%% VBM diagram
M_VBM = M_target - min(M_VSF);

M_total = M_VSF + M_VBM;

%% Plot
img = imread('Equivalent_Stress_State.png');

figure('Color','w','Position',[100 100 1150 520]);

% Compress the diagram area and leave more space for left/right labels
ax = axes('Position',[0.12 0.14 0.76 0.76]);
hold on;

yyaxis left
ylim([-50000 50000]);
xlim([0 L]);

% Insert image
imgHeight = 22000;
image([0 L], [-imgHeight/2 imgHeight/2], img);
set(gca,'YDir','normal');

h1 = stairs(x_vsf, V_vsf, ...
    'LineWidth', 2.8, ...
    'Color', [1 0 1]);

% VSF
ylabel('VSF [kN]');
yline(0, '-', ...
    'Color', [0.2 0.2 0.2], ...
    'LineWidth', 1.0, ...
    'HandleVisibility','off');


% VBM
yyaxis right
h2 = plot(x_VBM, M_total, ...
    'LineWidth', 2.8, ...
    'Color', [1 0.35 0]);

% Other details
ylabel('VBM [kNm]');
ylim([min(M_total)*1.10 0]);
xlim([0 L]);
```

```
xticks(0:10:L);
xlabel('x [m]');
title('Shear Force and Bending Moment Diagram Based on Beam Theory');
legend([h1 h2], {'VSF','VBM'}, 'Location','northeast');
grid on;
box on;
```

INSTITUTIONEN FÖR MEKANIK OCH MARITIMA VETENSKAPER
CHALMERS TEKNISKA HÖGSKOLA
Göteborg, Sverige 2025
www.chalmers.se

CHALMERS